



## AN ABSTRACT OF THE THESIS OF

Una Savić for the degree of Master of Science in Civil Engineering presented on June 12, 2019.

Title: Assessment of the Active Absorption System of the Large Wave Flume

Abstract approved:

---

Pedro Lomónaco

The Large Wave Flume at the O.H. Hinsdale Wave Research Laboratory houses a piston wavemaker with a built-in active absorption system designed by MTS Systems Corporation. The performance of the active absorption system has not been properly assessed yet. This thesis evaluates the performance of the MTS active absorption system in parallel with a new system designed at Aalborg University called AwaSys7. The results of this thesis have a direct impact on the quality of data collected in future experiments.

The collection of high-quality data in a wave laboratory is vital for coastal engineering design testing and expanding our understanding of physical ocean processes. Confidence in data is obtained by working with a reliable wave generator, particularly if an active absorption system is present and whose capabilities are known. It is understood that experiments requiring regular and irregular waves are impacted by re-reflection from the wave board if an active absorption system is not present or poorly designed. The presence of re-reflected waves leads to a build-up of energy, altering the desired sea state the experimental model is tested in.

The experiment at the Large Wave Flume tested a series of regular and irregular wave conditions in a highly reflective environment. The flume was equipped with five resistance wave gauges and eight ultrasonic wave gauges.

The performance of the two systems for the regular wave cases was based on calculated reflection coefficients, uniformity of incident waves, and the length of time required to eliminate the existing waves in the flume after testing was completed. For irregular wave cases the change in variance during simultaneous generation and absorption and its exponential decrease at the culmination of generation were used.

The performance parameters were calculated using a mixture of methods including zero down crossing analysis and the separation of incident and reflected waves conducted with the program WaveLab3.

The results show that the AwaSys active absorption system outperforms MTS for the irregular wave cases. However, neither system was able to remain stable for the entire duration of all of the irregular wave conditions. Both AwaSys and MTS had similar performance for the regular wave cases, but there was a trend in favor of AwaSys for all but one tested frequency.

©Copyright by Una Savić  
June 12, 2019  
All Rights Reserved

Assessment of the Active Absorption System in the Large Wave Flume

by  
Una Savić

A THESIS

submitted to

Oregon State University

in partial fulfillment of  
the requirements for the  
degree of

Master of Science

Presented June 12, 2019  
Commencement June 2020

Master of Science thesis of Una Savić presented on June 12, 2019

APPROVED:

---

Major Professor, representing Civil Engineering

---

Head of the School of Civil and Construction Engineering

---

Dean of the Graduate School

I understand that my thesis will become part of the permanent collection of Oregon State University libraries. My signature below authorizes release of my thesis to any reader upon request.

---

Una Savić, Author

## ACKNOWLEDGEMENTS

This project was made possible by the National Science Foundation through the Natural Hazards Engineering Research Infrastructure program.

I arrived at Oregon State University with a lifelong passion for the ocean and a hunger to learn a new set of skills. Although I lacked direction, I was excited to dive in and learn as much as possible. What transpired over the course of the next three years was one of the hardest and most humbling experiences of my life. Oregon State University has given me the priceless gift of a high caliber education and personal growth. I believe that the success I have experienced would not have been my reality were it not for the community I have surrounded myself with.

I would like to express gratitude to Tim Maddux for being a constant source of knowledge, patience, and laughter, Bret Bosma for his willingness to sift through code and listen to problems, and the remainder of the wave lab personnel for their persistent friendship and support. My friends pulled me up whenever my imposter syndrome yanked me down and insisted that I belonged here. I will be forever grateful to Sam Harry for continuously believing in me and being the best guide through my first years in engineering. Thank you to Marine Bentivoglio, Adam Keen, Carie Snowbarger, and David Brown for being my constant support beams.

I would like to thank Tuba Ozkan-Haller for always being willing to listen and to Harry Yeh for reminding me that my non-traditional path is a strength and not a weakness.

I wish to express my most sincere gratitude and appreciation to Pedro Lomónaco for being the best advisor a student could ask for. Your passion, warmth, and encouragement will never be forgotten! I appreciate the time you so graciously have given me in order to guide me through my thesis.

Finally, I cannot begin to express my thanks to my family: Tatu, mamili, Ivili, and Mile. Your support and unyielding belief in my ability to make it through graduate school has meant more than you will ever know.

# TABLE OF CONTENTS

	<u>Page</u>
1 Introduction.....	1
1.1 Literature Review.....	6
1.2 Project Scope.....	12
2 Wave Generation Methods.....	15
2.1 MTS Wave Generation and Control System.....	19
2.2 AwaSys7 Wave Generation System.....	21
3 Active Absorption Methods.....	24
3.1 MTS Wave Generation and Absorption System.....	24
3.2 AwaSys7.....	25
4 Experimental Setup.....	29
4.1 Flume Set-Up.....	29
4.1.1 2D Wave Generator.....	32
4.2 Experiment Instrumentation.....	35
4.2.1 Resistance Wave Gauges.....	35
4.2.2 Acoustic Wave Gauges.....	36
4.2.3 LWF Instrumentation.....	37
4.2.4 Wave Damper.....	39
4.2.5 Cameras.....	40
4.3 Test Wave Conditions.....	41
5 Experimental Procedure.....	44
5.1 Data Acquisition.....	44

## TABLE OF CONTENTS (CONTINUED)

	<u>Page</u>
5.2 Procedure for Testing with the MTS Controller.....	46
5.3 Procedure for Testing with AwaSys.....	46
5.4 Procedure Overview.....	47
6 Data Analysis.....	49
6.1 Data Filtering.....	49
6.2 Active Absorption Performance.....	52
6.2.1 Regular Wave Cases.....	53
6.2.2 Irregular Wave Cases.....	65
7 Results.....	66
7.1 Regular Wave Cases.....	66
7.1.1 Experiments with a Passive Absorber.....	78
7.2 Irregular Wave Experiments.....	84
Bibliography.....	93
Appendices.....	96

## LIST OF FIGURES

<u>Figure</u>	<u>Page</u>
1.1 2D piston wavemaker.....	5
2.1 Regions of applicability.....	18
2.2 AwaSys7 user interface.....	22
4.1 LWF coordinate system and instrument locations.....	31
4.2 MTS Systems Corporation wavemaker schematic .....	32
4.3 MTS Systems Corporation wavemaker schematic (motion frame).....	33
4.4 Resistance wave gauge.....	35
4.5 Acoustic wave gauges.....	36
4.6 Wavemaker wave gauge.....	38
4.7 Wave damper.....	40
4.8. Test wave conditions.....	43
5.1 ImTech.....	44
5.2 Acoustic wave gauge data system collection.....	45
5.3 AwaSys desktop setup.....	47
6.1 Pre and post filtered data .....	51
6.2 Time series with incident and reflected packets .....	55
6.3 Evolution of wave heights.....	59
6.4 Evolution of crests and troughs .....	60
6.5 Mean crest and trough plot .....	61
6.6 Evolution of wave height for both systems.....	62

## LIST OF FIGURES (CONTINUED)

	<u>Page</u>
6.8 Crests and troughs.....	64
7.1 Active absorption performance of MTS and AwaSys.....	68
7.2 Calm down time for regular cases.....	70
7.3 Wave height evolution for 1.4 s trial.....	72
7.4 Wave height evolution for 1.9 s trials.....	74
7.5a AwaSys beach crest and trough plot for 10.0 s and no absorption.....	79
7.5b MTS beach crest and trough plot for 10.0 s and not absorption.....	79
7.6a AwaSys beach crest and trough plot for 10.0 s.....	80
7.6b MTS beach crest and trough plot for 10.0 s.....	80
7.7a AwaSys beach crest and trough plot for 3.0 s.....	81
7.7b AwaSys beach crest and trough plot for 3.0 s.....	82
7.8a MTS beach crest and trough plot 3.0 s with absorption.....	83
7.8b MTS beach crest and trough plot 3.0 s without absorption.....	83
7.9 Variance for all 1.9 s peak period without absorption cases.....	85
7.10 Variance for all 5.0 s peak period without absorption.....	86
7.11 MTS and AwaSys 1.9 s peak period and 0.1 m comparison.....	87
7.12 MTS and AwaSys 1.9 s peak period and 0.25 m comparison.....	88
7.13 Fitted exponential function.....	89
7.14 Evolution of $H_{m0}$ for $T_p=1.9$ s and $H_s=0.1$ m.....	91
7.15 Evolution of $H_{m0}$ for $T_p=1.9$ and $H_s=0.25$ m.....	91

## LIST OF TABLES

<u>Table</u>	<u>Page</u>
2.1 Boundary conditions.....	16
4.1 Instruments.....	39
4.2 Test wave conditions.....	42
7.1 Absorption coefficients.....	67
7.2 Calm down time.....	71
7.3 Crest and trough data for regular waves with active absorption.....	76
7.4 Crest and trough data for regular waves without active absorption.....	76
7.5 Fitted exponent's coefficient.....	90

## LIST OF APPENDICES

<u>Appendix</u>	<u>Page</u>
A. List of symbols.....	99
B. Incident and reflected time series plots.....	100
C. 1.4 s and 1.9 s incident and reflected wave height evolution.....	102
D. Crest and trough evolution for regular beach trials.....	106
E. Crest and trough evolution for regular no beach cases.....	108
F. H evolution for all 1.4s and 1.9s cases.....	112
G. Alpha values.....	113
H. Percent variance.....	114
I. Crest and trough values.....	116
J. Crest and trough values in space.....	118

## DEDICATION

This thesis is dedicated to my parents for their courage, sacrifices,  
and for giving us roots and wings.

## **Chapter 1: Introduction**

The ocean environment covers approximately 70% of the planet, leading to a fundamental need to understand the physical processes that occur within and on the edge of our oceans [1]. For centuries, coastal communities have grown to accommodate an influx of people. In the United States, coastal counties were inhabited by 39% of the population in 2010 with an expected increase of 8% by 2020. This is the equivalent of approximately 133.3 million people living on the coast by 2020 [2]. Although the coastal habitat can be hazardous, communities have continued to expand, requiring further work in ocean related disciplines. Coastal communities require ports and other coastal infrastructure to remain functional. This need led to the recognition of a new civil engineering sub-specialty in 1930, i.e. coastal engineering [3]. Coastal communities are exposed to changing conditions such as a changing wave climate, sea level rise, hurricanes, storm surge, tsunamis, and erosion. Methods of protecting shorelines from erosion and an understanding of geological changes occurring on the coast are necessary. Offshore, new engineering advancements developed including floating structures, oil platforms, man-made islands, off shore wind and wave energy converter farms. Creativity, an iterative design process, and testing results in coastal engineering structures that are able to withstand random and extreme wave conditions. Examples of design testing include analysis of total forces on structure during hurricane storm surge events, sediment scour around piling, dune evolution, and stability of a rubble mound breakwater.

During the design process, engineers take into account wave conditions that have a low probability of exceedance; meaning, that they happen every five, fifty, hundred, or x number of years. The design wave condition is related to the probability of failure and the lifetime of the structure. A tsunami vertical evacuation structure planned for a coast needs to be designed to withstand earthquake forces and be structurally sound for the subsequent tsunami. Often, designs are required to undergo testing to ensure stability prior to the construction of the project. Testing occurs in a laboratory setting, especially in the end stages of design. A laboratory allows for control of variables during an experiment and can be tailored for the specific model needs. In addition, testing in a controlled environment without the corrosive habitat and unpredictability of the ocean is a necessity.

Testing is conducted with the use of numerical and physical models. Numerical models provide a mathematical representation or solution of the design and the interactions expected to occur [3]. A properly executed numerical model will produce a realistic representation of the event with high confidence, Kamphuis (1991) as cited in [3].

In coastal and ocean engineering, a physical model is a representation of a design or a natural process. Kamphuis (1991) and Dalrymple (1985) classified physical models into three categories with each representing a specific research goal [3]. Validation models confirm or further develop a numerical model while a design model tests a prototype's capability to withstand the limitations. An example of a design model is the testing of the base of an offshore wind turbine by scaling down the size of the model and measuring pressure and strain caused by wave forces. The third category is to

design a model in order to study a natural process that is not yet understood [3]. Physical models are able to reproduce extreme conditions, enable simultaneous collection of data, and control over the variability of factors during an experiment. Seeing a model undergo repeated testing offers a unique ability to visualize its behavior, allowing for immediate feedback by researchers and improvements to the model [3]. Examples of physical models tested in laboratories include breakwaters, jetties, wave energy converters, overland flow, and sediment transport. However, physical models have drawbacks which include scaling effects, cost, and unrealistic laboratory conditions, also known as laboratory effects.

The research laboratory used for experiments is chosen based on the physical model design, required ocean conditions, availability of laboratories, cost, and the physical process studied. Laboratories around the world offer a diverse set of tanks including multidirectional wave basins, flumes, and circular tanks. Basins are characterized by a wide box shape, flumes by a long and narrow channel, and circular tanks as a round pool. Wave tanks can be described by their characteristic shape, mostly with a wavemaker at one end and, typically, a mechanism for absorbing waves at the opposite end [4]. More recently built basins will have wavemakers on two walls with wave absorbers on the opposing two walls, including cases with a wave maker surrounding all sides of the basin. Primarily used wavemakers include, piston, plunger, flap, hinge, and pneumatic wavemakers as seen in water park pools [3]. A description of all tanks and wavemakers is not in the scope of this thesis and will not be discussed further. The

work will focus on the active absorption control system of a piston wavemaker in a flume<sup>1</sup>.

A flume wave tank is described as a long and narrow channel and is classified as a two-dimensional vertical (2DV) space, where alongshore processes (i.e. across the width of the flume) are considered uniform. The propagation of waves from the wavemaker to the opposite end of the flume are examined. The wave characteristics along the crest of a wave are assumed uniform and disregarded. In this study, waves propagating along the flume are generated by a so-called piston-type wavemaker. A piston wavemaker is a non-permeable flat surface that moves in a periodic fashion, backwards and forwards, exerting force on the water resulting in waves [3]. The wavemaker stroke,  $S$ , is the distance the piston moves in the negative and positive  $x$  direction as shown in Figure 1.1 [4]. As waves are generated by the piston, they displace the water surface that may be described in the simplest form by Linear Wave Theory with a harmonic motion:

$$\eta = \frac{H}{2} \cos(kx - \sigma t) \quad (1.1)$$

With  $\eta$  representing surface elevation,  $H$  is wave height,  $k$  is the wavenumber,  $x$  is the position of the wave in the direction of propagation,  $\sigma$  is the one over the period of the

---

<sup>1</sup> For information regarding the omitted wavemakers, the reader is encouraged to read *Water Wave Mechanics for Engineers and Scientists* by Robert G. Dean and Robert A. Dalrymple; Ch 6: *Wavemaker Theory and Physical Models*, *Offshore Structure Modeling* by Subrata Kumar Chakrabarti, and *Laboratory Techniques in Coastal Engineering* by Steven A. Hughes; Ch 7: *Laboratory Wave Generation*.

wave, and  $t$  is time. A complete list of symbols can be found in appendix A. In Figure 1.1 the wavemaker's periodic motion displaces a volume of water represented by the greyed-out area. The water propagates away from the wavemaker until it reaches a beach or structure, such as a test model shown in Figure 1.1. At this moment the wave will be either fully or partially reflected and travel in the opposite direction towards the wavemaker. In addition, any other feature introduced along the flume, like the foreshore bathymetry, could introduce partial reflection at multiple locations along the flume.

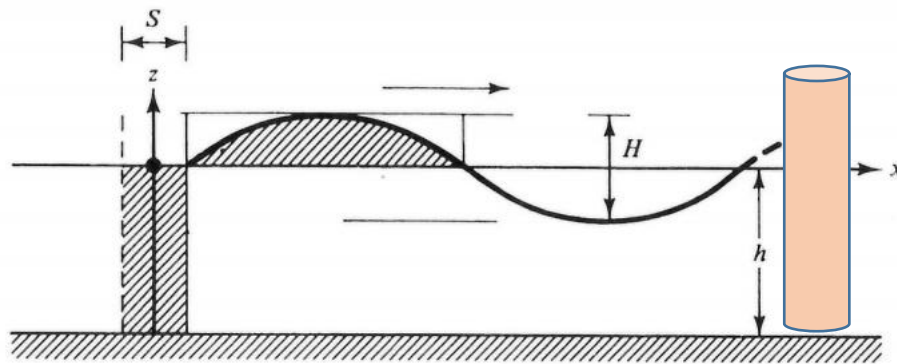


Figure 1.1: Representation of a 2D piston wavemaker and a typical test model.  $S$  is wavemaker stroke;  $H$  is wave height, and  $h$  is depth [4].

In the ocean, when a wave reaches a breakwater, it might be reflected and propagates back offshore. In a flume, the reflected wave is unable to continue propagating away from the structure due to the presence of the wavemaker, from which it will re-reflect back into the flume. As waves continue to be generated by the motion of the wave board, they become trapped within the flume causing an increase in energy and altering the wave train [5]. As energy cannot be created or destroyed, dissipation of energy from turbulence and friction will occur over a period of time. However, for testing purposes,

this does not occur quickly enough. This boundary problem led to the development of the active absorption system. The system detects waves approaching the wave maker by measuring the difference between the target and existing wave conditions. The motion of the wave maker is modified in such a way to produce a time series that is as close as possible to the desired wave train. The active absorption is implemented by the wave maker generating “negative” waves superimposed on the motion of the wave board required for wave generation. This superposition eliminates unwanted waves by shifting the phase of the wave 180 degrees. A reliable active absorption system will give the appearance that the waves pass through the wave board maintaining the desired sea state for testing purposes.

### *1.1 Literature Review*

Currently, it can be considered that there are two types of wave absorbers, active and passive [6]. Passive absorbers are any object whose purpose is to transform or disrupt the water particle velocities and dissipate its energy. Typically, passive absorbers are seen in the shape of a mildly sloping beach. Non-beach passive absorbers are made of various materials including horse hair or wooden slats [6].

Two different approaches have been developed for active absorption; near field and far field. Far field active absorption uses instruments to record surface elevation or wave velocity far from the wave board to estimate the reflected wave field approaching the wavemaker. The incoming waves are mathematically propagated to

the wavemaker allowing for proper motion compensation to occur. Near field active absorption uses the surface elevation at the wave board or the forces acting on the wave board. In this work, the focus will be on near field active absorption using the measured surface elevation at the wave board.

The groundbreaking research work on absorption began with the PhD of J.H. Milgram completed at MIT in 1965 [7]. Milgram continued his work by conducting the first study on active absorbers in 1970 [8]. The experiment was focused on analyzing the ability of a hinged paddle to absorb a generated wave. The objective was to calculate the paddle's horizontal movement from present and past input signals, including the surface elevation in the near field without destabilizing the system [8]. J.H. Milgram arrived at four criteria for active absorption systems [8].

1. Destabilization was not permitted.
2. The paddle was not allowed to drift.
3. At higher frequencies, the amplitude of the function for the absorber should be less than the generating paddle, decreasing noise.
4. Decrease of second order harmonics formed due to non-linearities from wave generation is permitted.

Milgram's experiment was conducted in a 335 cm long, 30.5 cm wide, and 19.1 cm deep aluminum channel with two aluminum hinged paddles, one at each end of the channel. Generation and absorption occurred separately with one paddle generating waves while the second paddle absorbed the waves [8]. Monochromatic waves and bursts of regular waves were generated with active absorption. The same wave conditions were tested again without active absorption, but a 10-degree beach was placed in the channel. The surface elevation was recorded a short distance from the

hinged paddle with a transducer whose data was sent to a filter as a voltage signal that moved the paddle accordingly. The result of Milgram's work was that active absorption was possible with the use of an input signal. While Milgram chose to pursue the use of water surface elevation, other researchers chose to use measured forces on the wave board [5]. G. Gilbert stated that the use of forces is not as convenient as surface elevation in his description of absorbers. Gilbert elaborated that the absorption signal could be added to the feedback generation loop signal and that the new signal would need to be checked for stability to avoid drift [9].

S.H. Salter conducted an experiment on a hinge-flapped system using the forces on the wave board [10]. Subsequent work using forces was conducted by Chatry et al. (1998) and Spinekken and Swan (2009). According to them, using surface elevation collected via wave gauges could lead to a lag due to the accumulation of dirt on instrumentation over time and changes in conductivity may require regular calibration. Accumulated lag and conductivity changes could drive instability as referenced in Milgram's first criteria. In addition, Salter argued that by using wave gauges, too much importance is placed on a sinusoidal wave shape. By using wave forces, the system may incorporate asymmetries as the waves become more nonlinear [10]. In addition, wavemaker systems with water present behind and in front of the wave board (wet-back) experience enhanced forces along with forces developed from evanescent modes in higher frequency waves. This increases error of active absorption systems using measured forces and can only be done in a dry-back system. [11] [5]. A dry-back wavemaker does not have water behind it.

Further work was conducted by Bullock and Murton using a wedge-type wavemaker and running regular and irregular waves in a channel which had either a beach or adjustable slats for wave dissipation and varied reflection, respectively [12]. Water surface elevation was recorded by a traversing wave gauge for the regular cases and by three stationary wave gauges for the irregular cases. The signal generated by the wave gauges was successfully used as the input for the servo controller driving the movement of the wavemaker by the use of analog filters. Bullock and Murton argued for the need for active absorption systems in highly reflective environments because of the development of unrealistic sea states due to reflected waves by the wave board [12].

In 1994 Hemming A. Schäffer, Thomas Stolborg, and Peter Hyllested presented their work on the analysis of a new wavemaker active absorption system called Active Wave Control System (AWACS) [13]. AWACS provided the ability of simultaneous generation and absorption by way of digital recursive filters with the input signal coming from two self-calibrating wave gauges located on the face of the piston wavemaker. The wave gauges on the piston face caused a lag of 50-100 ms [13]. The experiment was conducted in a 46.3 m long and 2.0 m wide channel with a vertical plate on the shoreward side and a piston wavemaker on the offshore side. Regular waves were generated and not simultaneously absorbed by the wavemaker due to the short duration of the waves. The irregular cases were simultaneously generated and absorbed [13]. A total of four wave gauges were used on the surface of the piston wavemaker with a single wave gauge placed halfway down the flume. An array of

three wave gauges placed approximately 30-35 m from the wavemaker were used for the separation of incident and reflected waves. The performance of the AWACS system was assessed by the comparison of reflection coefficients and incident and reflected wave spectra. The authors noted imperfections within the system as seen by small re-reflected waves, but did not suggest the cause [13].

Schäffer continued building on previous work on simultaneous generation and absorption by hydrodynamic feedback via wave gauges using linear wavemaker theory with the inclusion of evanescent modes. The work produced governing equations in Fourier space which were transitioned to the time domain by the use of a recursive digital filter used by the wavemaker to alter the movement based on hydrodynamic feedback from the wave gauges located on the wave maker [14]. Further work in Fourier space was completed by Schäffer and Jakobsen in 2003 with nonlinear wave generation and active absorption occurring simultaneously. The authors proposed the separation of the two systems, called dual mode [15]. Dual mode separates the wave generation from the active absorption system requiring two separate time series. By permitting the linear active absorption signal to be added to the non-linear wave generation signal as a perturbation prevents the active absorption from altering the incident waves. This is achieved by measuring the surface elevation at the wave maker and comparing it to the expected surface elevation allowing an adjustment in the active absorption signal to make appropriate adjustments. The transformation of Fourier space into the time domain with the use of a recursive filter is explained as a necessary method to allow a faster reaction time by the system [15].

The experiment was conducted in a 0.75 m wide, 1.20 m deep, and 23 m long flume with a beach (1:20). The AWACS system was successfully used in the comparison of the single and dual modes. Schäffer and Jakobsen stated that the dual mode successfully generated and absorbed non-linear waves regardless of the wavemaker theory [15]. The experiment tested regular waves with a period of 1.25 s that were generated for 10.0 s, preventing simultaneous generation and absorption. By keeping the duration of the test short, the authors were able to easily separate the incident and the reflected waves throughout their experiment. The irregular wave case allowed for simultaneous generation and absorption with the data assessed using spectral analysis [13].

A new active absorption system was developed in the early 2000s at Aalborg University called, AwaSys 1. An updated version, AwaSys6, was developed at Aalborg in 2016 that uses linear and non-linear waves. A decrease in lag in the feedback loop occurs due to the allowance of a small gap to exist between the wave gauges and the face of the wavemaker [13]. The authors state that a pervasive issue is that not all active absorption systems are efficient at absorbing low frequency waves, such as seiches which develop in flumes [5]. The AwaSys system uses a causal digital FIR filter that allows the alteration of the span of frequencies used in order to maximize the capability of the active absorption system. The experiment was conducted in a flume with two wavemakers on each end, separated 15.84 m. Wave gauges were mounted on the board faces without a gap. An array of wave gauges placed between the two wavemakers were used for the separation of incident and

reflected waves. One wavemaker generated and absorbed waves while the second only absorbed. The setup allowed for the assessment of uniformity of generated waves, which is an important property in laboratories. By allowing the second absorber to be active, the experiment minimized the reflection of the propagating waves. Regular and irregular cases were tested with positive results of regular waves generated using approximate stream function theory and irregular waves using InvFFT random phase method [5]. The analysis of the waves was conducted with the separation of incident and reflected waves as described by Lin and Huang (2004) and improved upon by Lykke Andersen et al. (2016). The analysis was done on a section of the time series which contained a mixture of incident and reflected waves 80 s following the start of the experiment [5]. AwaSys performed well by absorbing second order super and subharmonics for regular waves, with further work in irregular waves being presented later [5]. The authors note that AwaSys will have issues if the wave gauges are not properly calibrated.

### *1.2 Project Scope*

Wave laboratories around the world have acquired wavemakers with active absorption systems. Typically, a wavemaker supplier may incorporate their own active absorption system. Although the active absorption capability has been implemented in numerous wave laboratories around the world in the last several decades, there is little information on how well the system works. This project study aims the development of a methodology to assess the performance of active absorption systems of wave generators in coastal laboratories. The performance

assessment includes the wave energy absorption capability of the system, as well as the uniformity and homogeneity of the generated wave system in space and time. This project has been executed in the Large Wave Flume at O.H. Hinsdale Wave Research Laboratory (HWRL) in Oregon State University. The flume is equipped with a piston-type wave maker and active absorption capabilities. The performance of the active absorption has not been assessed yet.

The construction of the Large Wave Flume (LWF) began in 1972 with approximately half of the cost provided by O.H. Hinsdale, vice president of the Umpqua River Navigation Co. [16]. O.H. Hinsdale was specifically interested in testing the stability of concrete and rock used to construct jetties at river mouths and his desired project was the first to be scheduled in the LWF as soon as it opened [17]. Originally an outdoor lab, a limited roof was built in 1982 [18] and became a completely enclosed structure in 1989 with funding from the Office of Naval Research [19]. From 2004 to 2014 the National Science Foundation classified the lab as an experimental facility for its Network of Earthquake Engineering Simulation Program (NEES). During this time, the current piston wavemaker built by MTS Systems Corporation replaced the original hinged piston wavemaker in 2009 [19]. By 2016, HWRL was incorporated into the Natural Hazards Engineering Research Infrastructure program (NHERI) [19]. HWRL has grown with the addition of a multidirectional wave basin in 1989 that was expanded in 2003 with the support of NSF [19]. Both of the wave tanks were designed with flexibility in mind to further research capabilities making the HWRL facility vital for research [20, 21].

The current dry-back piston wavemaker in the LWF has the capability of active absorption whose performance has yet to be evaluated. This thesis will discuss the method that was implemented in order to assess performance of the current active absorption system in parallel with a new state of the art system, AwaSys7, supplied by Aalborg University.

Both systems, MTS and AwaSys, were assessed by running a set of regular and irregular waves, with and without active absorption. The majority of the wave conditions were conducted without a beach to test the systems with full reflection at the end of the flume. Two regular wave conditions were tested with a 1:12 sloped beach installed later along the flume. The performance of the systems for the regular wave cases were analyzed using reflection coefficients, uniformity of incident waves, and the length of time needed to remove the generated waves from the flume, also known as calm-down time. For the irregular wave cases, change in variance during generation and its exponential decrease at the end of wave generation were used for analysis. The data was processed using zero down crossing analysis and separation of incident and reflected waves with WaveLab3.

The following two chapters will discuss the wave generation and active absorption of MTS System Corporation and AwaSys7. The experimental setup including the arrangement of the flume and instrumentation will be discussed in chapter 4. The process of data acquisition and the experimental procedures will be discussed in chapter 5 with the data analysis described in chapter 6. Results and discussion will follow.

## Chapter 2: Wave Generation Methods

To generate waves, a proper surface elevation solution has to be chosen. In the case of linear waves, the fluid is assumed to be irrotational and incompressible leading to the establishment of the fluid potential velocity satisfying the well-known Laplace equation shown in Table 2.1 [22]. The Laplace equation is solved by using known boundary conditions given in terms of velocity potential that include bottom, kinematic, dynamic, lateral, and far-field wave conditions, as listed in Table 2.1 [3, 22]. The boundary condition that is pertinent to the generation of waves is the lateral boundary condition associated with the wavemaker. With  $L$  representing the wavelength of the wave, the movement of the wavemaker generates a wave by the displacement of a volume of water equivalent to [4]:

$$\int_0^{\frac{L}{2}} \frac{H}{2} \sin(kx) \quad (2.1)$$

When the solved Laplace equation consisting of a homogeneous and partial solution is used in conjunction with the dispersion relationships, the surface elevation equation is obtained with  $C_0$  representing the Biésel Transfer Function for the far field,  $C_j$  the near field, and the  $\omega$  the radian frequency [22]:

$$\eta_1(x, t) = C_0 \sinh(k_1 h) \cos(\omega t - k_1 x) + \sum_{j=1}^{\infty} C_j \sin(k_j h) e^{-k_j x} \sin(\omega t) \quad (2.2)$$

By representing the displacement of our piston wavemaker with the equation

$e(z, t) = e_0 \sin(\omega t)$  and using definitions found in [22], we obtain the Biésel

Transfer Function for the far field solution and a sum of transfer functions for the near field solutions (evanescent modes) represented by  $C_{0,2D}$  and  $D_x$ , respectively.

Table 2.1: First and second order Boundary conditions. With  $h$  representing water depth and  $z$  representing the vertical coordinate, with the bottom being  $z$  equal to  $-h$  and the water surface represented with  $z = 0$ .

Boundary Conditions	First-Order	Second-Order
<b>Laplace</b>	$\frac{\partial^2 \phi_1}{\partial x^2} + \frac{\partial^2 \phi_1}{\partial z^2} = 0$	$\frac{\partial^2 \phi_2}{\partial x^2} + \frac{\partial^2 \phi_2}{\partial z^2} = 0$
<b>Bottom</b>	$\frac{\partial \phi_1}{\partial z} = 0$ at $z = -h$	$\frac{\partial \phi_2}{\partial z} = 0; z = -h$
<b>Lateral (wall)</b>	$\frac{\partial \phi_1}{\partial x} = 0$	$\frac{\partial \phi_2}{\partial x} = 0$
<b>Kinematic Free Surface</b>	$\frac{\partial \eta_1}{\partial t} - \frac{\partial \phi_1}{\partial z} = 0$ at $z = 0$	$\frac{\partial \eta_2}{\partial t} + \frac{\partial \phi_1}{\partial x} \frac{\partial \eta_1}{\partial x} - \frac{\partial \phi_2}{\partial z} - \eta_1 \frac{\partial^2 \phi_1}{\partial z^2} = 0$
<b>Dynamic Free Surface</b>	$\frac{\partial \phi_1}{\partial t} + g \eta_1 = 0$ at $z = 0$	$\frac{\partial \phi_2}{\partial t} + \eta_1 \frac{\partial^2 \phi_1}{\partial z \partial t} + \frac{1}{2} \left[ \left( \frac{\partial \phi_1}{\partial x} \right)^2 + \left( \frac{\partial \phi_1}{\partial z} \right)^2 \right] + g \eta_2 = 0$
<b>Lateral (piston)</b>	$\frac{\partial \phi_1}{\partial x} = \frac{dX_{01}}{dt}$ at $x = 0$	$\frac{\partial \phi_2}{\partial x} = \frac{dX_{02}}{dt} - X_{01} \frac{\partial^2 \phi_1}{\partial x^2}, x = 0$
<b>Wave</b>	$\frac{d\phi_1}{dt} = 0$	

With  $C_{0,2D} = \frac{H}{S}$  with  $S$  representing the wavemaker stroke [22]:

$$\frac{\eta(x,t)}{e_0} = C_{0,2D} \cos(\omega t - kx) + D_x(x) \sin(\omega t). \quad (2.3)$$

In the linear solution, and far from the wavemaker, the second term of the right-hand side of the equation disappears omitting the evanescent modes [3]. Thus, as noted in [3], in linear theory the surface elevation is presented as:

$$\eta_1(x, t) = \frac{H}{2} \cos(k_1 x - \sigma t) \quad (2.4)$$

The analytical solution to the Laplace Equation may be linear or apply a weakly nonlinear solution (i.e. a perturbation method). The accuracy of the solution improves as the order number increases. The n-th order Stokes solution to the Laplace Equation is a classical way to describe nonlinear waves. Other methods allow the development of the solution to wave propagation that are not solutions to the Laplace Equation, including cnoidal and solitary wave theories.

Linear waves can be solved past the first order to take into account the different combinations of harmonics that can be generated using second or higher order solutions. In a similar way as with Linear Wave Theory, proper boundary conditions and techniques have been implemented in the development of the generation of nonlinear waves (see e.g. [5] and [23]). However, the different linear and nonlinear wave theories have been derived assuming different conditions that limit the range of applicability. Figure 2.1 Shows the different regions of applicability for some wave theories that represent the typical waves generated in laboratories.

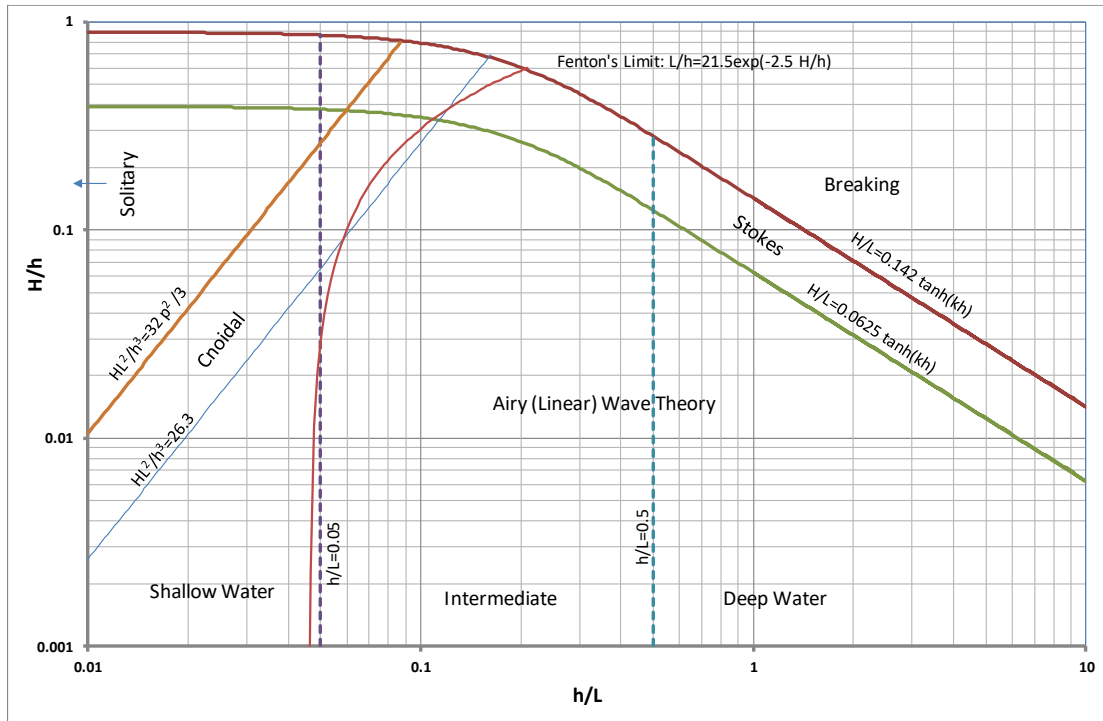


Figure 2.1: Regions of applicability of different wave theories.

The majority of intermediate water waves fall in the Airy wave, or linear theory. Stokes' theory is an expansion of linear theory by solving for second or higher orders. The cnoidal wave theory applies to shallow water waves. Stream function theory applies to waves that are in the shallow and intermediate water regimes<sup>2</sup>. As a conclusion, in proper wave generation and absorption, it is best to incorporate the corresponding wave theory according to the different ranges of applicability, providing the most accurate condition in testing. As will be seen in the following chapters, in this Thesis the active wave absorption assessment was performed with

<sup>2</sup> For further information on Cnoidal and Stream Function theory, the reader is referred to The Cnoidal Theory of Water Waves, Fenton J.D. (1999) and Approximate Streamfunction Wavemaker Theory for Highly Nonlinear Waves in Flumes, Schäffer (2007), respectively.

the generation of waves always using the corresponding theory according to the regions of applicability as seen in Figure 2.1, minimizing the generation of spurious waves and ensuring stability and quality in the experiments.

### *2.1 MTS Wave Generation and Control System*

The MTS system includes preset controls for generating cyclic, random, solitary, cnoidal, Stokes, and Airy waves. In addition, user-generated surface elevation and board displacement files can be uploaded. Recently, the system was suited to incorporate an external analog signal, which was implemented to enable the generation using alternative systems (e.g. AwaSys). Trials conducted with the MTS System used the option for user-defined surface elevation and board displacement files to generate the desired wave conditions. MTS calls the surface elevation file a wave height file, which is fundamentally inadequate, since what it is prescribed is the surface elevation, and not the wave height. The surface elevation data file is translated into board motion by applying the Biésel Transfer Function using a fixed water depth and period input by the user. No evanescent modes are calculated; therefore, MTS Systems applies the far field solution of eq. 2.3.

For regular wave generation, surface elevation and wave board displacement files were created using a MATLAB script written by Tim Maddux using the wave generation theory developed by Schaffer in [24]. The period, wave height, and duration were entered allowing the script to choose the appropriate wave theory from

linear, Stoke's second-order, cnoidal, and stream function theory by calculating the nonlinearity parameter,  $s$  found in [4].

$$s = \frac{ka \cosh kh(2 + \cosh 2kh)}{\sinh kh^3} \quad (2.5)$$

For  $s \leq 1$ , Stoke's second order theory is valid [24].

If  $s > 1$ , Stoke's theory is invalid and the linear, cnoidal, or stream function theories are evaluated. Using [25] as a reference:

If  $T < 7.256 \sqrt{\frac{h}{g}}$  and  $U > 100$  : T is the wave period and U is the Ursell Number.

This should be impossible to achieve. In the case that it does, linear theory is used.

If  $T < 7.256 \sqrt{\frac{h}{g}}$  and  $U \leq 100$ : Stream function theory is valid.

If  $T \geq 7.256 \sqrt{\frac{h}{g}}$  and  $U \leq 100$ : Stream function theory is valid.

If  $T \geq 7.256 \sqrt{\frac{h}{g}}$  and  $U > 100$ : Cnoidal theory is valid.

Once the appropriate wave theory for each condition is found, a corresponding wave generation theory is implemented. The wave generation technique may induce the generation of spurious waves that may be reduced by using wave generation to the second order [24]<sup>3</sup>. The spurious waves are free waves generated by irregularities

---

<sup>3</sup> For details on second order wavemaker theory the reader is referred to Second-Order Wavemaker Theory for Irregular Waves by Hemming A. Schäffer (1996) 24. Schäffer, H.A., *Second-Order Wavemaker Theory for Irregular Waves*. Ocean Engineering, 1996. **23**(1): p. 44-88. and Second-Order Wavemaker Theory for Multidirectional Waves by Hemming A. Schäffer and Catherine M. Steenberg (2003).

along the flume, the simplification of the generation method to a first order, and due to the nonlinear interaction with different harmonics; producing sub and super-harmonics. In addition to spurious wave, evanescent modes are generated by the misalignment of the wavemaker motion and the velocity profile of the generated waves. This is observed as a perturbation in the surface elevation in front of the wave maker and quickly fades away from the board. In shallow water, evanescent modes quickly disappear at a distance of three times the water depth from the wavemaker [3].

For irregular wave generation, a second MATLAB script using second order wavemaker theory was used to generate the surface elevation and wave board displacement files. The required inputs are peak period, significant wave height, duration, and spectral shape.

For both, regular and irregular trials, the waveboard displacement files are used to generate waves with the active absorption system deactivated, while the surface elevation files are used for the active absorption trials.

## *2.2 AwaSys7 Wave Generation System*

AwaSys7 gives the user a multitude of options for wave generation. The interface options are as follows: regular waves (Approximate Stream Function and Linear Method 1<sup>st</sup>/2<sup>nd</sup> Order - Stoke's), custom time series, custom spectrum,

solitary/tsunami, TMA, Generalized  $\Gamma$ , Jonswap, Bretschneider-Mitsuyasu modified, Bretschneider-Mitsuyasu, Bretschneider, Pierson Moskowitz, FRF, Gaussian Swell, Top-Hat, and Torsethaugen-Haver (Figure 2.2). Stream Function (10<sup>th</sup> order) was used for regular wave generation while Jonswap ( $\gamma = 3.3$ ) was used for the irregular wave cases. For consistency purposes, Stoke's theory was planned for the trials in which the generating MATLAB script chose Stoke's theory for the MTS portion of the experiment. However, AwaSys7 preferred stream function theory. By using higher stream function orders we increase the quality of the approximation [26].

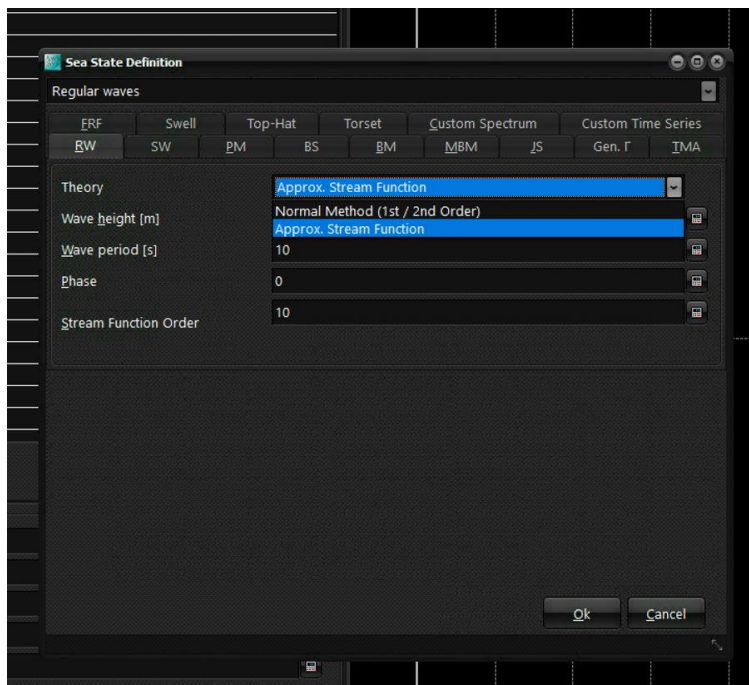


Figure 2.2: AwaSys7 user interface. Sea State Definition.

To generate waves, the sea state is defined by selecting the desired theory, water depth at the wavemaker, water depth at a reference point, sample time, and

succeeding calm down time. Calming down is used to absorb the existing waves in the flume after the experiment has concluded.

## Ch 3 Active Absorption Methods

### *3.1 MTS Wave Generation and Absorption System*

The MTS system uses the term ‘Wave Height Control’ for active absorption. Wave height control can be used for linear and cnoidal waves as well as the user generated files. Wave height control functions by measuring the surface elevation in front of the wave board and comparing it to the target surface elevation that is previously computed or defined by the user. The difference between the two values is calculated and considered as an error that requires a correction. The motion of the wave board is adjusted by applying a Biésel Transfer Function to its movement. The Biésel Transfer Function has been derived for Linear Theory and the solution is based on the relative wave number,  $kh$ , which requires for its computation the wave period and the depth at the paddle. Since the period of the reflected wave is unknown beforehand, (the system would need to record the entire wave to calculate the period, which would delay the adjustment of motion) the system requires as an input a “nominal” wave period in order to calculate the transfer functions. This is required for irregular waves, uses the wave period of the regular waves, and the water depth when ‘Wave Height Control’ is activated. A limitation for the input period for the MTS system was discovered during the early phases of the experiment to be 15.0 s. While the system is generating waves, the measured signal of two wave gauges located at the wavemaker board are averaged and introduced to the absorption system as the current surface elevation at the piston. The feedback information is used to modify the board displacement required to generate the desired waves. The MTS system uses a linear

Biéssel Transfer Function to convert the wave height to the required board displacement, and uses the board velocity for controlling the position [27]. As noted in chapter 2, the wave height control system used by MTS does not take into account the evanescent modes that occur at the face of the board, hence, the evanescent modes will be interpreted by the MTS system as part of the error, which will be tried to be absorbed. In addition to the recurrent surface elevation feedback, a running average filter spanning 20.0 s is used to calculate the mean water level in the flume. The filter is used to remove low frequency (seiche) and higher frequency waves occurring in the flume that are outside the ability of the wave height control system. The mean water level is subtracted from the surface elevation to obtain the wave height and is sent to the system through the wave height feedback signal [27]. The amplitude of the wave height control signal is limited by the gain control.

### 3.2 *AwaSys7*

AwaSys provides flexibility by allowing the user to select if near or far field wave gauges will be used. The surface elevation feedback measured by MTS at the board was connected to and used by AwaSys as an input. Hence, during these experiments, near field wave absorption was used. For the nearfield one-gauge mechanism, AwaSys applies the active absorption as described in [5]. The active absorption method uses linear theory in the nearfield but includes the presence of evanescent modes occurring at the wavemaker. As described in [5], the wave amplitude at the wavemaker wave gauge is provided in complex form with the Biéssel Transfer

Function that describes the wave amplitude at the wavemaker wave gauge by the equation given in [5]:

$$A_{WG} = (-iC_{02,D}e^{ikd_{WG}} + D(d_{WG}))X_{gen} \quad (3.1)$$

Here,  $d_{WG}$  represents the distance from the wave gauges to the piston,  $X_{gen}$  is the motion of the wave maker during wave generation, and  $A_{WG}$  is the wave amplitude at the wavemaker wave gauge. The motion of the wavemaker required to make necessary corrections to the surface elevation is inserted into equation 3.1 along with the assumption that the reflected and re-reflected wave amplitudes are equal resulting in equation 3.2:

$$A_{WG} = \left(-iC_{02,D}e^{ikd_{WG}} + D(d_{WG})\right)X_{gen} + X_{abs} + 2\cos(kd_{WG})A_R \quad (3.2)$$

With  $X_{abs}$  and  $A_R$  representing the motion of the wavemaker during active absorption and the amplitude of the reflected wave, respectively. In [5], with  $A_I$  representing the amplitude of the incident waves, the far field incident waves are generated by the motion of the wavemaker during generation and absorption with the reflected wave amplitude summed.

$$A_I = -iC_{02,D}(X_{gen} + X_{abs}) + A_R \quad (3.3)$$

By plugging the far field incident amplitude into the equation for wave amplitude at the wavemaker, an equation describing wavemaker displacement is reached [5] as shown in equation 3.4. With  $H(f)$  representing the transfer function for active absorption. Not stated in the equation but stated as a vital addition is the inclusion of the phase shift and gain.

$$X_{gen} + X_{abs} = (2A_I \cos(kd_{WG}) - A_{WG})H(f) \quad (3.4)$$

$$H(f) = \frac{1}{iC_{0,2D}*(e^{ikd_{WG}} - 2 \cos(kd_{WG})) - D(d_{WG})} \quad (3.5)$$

[5] state that by measuring the surface elevation and calculating the desired incident wave height, the displacement of the wavemaker can be calculated. The displacement of the wavemaker is then sent to a digital causal FIR filter [5].

AwaSys features a dual mode design separating the signal for wave generation from the absorption signal [28]; preventing the active absorption signal from compromising the time series signal. The dual mode capability is achieved by omitting the wavemaker generation motion from equation 3.4 giving rise to the new absorption signal in equation [3.6] [5].

$$X_{abs} = -A_{WG,abs}H(f) \quad (3.6)$$

The authors state that by calculating the far field surface elevation of the desired wave condition and by adding the evanescent modes, the required surface elevation at the wavemaker face can be calculated [5]. For the absorption of irregular waves, Lykke et al. use equation 3.6 that contains linear and second order components [5]<sup>4</sup>. It is important to note that, unlike the MTS system which allows only one period to be absorbed, AwaSys accepts a span of frequencies that can be adjusted by the user.

---

<sup>4</sup> For a more detailed explanation regarding the active absorption system used by the AwaSys7 program the reader is encouraged to see, A new active absorption system and its performance to linear and non-linear waves by Thomas Lykke Andersen et al. (2016).

## Chapter 4: Experimental Setup

As indicated previously, this project study aims to assess the performance of the active absorption system of the Large Wave Flume at HWRL, Oregon State University. Two active absorption systems will be analyzed, i.e. the absorption system provided by MTS, the manufacturer of the wave machine; and the absorption system implemented in AwaSys, a wave generation software system developed in Aalborg University.

Active absorption relies on the measurement of wave reflections along a flume and reaching the wave board, and the absorption algorithm will modify the signal to ensure the generated waves are as close as possible to the target waves. If there is no reflection, the active absorption system should not modify the original signal. Hence, it is understood that, for a single paddle system, the most demanding condition would be to have full reflection of the generated waves, so the absorption system will significantly modify the steering signal. From the perspective of control stability, it is also understood that minimum or no reflection will be the other most demanding case in the performance assessment.

### *4.1 Flume Set-Up*

The Large Wave Flume (LWF) is a long and narrow channel with a removable and fully adjustable beach [21]. The flume is 110 m long, 3.7 m wide, and 4.6 m deep. The working length of the flume is 87.415 m, i.e. the distance from the paddle mid

position to the end of the flume where experiments can be executed. The flume is equipped with a dry-back hydraulically powered piston wavemaker with a max stroke of 4 m and a speed of 4 m/s [26]. More details on the wave machine can be found in the following sections.

To enable the full reflection of the waves at the end of the flume, the concrete slabs, typically used as a passive wave absorber, were laid horizontally on the bottom of the flume starting at bay 2 (Figure 4.1). The approximate height of each concrete slab is 6 inches, equivalent to 0.1524 m. The back wall of the flume was exposed leaving a smooth and fully reflective surface. It should be noted, that for two additional regular cases, the concrete slabs were put into a mild 1:12 slope configuration with the slope starting at bay 9 and finishing at the vertical wall, 87.415 m from the wavemaker. The LWF coordinate system can be found in Figure 4.1 and is defined as follows: the origin is located at the center of the bottom of the piston face while in a neutral position. The x-coordinate is positive in the north direction with the propagating waves. The positive y-coordinate moves from the midline of the piston face to the west, while the z-coordinate moves in a positive direction from the midline of the floor up along the face of the piston.

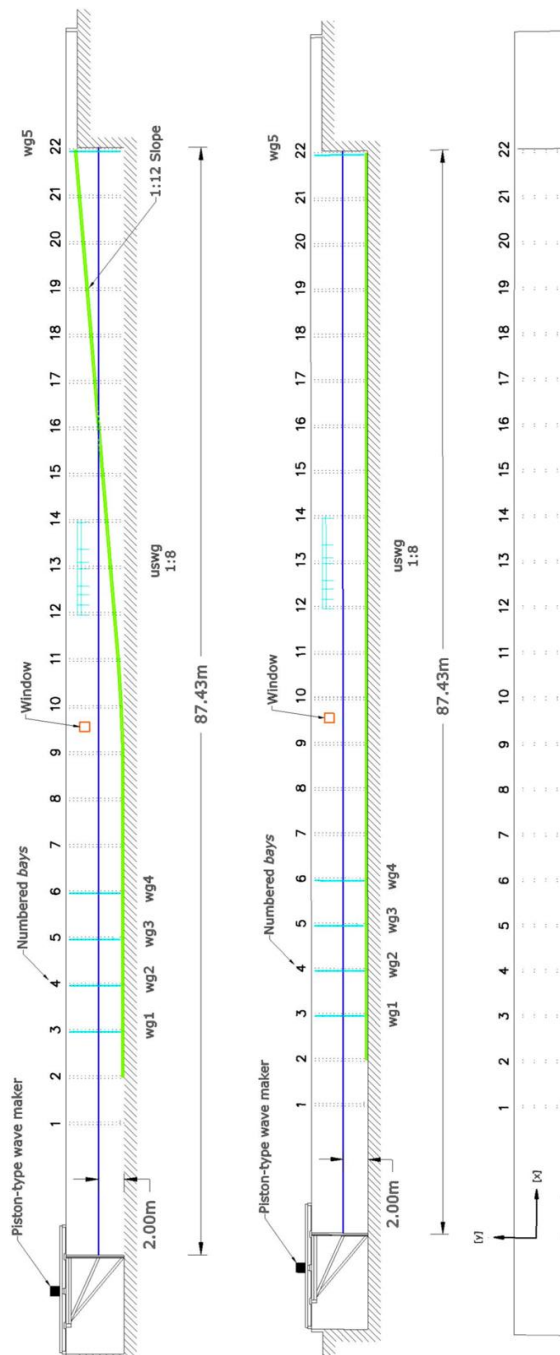


Figure 4.1: Left: longitudinal cross-section of the flume with the 1:12 dissipative beach with slab and gauge positions. Center: longitudinal cross-section of the flume for the fully reflected wave conditions with slab and gauge positions. Right: Longitudinal top view of the flume with coordinate system. Courtesy of Pedro Lomónaco.

### 4.1.1 2D Wave Generator

The 2D hydraulically powered generator is a dry back piston wavemaker that was installed by the MTS Systems Corporation in 2009 [26]. A labeled Figure of the wave generator system provided by MTS can be seen in Figures 4.2 and 4.3.

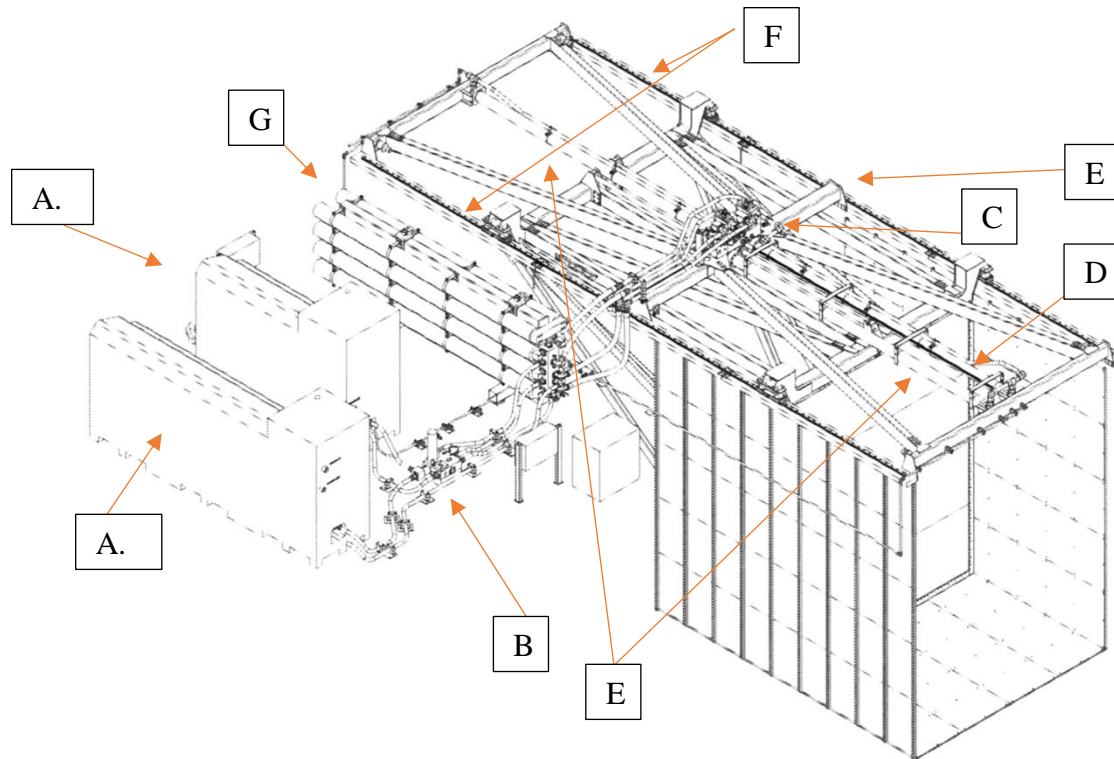


Figure 4.2: Wave generator system figure from the MTS Systems Corporation user manual, 2009, [26]. **A.1:** MTS Model 505.60 HPU, **A.2:** MTS Model 505.120 HPU, **B:** MTS Model 293.32 HSM, **C:** actuator manifold, **D:** teposonics transducer, **E:** actuator assembly, **F:** bearing rails, **G:** bank of accumulators

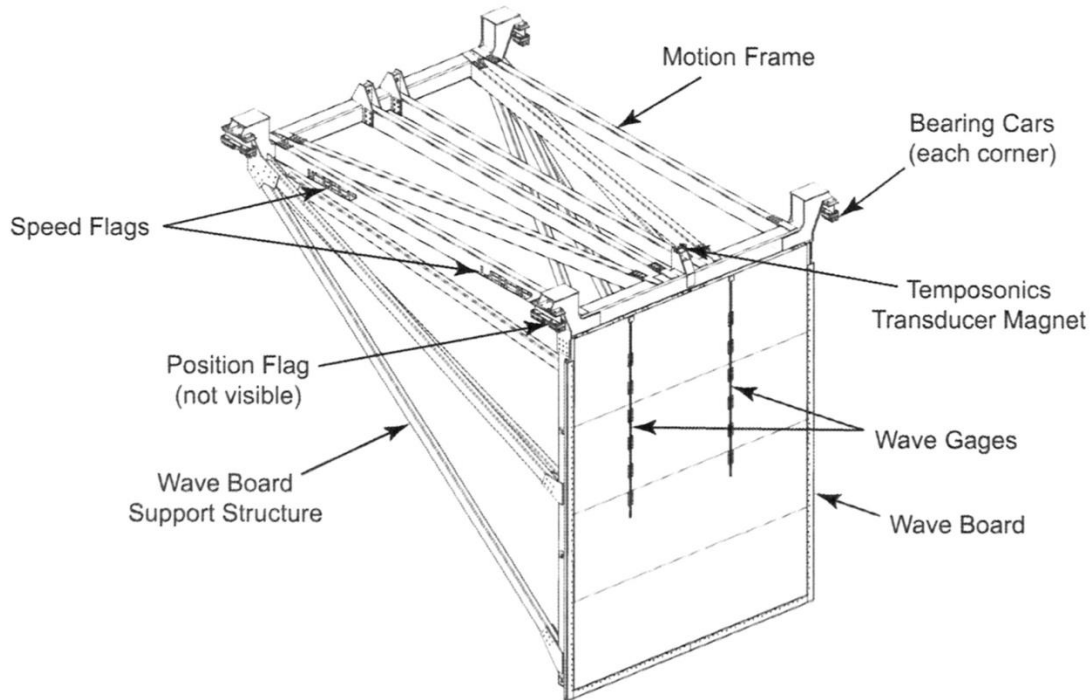


Figure 4.3: The motion frame and wave board from the MTS Systems Corporation user's manual, 2009, [26].

The piston wavemaker was designed to produce solitary, regular, and irregular waves with the movement of its wave board against water contained in the flume. The desired waves are determined by the user from a computer station that is housed in the control room overlooking the LWF. The wave board is hydraulically powered by two MTS Model 505 hydraulic power units (HPU) that are heated to 100°F+. The heated oil provided by the HPU is controlled by the MTS Model 293.32 hydraulic service manifold (HSM) with a servo hydraulic drive system. A servo hydraulic drive system is an electronically controlled valve programmed to control the volume of oil that flows to the actuator (mechanical component that controls movement). The required volume is sent through the HSM to the actuator manifold located on top of the drive frame assembly [26]. The actuator manifold houses servo valves that control

the actuator's velocity and direction as directed by the command received from the MTS controller. A position transducer is housed on the north end of the drive assembly. This particular transducer, developed by MTS and known as Temposonics™, is composed of a magnet on the motion assembly and a sensor housed on the drive assembly. As the wavemaker moves, the MTS controller receives position feedback as the magnet and sensor pass each other [26]. A bank of accumulators housing additional oil required for tests with large displacements are located on the southeast side of the flume. The piston face is connected to the moving frame that is powered by the control manifold and actuator assembly. Bearing cars found on each corner move by gliding on bearing rails located on top of the flume walls. Sensors are located on the drive frame and track the location of the speed flags on the motion frame. This system is used to provide the wavemaker with acceleration and deceleration feedback. An added feature of the system are the position flags located in the front of the wave board assembly. The flags are used to prevent the wavemaker from exceeding its limits by obstructing the view of the sensors [26]. Finally, two resistance wave gauges are located on the piston face and provide the system with water surface elevation feedback. The resistance wave gauges are discussed in Section 4.2.3.

## *4.2 Experiment Instrumentation*

A combination of resistance wave gauges, acoustic wave gauges, and instruments routinely used for testing in the LWF were used for the experiment. The locations of the wave gauges along the flume are indicated in Figure 4.1.

### *4.2.1 Resistance Wave Gauges*

Resistance wave gauges track surface elevation by recording the conductivity of the water as it changes based on the temperature and salinity by using two wires as conductors. The measured resistance has an inverse relationship with the length of wire that is submerged [28]. A total of five resistance wave gauges were installed along the east wall of the flume and were used to record the surface elevation during each trial. The twin wire resistive wave gauges (wg) seen in Figure 4.4 were calibrated during the draining process at the end of the experiment.



Figure 4.4: Resistance wave gauge 2 during testing.

#### 4.2.2 Acoustic Wave Gauges

Acoustic wave gauges (uswg), shown in Figure 4.5, measure the surface elevation of the water in the flume by emitting sound waves that travel through the air to the water surface. The sound waves are reflected back to the gauge measuring and recording the distance. A total of eight acoustic wave gauges were installed in a lagged array along the east wall of the flume with each gauge having at least a distance of 0.6 m from the adjacent gauge(s) to prevent cross-talking. The array of ultra-sonic wave gauges were used for the separation of incident and reflected waves for all irregular wave conditions and regular wave conditions with a period greater than 1.9 s and without a beach.



Figure 4.5: Acoustic wave gauges 1-8 shown during testing.

#### 4.2.3 LWF Instrumentation

The wavemaker piston houses two wave gauges that consist of two off-set pre-calibrated resistive wave gauges mounted on the wave board that are called the wavemaker wave gauge or wmwg (Figure 4.6). The stainless-steel wave gauges are housed in ultra-high molecular weight (UHMW) polyethylene wire guides. The surface elevation recorded by the two gauges is averaged together cancelling the effect of cross waves formed in front of the piston. The wmwg is used to obtain a surface elevation feedback to the system, where the surface elevation is zero at the still water level [26]. The distance of the wave maker wave gauges from the piston face were measured with a Dura-cal IP65 caliper. For the west gauge the distance from the piston face was estimated to be 1.07 cm and 1.14 cm for the east gauge. The wavemaker displacement (wmdisp) is a Temposonics<sup>TM</sup> transducer sensor that tracks and records the displacement of the piston. The level sensor, located at bay 2, is a NIST calibrated pressure sensor used to measure the still water depth.



Figure 4.6: Wavemaker wave gauges (wmwg).

Wavemaker start (wmstart) records a signal which is initiated with the activation of the wavemaker and maintains a positive value while the wavemaker is active after which it drops to zero as a step function. This signal is used to synchronize multiple data acquisition systems and for post-processing. Instruments and their locations are summarized below in Table 4.1.

Table 4.1: Instruments: courtesy of Tim Maddux.

Instrument	Sensor Name	Placement (m)		
		(X)	(Y)	(Z)
standard	VSTD-7208	-	-	-
wmstart	Wmstart	-	-	-
wmdisp	TMPO-LWM	-	0	-
wmwg	RWG-LWM	-	0	-
level	PRES-9959	13.961	-1.532	0.323
wg1	RWG-2263-01	17.827	-1.384	-
wg2	RWG-2263-02	21.479	-1.388	-
wg3	RWG-2263-03	25.142	-1.371	-
wg4	RWG-2263-04	28.799	-1.372	-
uswg1	DS-6553	50.656	-1.302	3.493
uswg2	DS-6662	51.272	-1.314	3.482
uswg3	DS-6665	52.187	-1.312	3.484
uswg4	DS-6663	52.82	-1.291	3.486
uswg5	DS-6486	54.003	-1.306	3.491
uswg6	DS-6554	54.619	-1.306	3.488
uswg7	DS-6666	55.831	-1.31	3.496
uswg8	DS-6555	57.657	-1.274	3.479
wg5	RWG-2264-01	87.097	-1.369	-

#### 4.2.4 Wave Damper

The experimental setup of the flume created highly reflective conditions. For trials with the active absorption capability turned off, the reflective conditions on both ends of the flume would have created waves propagating in the flume for an extended period of time. A preliminary test resulted in a long wave that propagated for a total of 4 hours. To decrease the time between trials, a simple damper was built using unistruts, horse hair, and sheets of perforated plywood as seen in Figure 4.7. The damper was used to disrupt the maximum horizontal water particle velocities

occurring at the node of a standing wave. The location of the nodes for each trial changed depending on the wave period and were not located in the same position, but for consistency, the damper was lowered at the midway point of the flume, 43.7 m, during each trial except for one particular case (MTS no absorption,  $T=1.4$  s  $H=0.05$  m). The damper was raised and lowered using a 6-ton gantry crane. Four ropes were tied to the top corners of the damper and attached to the closest eyehole in the appropriate flume wall with enough tension to allow the damper to dissipate as much wave energy as possible when submerged.



Figure 4.7: Wave damper during deployment.

#### 4.2.5 Cameras

Two GoPro cameras were used for ten of the trials. The locations of the GoPro cameras varied throughout the experiment. An iPhone 6 was used to take photos and videos when necessary. A Panasonic AW-HE50S camera mounted in the ceiling

above bays 16 and 17 was used for the recording of one of the trials ( $T=10.0$  s  
 $H=0.50$  m).

#### *4.3 Test Wave Conditions*

MTS and AwaSys7 were tested in two phases. In phase one waves were generated with the active absorption deactivated. In the second phase the identical wave conditions were generated with active absorption activated. The wave conditions included both regular and irregular waves. The wave conditions were chosen to allow for the changing of one variable at a time while providing an evenly spread array of wave conditions, where the dimensionless properties are typically found in nature. The regular cases consisted of shallow, intermediate, and deep-water waves, while all of the irregular cases were in the intermediate water regime. The tested wave conditions are listed in Table 4.2 and Figure 4.8. The regular wave cases were designed to generate a short burst of 20 waves, while the irregular cases had more than 400 waves to ensure a proper wave distribution. The labels marked in gray in Table 4.2 represent wave conditions that either had an antinode located below the uswg hitting the instruments repeatedly, or that the waves were too steep to be properly measured by the uswg. Those cases were executed once and not repeated during the different phases of testing. Both phases were conducted in the flume with the beach removed allowing for a highly reflective environment for testing. Also, each phase included the testing of two regular cases with a 1:12 slope beach installed in the flume. The water depth in the flume was set to 2.0 m for every trial. The

presence of the concrete slabs on the bottom of the flume decreased the water depth by 0.15 m from bay 2 to the back wall.

Table 4.2: Test wave conditions. The grey rows represent the regular experiments that were not further considered due to the limitations of the uswg position or recording.

<b>Regular</b>		without beach			
<b>T</b>	<b>H</b>	<b># of waves</b>	<b>wave duration</b>	<b>time with ramps</b>	<b>total test time</b>
<b>(s)</b>	<b>(m)</b>		<b>(s)</b>	<b>(s)</b>	<b>(s)</b>
1.4	0.05	20	28	68	900*
1.9	0.05	20	38	78	900
1.9	0.10	20	38	78	900
1.9	0.16	20	38	78	900
2.4	0.25	20	48	88	900
3.0	0.05	20	60	100	900
3.0	0.10	20	60	100	900
3.0	0.25	20	60	100	900
3.0	0.35	20	60	100	900
5.0	0.05	20	100	140	900
5.0	0.10	20	100	140	900
5.0	0.25	20	100	140	900
5.0	0.50	20	100	140	900
10.0	0.05	20	200	240	900
10.0	0.25	20	200	240	900
10.0	0.50	20	200	240	900
1.9	0.25	20	38	78	900
3.0	0.50	20	60	100	900
8.0	0.50	20	160	200	900
<b>Regular</b>		with beach			
3.0	0.35	~186	560	600	1500
10.0	0.50	20	200	240	900
<b>Irregular</b>		without beach			
<b>T<sub>p</sub></b>	<b>H<sub>s</sub></b>				
<b>(s)</b>	<b>(m)</b>		<b>(s)</b>	<b>(s)</b>	<b>(s)</b>
1.9	0.10	453	860	900	1800
1.9	0.25	453	860	900	1800
5.0	0.10	448	2240	2280	3180
5.0	0.25	448	2240	2280	3180

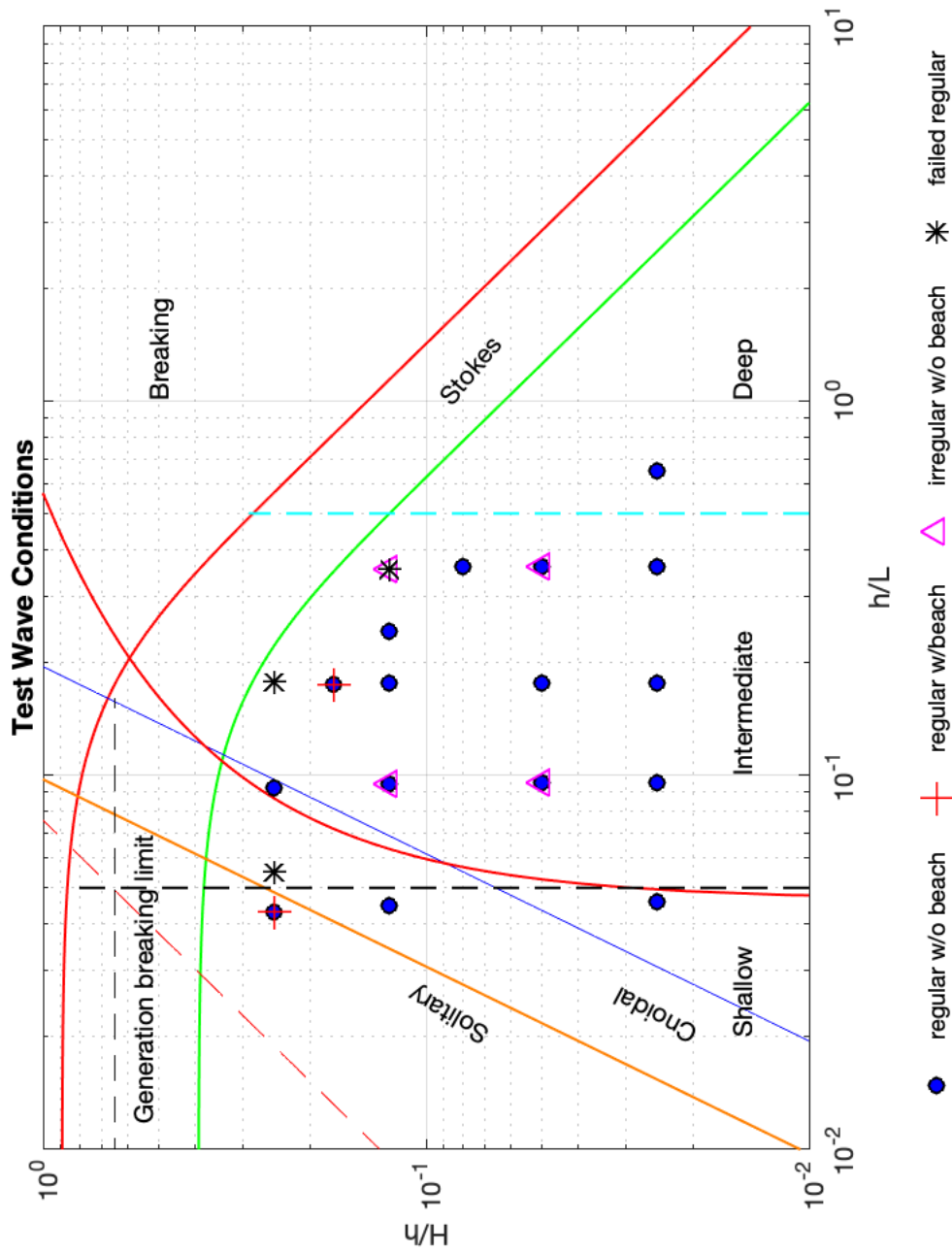


Figure 4.8: Test Wave Conditions in dimensionless form, plotted with the regions of validity of the different wave theories

## Chapter 5: Experimental Procedure

### 5.1 Data Acquisition

The data collected by the data acquisition system (DAQ) at HWRL included a voltage reference for QC&QA, the flume water level, the wavemaker displacement, wavemaker start, the average of the wave gauges at the paddle (wmwg), and the ultrasonic and resistance wave gauges. The resistive wave gauges used were fabricated by ImTech (Figure 5.1) which measures the changes in electrical current along two surface piercing wires as the surface elevation changes. The current data is measured as a voltage signal by the data acquisition system. The DAQ was located on the east side of the flume wall in proximity to the resistance wave gauges.



Figure 5.1: ImTech resistance wave gauge, voltage standard, and DAQ.

The ultrasonic wave gauge data had a similar setup as the resistance wave gauges, shown in Figure 5.2. The data was recorded as a voltage signal that was converted from volts to meters during the post processing of data using a transformation constant obtained during calibration.

A computer receiving information from the data acquisition system was used to update the trial number, file name, trial description, and conditions for each trial along with the sampling rate. All of the instruments used for the experiment had a sampling rate of 100.0 Hz.



Figure 5.2: System setup used to send the ultrasonic wave gauge measurements to the data acquisition system.

### *5.2 Procedure for Testing with the MTS Controller*

The MTS computer was used to select the desired displacement or surface elevation file for the trial, enable the wave height control, and to start the wavemaker. Prior to starting the MTS system, the DAQ was initiated in order to record 30 seconds of still water conditions prior to each trial. For trials tested with active absorption, the wave height control was activated immediately prior to the generation of waves.

### *5.3 Procedure for Testing with AwaSys*

During the AwaSys phase, three computers in two separate locations were used. The computer connected to the data acquisition system was used in the same manner as during the MTS phase, recording the still water level for a total of thirty seconds prior to start of the wave generation. The MTS computer was utilized by selecting the external analog option. The external analog permits another system to override the MTS wave generation system.

At the end of the thirty seconds, the user turned on the external analog function. With AwaSys overriding the MTS system, the run button was pushed on the AwaSys computer starting the trial.



Figure 5.3: AwaSys desktop computer at bay 2.

#### *5.4 Procedure Overview*

As previously stated, there is a total of thirty seconds of still water level data recorded prior to each trial. Once the appropriate system for generating and absorbing waves was activated, the rest of the trial was completed in an identical manner. For the MTS trials using active absorption, the wave height control was deactivated immediately following the completion of the wave generation and calming down time of the trial. The calming down period began at the end of the wave generation and ended 10 minutes after the start of the trial. The damper was lowered at the end of the calm down time while the DAQ kept recording for an additional 5 minutes.

This time frame was kept consistent with both systems except for the first two trials of the MTS phase. The damper was not prepared in time for the initial MTS trial while the damper deployment was not recorded during the second trial. AwaSys allows the user to set a calm down time, which was replicated to match the MTS

experiments. Therefore, the calm down time was set to end 10 minutes after the start of the trial, terminating active absorption.

For trials without active absorption, the duration of the instrument recording and time of damper deployment was kept consistent as for the active absorption trials.

The irregular wave trials with and without active absorption were conducted in the same manner as the regular trials in terms of calm down time and damper deployment except that the 10-minute calm down time began after wave generation ended.

## Chapter 6: Data Analysis

### *6.1 Data filtering*

As indicated in the previous chapters, laboratory wave generation is subject to various imperfections such as wave board displacement, wave board type, wave theory approximation, and limited-order wave generation compensation. In practice, nonlinear interactions with all the existing harmonics, may enhance the generation and propagation of spurious waves, some shorter and some longer than the period of the target waves. This process requires space and time, and eventually all the different components may interact with each other. Moreover, only those frequencies with a wavelength close to an integer fraction or proportion of the flume length, will excite the resonant modes. As a result, these (long) waves will increase wave amplitude, which is known as tank seiching.

This phenomenon was observed during the experiments, which was expected given the highly reflective boundary at the end of the flume. Hence, as part of the data analysis, the long-wave component of the signal was separated from the shorter-wave components.

Moreover, in a similar way, high-frequency spurious waves can also be observed due to wave scattering of the different protruding elements along the flume, from the splashing of the make-up pump used to return the leaked water through the moving seal of the dry-back paddle, nonlinear interaction of the different wave components, or even due to wave splashing and clapotis. These high-frequency waves are also measured and can be considered as noise. Then, further in the analysis, the high-

frequency component of the obtained signal is separated from the short-wave components. The analysis of the performance of the active absorption of both systems was executed on the resulting, filtered, short-wave time series.

In order to separate the high frequency and low frequency data from the desired short waves time series, the calibrated data was filtered using a Butterworth low pass filter.

The expected seiche modes in the flume were calculated using Table 5.1 from [4].

$$\frac{2L}{\sqrt{gh_0}} = \frac{2*87.415 \text{ m}}{\sqrt{9.81 \frac{\text{m}}{\text{s}^2} * 1.85 \text{ m}}} \approx 41 \text{ s for the first mode.} \quad (6.1)$$

Frequencies beyond 0.05 Hz were filtered out in order eliminate long waves from the data. The same data was passed through a Butterworth bandpass filter that allowed frequencies from 1.67 Hz to 0.05 Hz to pass leaving only waves whose frequencies were in a range between the noise in the flume and the long waves or seiche. The bandpass filter eliminated the seiche and noise from waves generated by the fill pump. Great care was taken to avoid filtering the data too much in order to not compromise the results. Figure 6.1 shows an example of calibrated and filtered uswg data for a 1.4 s case tested using the MTS system with active absorption. As mentioned earlier, it is interesting to note that, in the low pass filter section, a generated and developing seiche in the tank is visible. For purposes of data analysis, the broadband passed data, seen in the far-right column in Figure 6.1 was used.

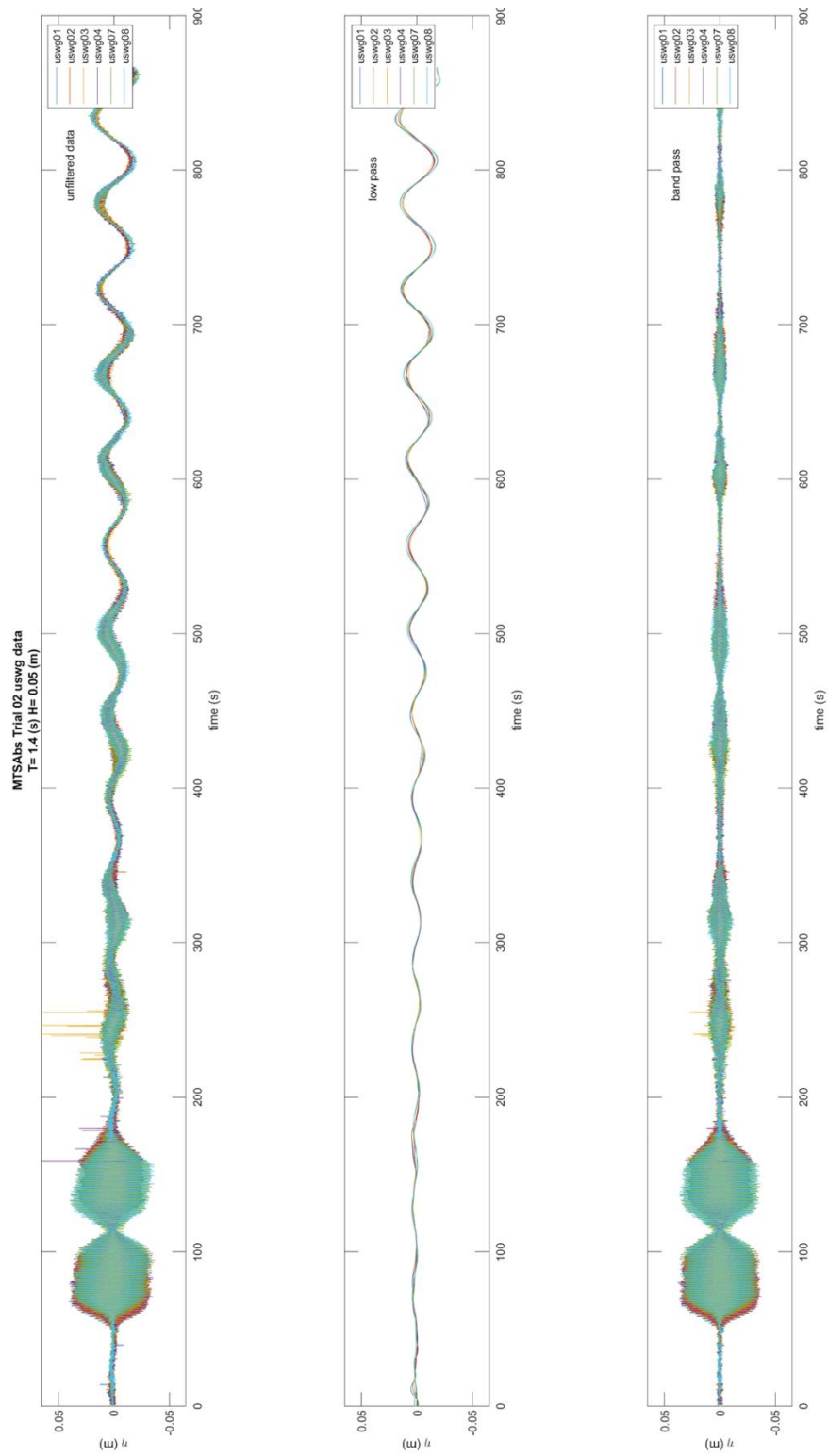


Figure 6.1: Sample of data pre-filtering, post low-pass, and bandpass filtering for a case with active absorption enabled.

## *6.2. Active Absorption Performance*

The assessment of the active absorption system was analyzed by computing the statistics of the incident wave height, crests, and troughs for each trial of the regular wave cases. These parameters show the ability of the wavemaker to produce consistent waves. Moreover, the shape of the waves can be established by analyzing the crest and the trough of the waves and compare them with the theoretical profile of the wave. The reflection coefficient of the wavemaker was calculated for all of the regular wave trials using the measured or computed incident and reflected wave heights.

The reflection coefficient shows how well the active absorption system works during each wave condition by providing the percent of the wave height that is reflected off the piston face. The reflection coefficient at the wave board is, actually, the inverse of the absorption coefficient. Perfect 100% absorption means 0% reflection, and vice-versa. The final parameter used was the calm down time. This was the time duration required for the active absorption system to reduce the waves in the flume below a given threshold after generation ends. By analyzing the calm down time for each trial, we can better adjust the time between testing for future experiments.

For the irregular wave cases, the system was assessed by calculating the wave height percent variance of each trial. Variance shows the trend in energy in the flume for the duration of the trial and can be used to assess whether the energy content is increasing, or how quickly the energy decreases when simultaneous generation and absorption ends.

### 6.2.1 Regular Wave Cases

As mentioned in chapter 4, short bursts of 20 waves were generated for each regular trial. The number of waves was chosen in order to limit the number of wave trains travelling in each direction, while keeping enough waves to have a representative sampling series. The burst of 20 waves propagated from the wavemaker to the wall. When the waves reflect from the wall, create a standing wave pattern near the wall. The waves then propagated from the flume back towards the wavemaker. The 1.4 s and 1.9 s cases had a short period leading to situations of purely incident and purely reflected portions of the wave train visible in the timeseries. This is useful since for those cases the reflection coefficient from the paddle (or the vertical wall) can be computed without the need of using incident-reflected estimation methods.

Figure 6.2 shows the timeseries for the entire duration of an MTS 1.4 s period trial conducted without active absorption<sup>5</sup>. The x axis represents the test elapsed time, while the y axis represents the length of the flume longitudinal coordinate in meters. The vertical axis is a longitudinal coordinate, where each of the wave gauges have been plotted according to their corresponding position (in order wmwg, wg1, wg2, wg3, wg4, uswg 1-8, and wg5). In order to plot the measurement of the surface elevation, the time series was scaled appropriately. Figure 6.2 is used for representation of the different wave trains as they propagate along the flume and helps understanding the selection of the time windows used during the data analysis.

---

<sup>5</sup> The plot in Figure 6.2 can be found in appendix B for every trial and both systems.

Wave generation at the paddle is seen at  $y=0$  m, with the main 20 waves identified by the red shaded section. The incident waves can be followed up to the wall as they pass each instrument. The incident waves appear to stay uniform until they reach the wall. An increase in wave height is evident at the wall due to the formation of a stationary wave. As the burst of waves propagate back in the direction of the wavemaker, wave-wave interaction and frequency dispersion produce some variability, and the packet of waves reduces its uniformity. This plot also helps in the identification of the superposition of incident and reflected waves, and the effect in the time series. Lack of uniformity in the wave profile is due to the superposition of waves travelling in different directions and is not related to the quality of the generated waves.

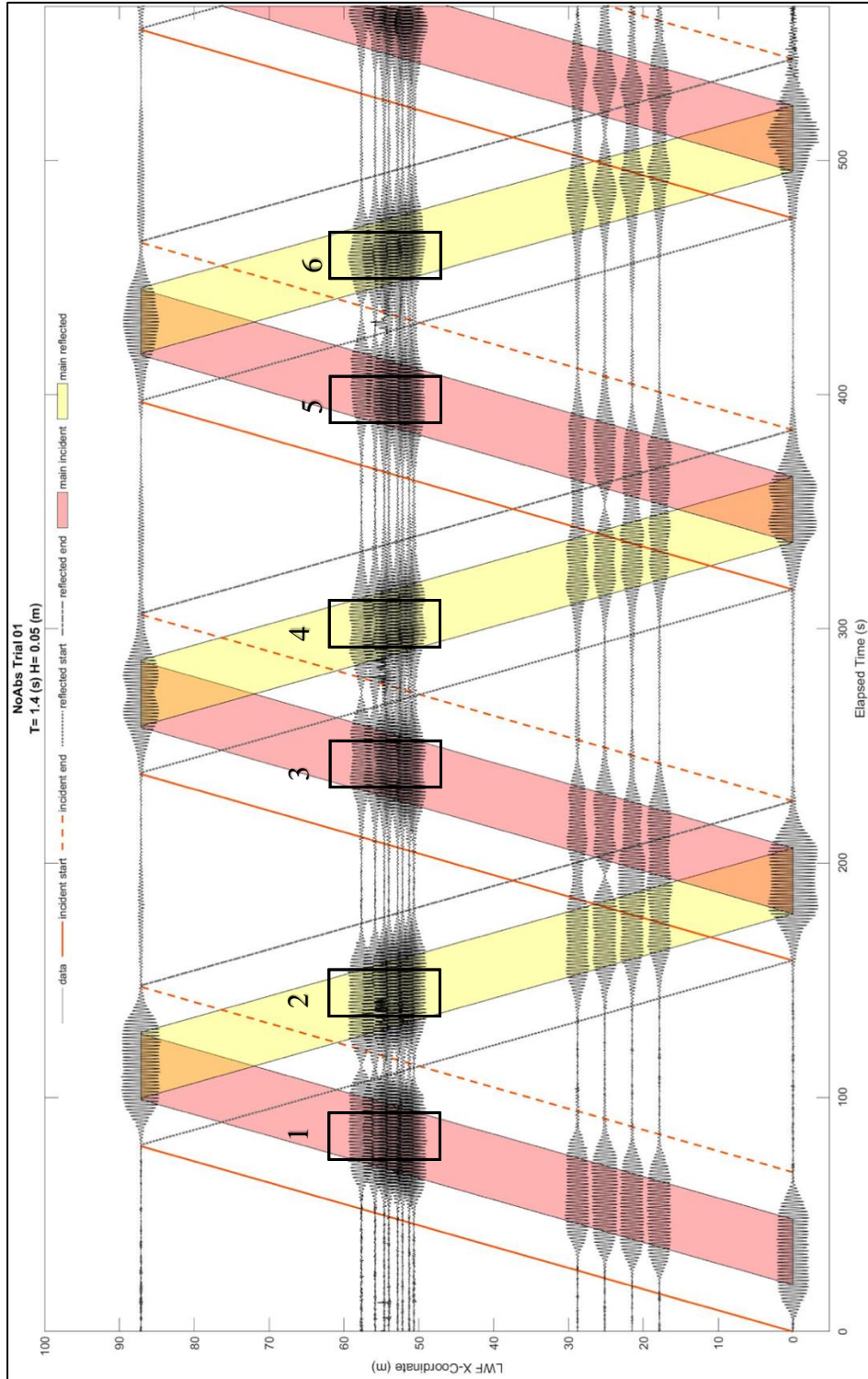


Figure 6.2: Time series showing the incident and reflected wave packets along the flume. The numbered boxes represent sections of pure incident or reflected wave trains.

In the cases of 1.4 s and 1.9 s, the windows used for analysis were extracted from the purely incident and reflected sections identified by the numbered black squares as in figure 6.2. The sections were identified by calculating the group velocity and wave speed using equations 4.82b and 3.35 for from [4] .

$$C_g = \frac{c}{2} \left( 1 + \frac{2kh}{\sinh 2kh} \right) \quad (6.2)$$

$$C = \frac{L}{T} \quad (6.3)$$

The recorded water depth from each trial was used for computing the wave celerity; taking into account a change in water depth occurring at bay 2 due to the thickness of the concrete slabs. The wavelengths were calculated in WaveLab3 using the Stream Function theory.

As the wave period becomes longer, the wave paddle is still generating the 20-wave train when the reflected waves from the vertical wall arrives. This is significant because at a point in time at any location in the flume there may be several wave trains passing through. For trials with a period of 3.0 s or greater, the numbered boxes in 6.2 that represent the purely incident or reflected sections no longer exist.

Therefore, two separate processing methods to obtain the wave height, crest, trough, and reflection coefficients was required.

The regular cases with a period of 1.4 s and 1.9 s were analyzed using zero crossing analysis of the purely incident or reflected sections of the time series. The purely incident or reflected sections were significantly decreased with the 2.4 s period and nonexistent with periods of 3.0 s and greater. Trials without purely incident and reflected wave data ( $T > 2.4$  s) were analyzed with reflection analysis using WaveLab3. The program offers a wide variety of theories for the separation of incident and reflected waves each with specific wave gauge requirements. The trials with a period of 2.4 s or greater were analyzed in WaveLab3 using the irregular (nonlinear) separation of incident and reflected waves by Eldrup and Skjelbreia (2016).

The separation of incident and reflected waves provided two separate time series that were processed using zero crossing analysis in MATLAB. Equations 6.2 and 6.3 were used on the main burst of 20 waves, ramp up and ramp down waves as they propagated from the wavemaker to each instrument, to the wall, and back to each instrument until reaching the wavemaker. The trial shown in figure 6.2 was conducted without absorption thus the waves reflected off of the wavemaker and were recorded while they traveled back and forth.

All MTS trials had a known start of the 20.0 s ramp up due to an internal trigger system (wmstart signal). As soon as the run button was hit, the 20.0 s ramp up began. However, AwaSys did not have a wmstart signal, so the time from running a case to the start of the 20.0 s ramp up varied. In order to properly set the start time of

AwaSys trials, a cross-correlation analysis was used. The cross-correlation analysis was conducted using WaveLab3 by comparing an AwaSys trial with its MTS counterpart.

The zero down crossing analysis was conducted in MATLAB and identified individual waves for each ultrasonic and resistance wave gauge. The characteristics of the waves that were obtained include the number of waves in each analyzed section, wave height, crest, and trough. The wave characteristics were analyzed statistically to evaluate its variability.

Figure 6.3 presents the evolution of the wave height during a full trial of regular waves ( $H=0.05$  m,  $T=1.4$  s) as generated with MTS and AwaSys with no absorption. This is the same case as the one presented in Figure 6.2. Each point represents an individual wave, and each cluster corresponds to the bursts of waves travelling in different directions. The data shown was measured at uswg1, due to its proximity to the mid-point of the flume, decreasing the exposure to disturbances and reflections occurring at either ends of the flume. In other cases, ultrasonic wave gauge 2 was used if uswg 1 had excessive noise.

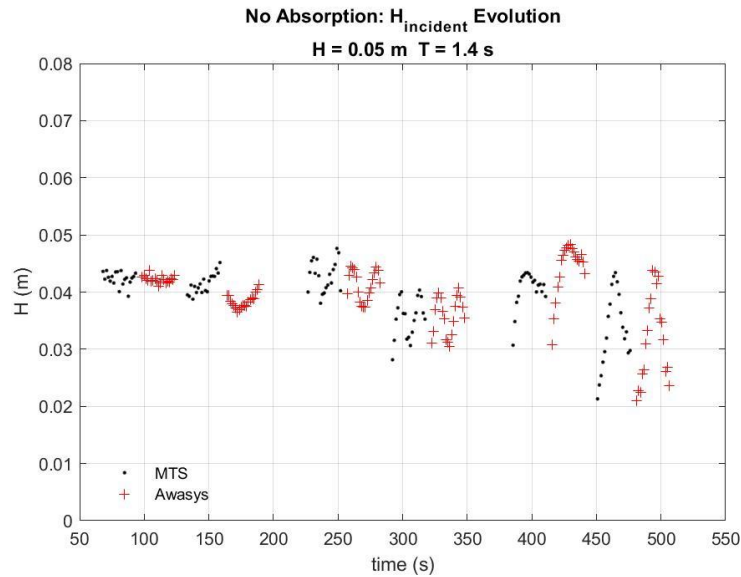


Figure 6.3: Comparison of the evolution of the incident wave height between MTS and AwaSys for the  $T = 1.4 \text{ s}$   $H = 0.05 \text{ m}$  wave condition.

In Figure 6.3, we can observe how the wave height changes as the waves travel back and forth in the flume. Each black dot or red cross represents one wave. We can further assess each wave by looking closer at each wave's crest and trough characteristics as seen in figure 6.4.

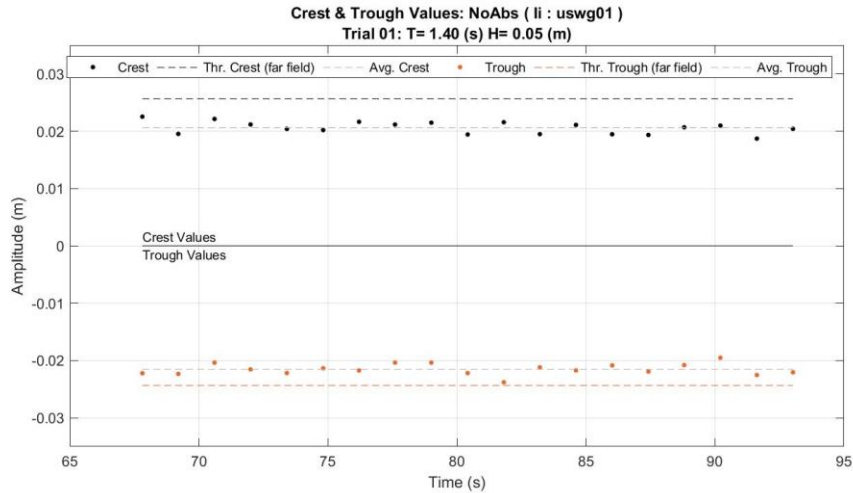


Figure 6.4: Evolution of crests and troughs for uswg1 during the first incident burst of waves for the MTS system without absorption for the  $H = 0.05$  m,  $T = 1.4$  s wave condition.

Figure 6.4 is an in-depth view of first incident wave train propagating past ultrasonic wave gauge 1 by focusing on the individual waves' crests and troughs.

In order to take a broader look at what is happening to the waves in space and time, the wave height, crest, and trough data within each purely incident and reflected section was averaged for each instrument. This produced a single value with a standard deviation for wave height, crest, and trough for each instrument and an example can be seen in figure 6.5. As expected, the wave amplitudes are higher at the wavemaker and the back wall of the flume due to the superposition of the incident and reflected waves.

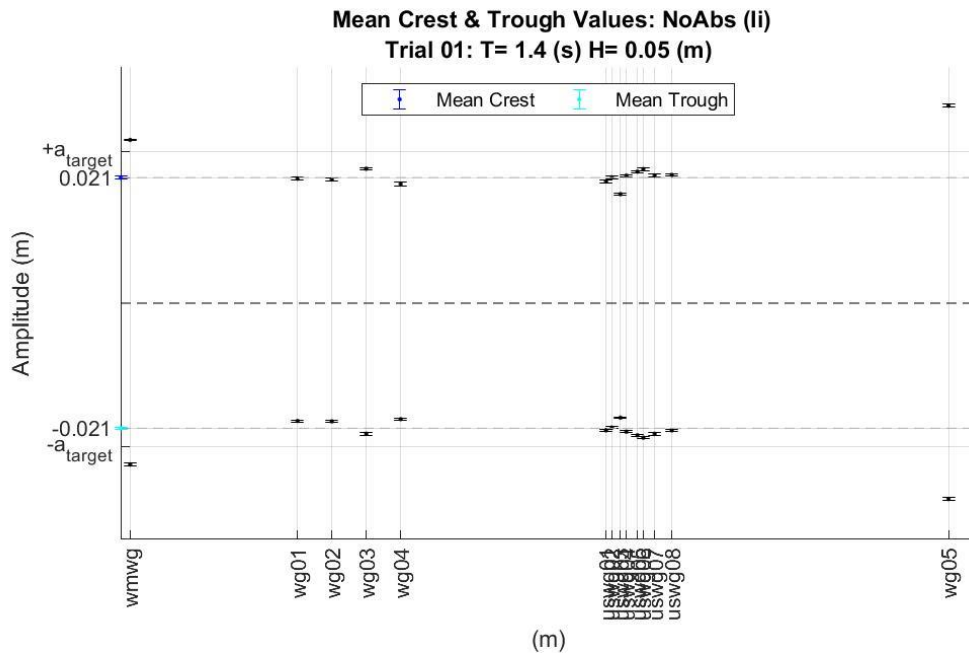


Figure 6.5: Mean crest and trough data for each instrument for an MTS trial without absorption.  $H = 0.05$  m,  $T = 1.4$  s wave condition.

The wave height, crest, and trough for each ultrasonic wave gauge was summed and averaged giving us a single value for the wave height in each purely incident or reflected window for every ultrasonic wave gauge. Figure 6.6 shows how the averaged wave heights evolve for the  $H=0.05$  m,  $T=1.4$  s wave case with and without absorption for both of the systems.

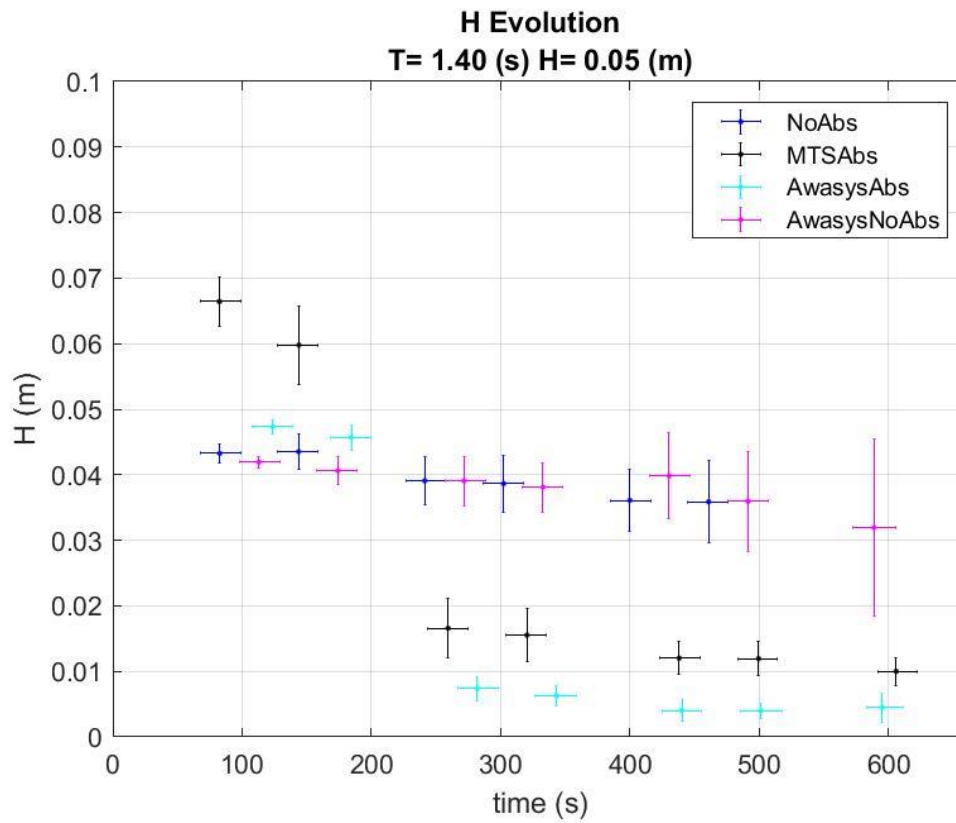


Figure 6.6: Wave height evolution for MTS and AwaSys with and without absorption for the  $H = 0.05$  m,  $T = 1.4$  s wave condition. Cross-hairs shows the variability in wave height and the span of time from which all of the data was extracted.

The final assessment was completed by using the averaged wave heights from the ultrasonic wave gauges to calculate the reflection coefficient. Equation 6.4, used for the calculation of the reflection coefficient, can be found on page 143 in [4] and is consistent to what was used in [13] and [5].

$$K_r = \frac{H_r}{H_i} \quad (6.4)$$

Where  $H_r$  is the height of the waves reflected off of the wavemaker and  $H_i$  represents the height of the waves that are approaching the wavemaker. For this experiment, the wave heights calculated from the zero down crossing analysis for each uswg were averaged to obtain one value for the wave height within each boxed section in figure 6.2. To calculate the reflection coefficient of the wavemaker using equation 6.4, the averaged reflected wave height from window 3 was divided by the averaged incident wave height from window 2.

The final parameter was the calm down time. The calm down time was calculated using zero crossing analysis and assessing the wave heights until a threshold of 0.1 cm was reached. While all of the wave data was saved, the incident and reflected wave heights were used to calculate the reflection coefficients while the incident crest and trough data was used to show the system's consistency throughout a trial. A sample trial with  $H=0.25$  m,  $T=2.4$  s is shown in figure 6.8.

In order to properly assess the active absorption system for cases with simultaneous generation and absorption, the lowest calculated reflection coefficient was used. This is because while simultaneous generation and absorption are occurring, the method of separation assumes that only one wave train is propagating in each direction. An estimation of the system is possible if only the wave trains propagating away from the wavemaker are analyzed. If the wave amplitudes increase, then we can assume that it is due to the waves re-reflecting off of the paddle.

This procedure was executed for each and every trial, yielding the data results of the active absorption performance assessment. The results will be discussed in Section 7.

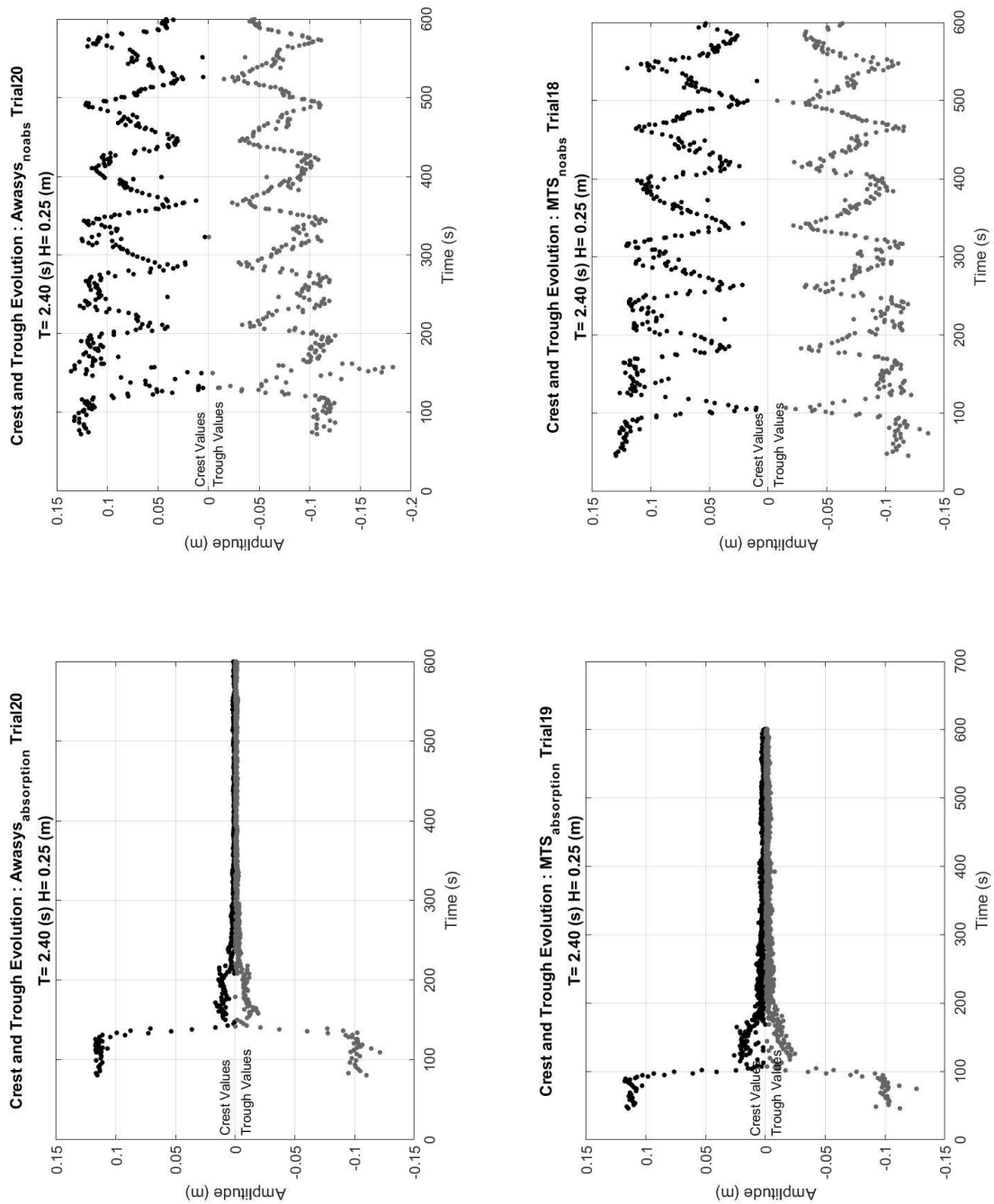


Figure 6.8: The evolution of crests and troughs from each analyzed window plotted together. Obtained by separation of incident and reflected waves with WaveLab3.

### 6.2.2 Irregular Wave Cases

The irregular wave cases consisted of four different wave conditions with the energy content assessed along the time series and how efficiently the waves were absorbed. Each trial was separated into windows and processed in WaveLab3 using the reflection analysis routine. The 1.9 s cases were analyzed using the irregular (with cross mode) method by Zelt and Skjelbreia (1992) while the 5.0 s cases were analyzed using the irregular (nonlinear) method by Eldrup and Skjelbreia (2016). The 1.9 s cases were processed differently due to a cross wave mode discovered by using equation 6.1. Cross-waves were confirmed visually during the experiments for all of the regular and irregular  $T = 1.9$  s cases.

$$\frac{2L}{\sqrt{gh_0}} = \frac{2*3.658 \text{ m}}{\sqrt{9.81 \frac{\text{m}}{\text{s}^2} * 1.85 \text{ m}}} \approx 1.72 \text{ s for the first mode.} \quad (6.5)$$

The trend in energy was obtained by calculating the percent variance over the entire duration of each trial. The performance of the absorption was assessed by windowing the data into significantly smaller sections. This provided a more sensitive variance calculation at the end of generation during which only absorption was occurring. The variance was fit with an exponential function:

$$e^{-\alpha t} \quad (6.6)$$

The alpha coefficient in the exponent was used to develop a relationship with the performance of the active absorption system.

## Chapter 7: Results

### *7.1 Regular Wave Cases*

The most direct way to assess the performance of the active absorption system is by calculating the reflection coefficients from the average incident and reflected waves. A reflection coefficient of 1.0 means that 100% of the waves approaching the wavemaker were reflected. In other words, there is full reflection occurring and zero absorption. We expect to have a reflection coefficient around 100% for all of the trials conducted without active absorption and during simultaneous generation and absorption. A reflection coefficient greater than one means that an increase in energy is occurring in the flume. A reflection coefficient less than one means that absorption or a decrease in energy is occurring. When using active absorption, the goal is to achieve the smallest reflection coefficient proving that the system is absorbing the majority of the waves. Alternatively, this can be expressed with the absorption coefficient that is calculated from the reflection coefficient. Our goal is to obtain an absorption coefficient of one, signifying that 100% of the energy has been absorbed. As given in [4], the absorption coefficient is defined as:

$$K_a = 1 - K_r \tag{7.1}$$

Table 7.1 summarizes the absorption coefficient for the MTS and AwaSys systems for each wave height and frequency while figure 7.1 summarize the reflection coefficients with the theoretical prediction as provided by Lykke, 2016.

Table 7.1: Absorption coefficients for MTS (M) and AwaSys (A).

K <sub>a</sub>												
1/T	0.71 Hz		0.53 Hz		0.42 Hz		0.33 Hz		0.2 Hz		0.1 Hz	
T	1.4s		1.9s		2.4s		3.0s		5.0s		10.0s	
H(m)	M	A	M	A	M	A	M	A	M	A	M	A
<b>0.05</b>	0.72	0.84	0.81	0.86			0.69	0.70	0.60	0.62	0.45	0.35
<b>0.1</b>			0.88	0.93			0.73	0.76	0.77	0.77		
<b>0.16</b>			0.90	0.94								
<b>0.25</b>					0.82	0.88	0.73	0.77	0.78	0.86	0.54	0.39
<b>0.35</b>							0.65	0.67				
<b>0.5</b>									0.61	0.74	0.42	0.35

The performance of the active absorption systems in Table 7.1 and figure 7.1 shows a trend with AwaSys outperforming MTS for every frequency and wave height tested except at T=10.0 s (0.1 Hz). The reason for this behavior is unknown, but more work can be done on setting up the filter within the AwaSys system. The filter was set for a frequency range from 0.1 to 1 Hz. During set up, the frequency range for the filter was successful, in theory. However, it is possible that the filter would need to be adjusted for longer waves.

Examining each wave height, the data shows that the biggest performance difference for a wave height of 0.05 m occurs at a period of 1.4 s (0.71 Hz) with AwaSys absorbing 12% more wave height than MTS. For the trials with a period of 1.9 s, 3.0 s, and 5.0 s the performance is nearly identical while MTS outperforms AwaSys by absorbing 10% more of the wave height for the 10.0 s trial.

MTS and AwaSys both seem to perform quite similarly at all frequencies tested for a wave height of 0.1 m, with AwaSys outperforming MTS by only 5% at a frequency of 0.53 Hz. The wave height of 0.16m was tested only at a period of 1.9 s (0.53Hz) with AwaSys absorbing 4% more.

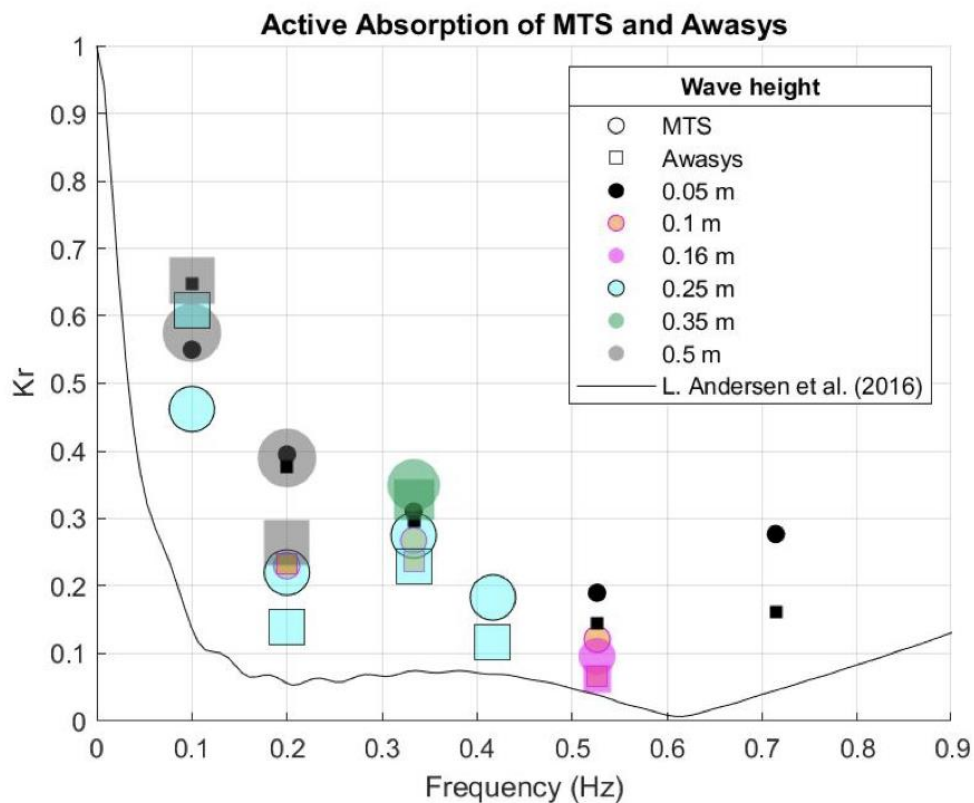


Figure 7.1: Active absorption performance in terms of reflection coefficient  $K_r$  with the AwaSys theoretical prediction for active absorption trials.

The trials with a wave height of 0.25 m were tested with four different frequencies.

AwaSys outperformed MTS for 2.4 s, 3.0 s, and 5.0 s by 6%, 4%, and 8%,

respectively. Only one case was tested for a wave height of 0.35 m at a period of 3.0 s

(0.33Hz) with AwaSys outperforming MTS by 2%. Due to restrictions in wave

steepness, only two frequencies were used to analyze the 0.5 m wave height

condition. At 5.0 s (0.2 Hz) AwaSys outperformed MTS by 10% and MTS outperformed AwaSys by 7% at a period of 10.0 s (0.1 Hz).

For all tested frequencies there is a trend that shows that AwaSys outperforms MTS with the greatest difference at 1.4 s with a wave height of 0.05 m. In order to obtain the reflection and absorption coefficients a series of assumptions and averaging was conducted. Therefore, the uncertainty of the reflection and absorption coefficients might be large. Hence, it is considered that the difference in absorption performance between MTS and AwaSys can be considered small, showing that even though MTS oversimplifies the analysis by not considering the evanescent modes and applying the same frequency to compute the Biésel Transfer Function, MTS is able to absorb surprisingly well, almost as good as AwaSys.

A second parameter used to assess the performance of the active absorption performance was to evaluate its ability to remove the generated waves from the flume to allow for a quicker turnover between each trial. Figure 7.2 is a plot of the time needed from the end of the wave generation to bring the wave height to 0.1 cm or lower for each wave condition.

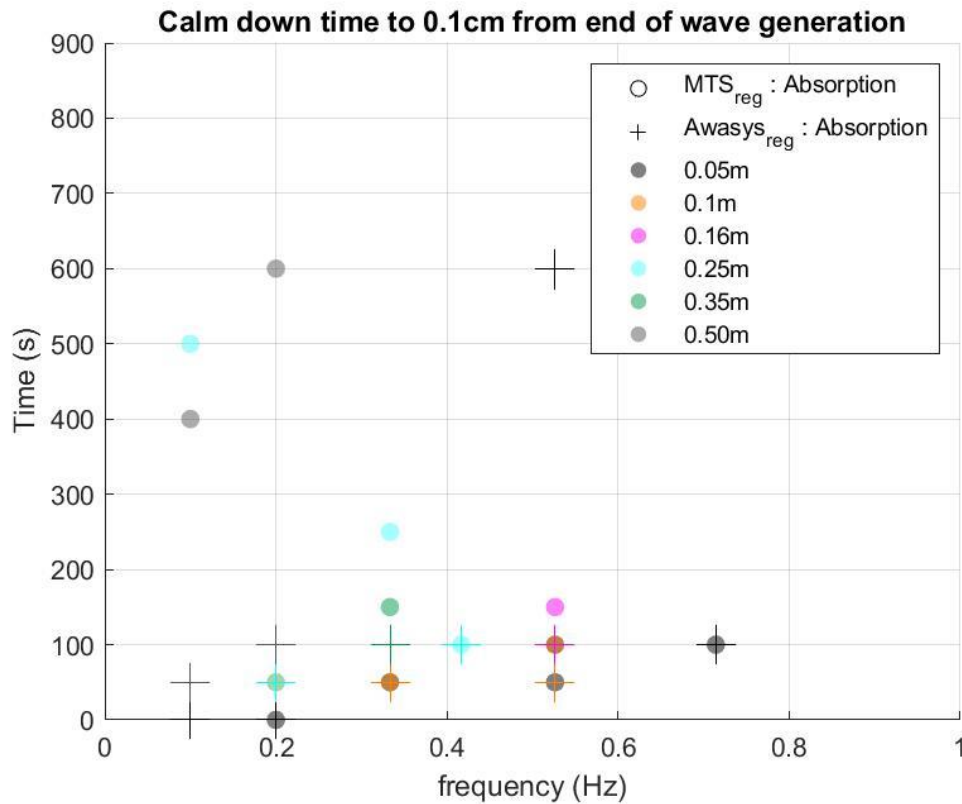


Figure 7.2: Calm down time for regular cases without a beach.

For 0.71 Hz and 0.4 Hz both of the systems required 100 s to bring the flume to a still water condition. Tests conducted with a 0.55 Hz frequency show an increase of 50 s in calm down time from the smallest to the largest wave height for the MTS system. The AwaSys system requires on average, 50-100 s less than MTS. Wave heights of 0.1 m and 0.05 m at 0.33 Hz required 50 s for both systems. 0.25 m and 0.35 m cases tested at 0.33 Hz required 100 s for AwaSys and 250 s and 150 s for MTS.

Wave heights with a frequency of 0.2 Hz had a varied performance. Both systems did not require any time for the 0.05 m cases, and both needed 50 s for 0.1 m and 0.25 m.

MTS needed 600 s while AwaSys needed 100 s for the 0.5 m case. Table 7.2 presents calm down times in non-plot form.

Table 7.2: Calm down time summarized in table form.

	f=0.1Hz T=10.0s		f=0.2Hz T=5.0s		f=0.33Hz T=3.0s	
H (m)	MTS (s)	AwaSys (s)	MTS (s)	AwaSys (s)	MTS (s)	AwaSys (s)
0.05	20	5	5	5	50	50
0.1			50	50	50	50
0.16						
0.25	500	50	50	50	250	100
0.35					150	100
0.5	400	-	600	100		
	f=0.4Hz T=2.4s		f=.55Hz T=1.9s		f=.78Hz T=1.4s	
H (m)	MTS (s)	AwaSys (s)	MTS (s)	AwaSys (s)	MTS (s)	AwaSys (s)
0.05			50	50	100	100
0.1			100	50		
0.16			150	100		
0.25	100	100				
0.35						
0.5						

The 0.1 Hz, 0.05 m case required less than 5 seconds to reach a calm state for both systems. The 0.25 m case required 500 s during the MTS test and only 50 s for Awasys. The largest wave at 0.5 m and 0.1 Hz required 400 s for MTS while threshold was not reached for the AwaSys system. This was due to a long wave being generated while the AwaSys active absorption was turned on. In general, AwaSys requires a shorter period of calm-down time in between testing.

Finally, all wave heights, crests, and troughs were evaluated for the non-beach regular cases. As mentioned in chapter 6, the wave heights were evaluated for all of the 1.4 s and 1.9 s cases to see how consistent the incident packets would remain after traveling back and forth in the flume.

Figure 7.3 shows the incident and reflected wave heights as they evolved for all of the 1.4 s and 1.9 s trials. We can see a pattern between the absorption and no absorption trials that the waves become increasingly dispersed with each pass in the flume without absorption. MTS significantly increases the wave height of the initial generated packet of waves while AwaSys maintains a uniform packet of waves for the 1.4 s 0.05 m trial with absorption. As the waves are absorbed by both systems, we see that the re-reflected waves by AwaSys system remain more uniform than those re-reflected during the trial with the MTS system.

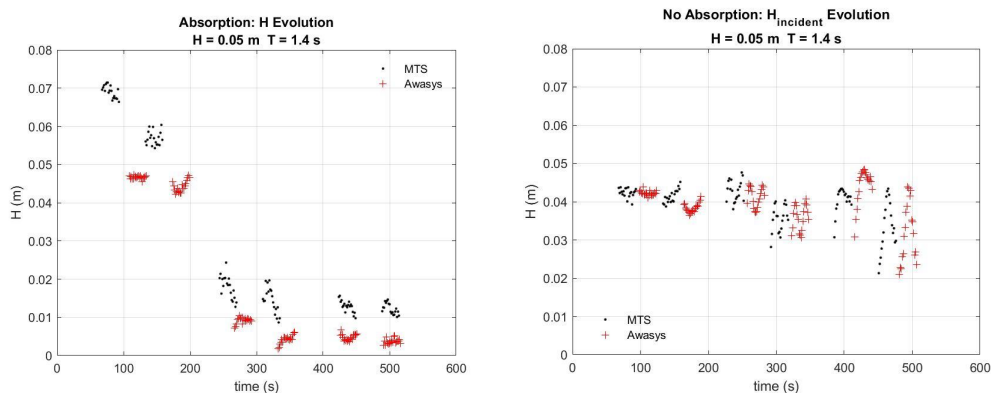


Figure 7.3: Comparison of the wave height evolution during absorption and no absorption trials with both systems.

For the 1.9 s, 0.05 m case, it is apparent in figure 7.4 that MTS performs better at generating wave heights closer to the desired value. Both systems seem to perform nearly identically for trials with and without absorption. All of the no absorption trials shown in figure 7.4 have the same characteristics of waves becoming increasingly non-uniform as they reflect off a highly reflective surface such as the wavemaker or wall. It does seem that for the active absorption trials (left column in Figure 7.4) that the uniformity of the re-reflected waves increases for both systems. Perhaps, due to the wavemaker having an easier time adjusting its stroke for larger wave heights.

The plots shown in figures 7.3 and 7.4 can be additionally found in appendix C.

As mentioned in the previous chapter, all of the wave height data for the 1.4 s and 1.9 s cases was compiled for the eight ultrasonic wave gauges and averaged together to see how the variability of our waves changed. All of the plots can be located in appendix F.

In addition to wave heights, crests and troughs were evaluated to assess wave shape consistency. Wave shape can be analyzed by comparing the crest and trough values for each wave height. A linear sinusoidal wave's crest would be equal to and opposite in sign to the trough. However, as waves become nonlinear, their crests and troughs are no longer mirror images of each other, thus evolving from a sinusoidal shape to a so-called trochoidal shape.

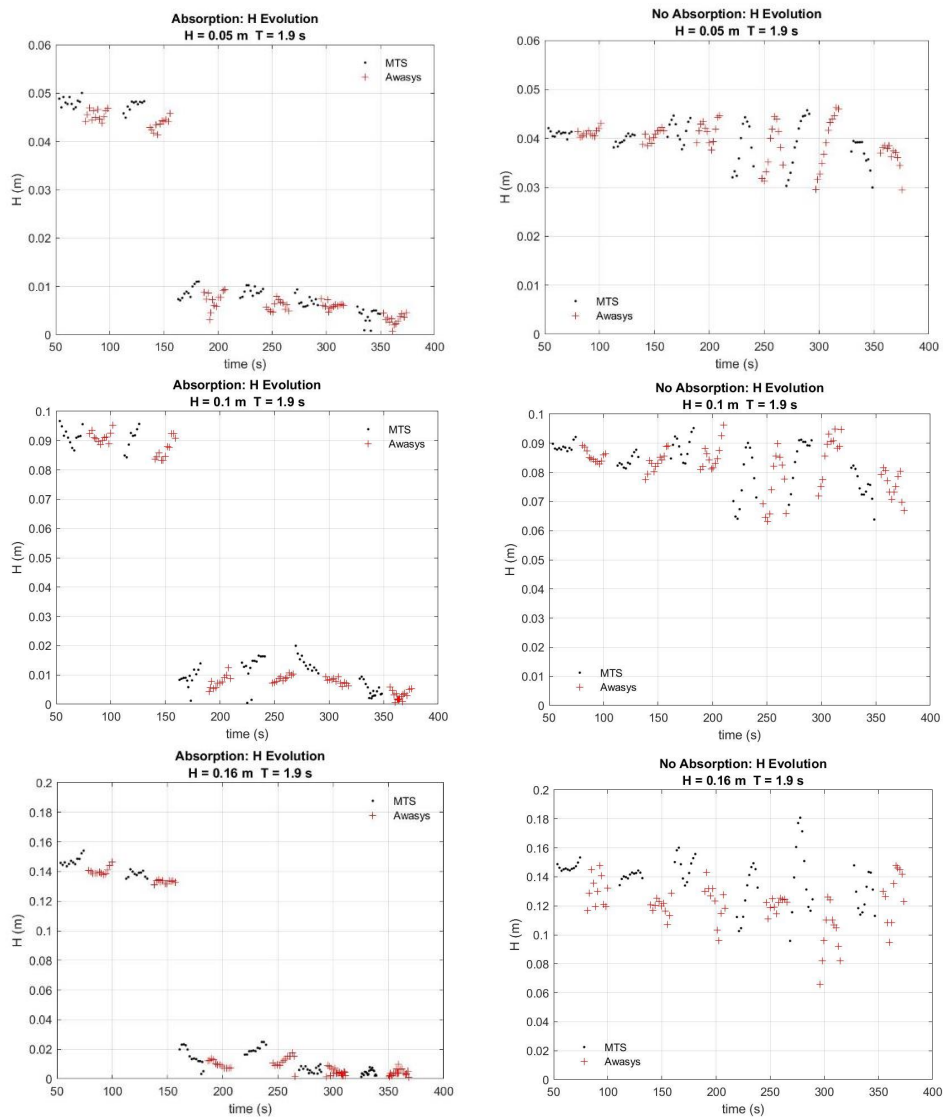


Figure 7.4: Plots of all of the 1.9 s regular wave trials with and without absorption for both of the analyzed systems.

As the waves traveled across the flume, it was expected that they would hit the back wall, reflect, and travel back to the wavemaker. Once at the wavemaker, they are supposed to be absorbed. If simultaneous generation and absorption is occurring, the

system should generate our desired sea state without altering the generated waves while absorption is active. Therefore, the focus of shape of the waves was on the incident wave packets, or the wave trains that were traveling from the wavemaker and not the waves coming from the wall.

If we imagine that we take the initial packet of black dots or red crosses from figures 7.3 and 7.4 and look at them in terms of the crests and troughs, we obtain figure 6.4 for every 1.4 s and 1.9 s trial. All of these figures are located in appendix I. The crest and trough were evaluated in space and in time in the entire flume as seen in figure 6.5 and can be found in appendix J.

The remainder of the trials with periods of 2.4 s and greater could not be analyzed in the same manner, but by doing zero down crossing analysis on their incident time series, crest and trough data was compiled.

Table 7.3 summarizes the calculated crests, troughs, and standard deviations along with the theoretical crest and trough values for trials with active absorption while the no active absorption trials are presented in Table 7.4 for comparison purposes. These tables represent every wave condition including the 1.4 s and 1.9 s tests.

Table 7.3: Crest and trough data for all regular trials with active absorption in conjunction with the theoretical crest and trough values.

THEORETICAL		ABSORPTION									
Crest	Trough	MTS				AwaSys					
(m)	(m)	T	H	Crest	std	Trough	std	Crest	std	Trough	std
(m)	(m)	(S)	(m)	(m)	(m)	(m)	(m)	(m)	(m)	(m)	(m)
0.026	-0.024	1.4	0.05	0.034	0.001	-0.034	0.001	0.023	0.000	-0.023	0.001
0.025	-0.025	1.9	0.05	0.003	0.005	-0.003	0.005	0.003	0.005	-0.003	0.005
0.052	-0.049	1.9	0.10	0.007	0.012	-0.007	0.012	0.005	0.011	-0.005	0.010
0.084	-0.076	1.9	0.16	0.008	0.017	-0.008	0.016	0.007	0.016	-0.007	0.015
0.134	-0.116	2.4	0.25	0.099	0.030	-0.091	0.024	0.106	0.025	-0.095	0.021
0.025	-0.025	3.0	0.05	0.021	0.005	-0.021	0.004	0.020	0.005	-0.021	0.005
0.052	-0.048	3.0	0.10	0.041	0.011	-0.041	0.008	0.041	0.010	-0.041	0.010
0.135	-0.115	3.0	0.25	0.115	0.021	-0.100	0.010	0.113	0.027	-0.097	0.022
0.195	-0.156	3.0	0.35	0.149	0.025	-0.123	0.012	0.155	0.038	-0.128	0.029
0.026	-0.024	5.0	0.05	0.023	0.007	-0.022	0.005	0.023	0.005	-0.021	0.005
0.053	-0.047	5.0	0.10	0.049	0.011	-0.043	0.002	0.048	0.011	-0.040	0.009
0.145	-0.105	5.0	0.25	0.143	0.032	-0.092	0.004	0.132	0.031	-0.089	0.021
0.325	-0.175	5.0	0.50	0.294	0.068	-0.162	0.012	0.290	0.067	-0.154	0.037
0.028	-0.022	10.0	0.05	0.023	0.006	-0.019	0.004	0.024	0.006	-0.018	0.005
0.180	-0.070	10.0	0.25	0.132	0.006	-0.058	0.003	0.150	0.036	-0.058	0.014
0.401	-0.099	10.0	0.50	0.323	0.014	-0.105	0.007	0.362	0.088	-0.098	0.025

Table 7.4: Crest and trough data for all regular trials without active absorption.

THEORETICAL		NO ABSORPTION									
Crest	Trough	MTS				AwaSys					
(m)	(m)	T	H	Crest	std	Trough	std	Crest	std	Trough	std
(m)	(m)	(S)	(m)	(m)	(m)	(m)	(m)	(m)	(m)	(m)	(m)
0.026	-0.024	1.4	0.05	0.021	0.001	-0.022	0.001	0.021	0.000	-0.021	0.000
0.025	-0.025	1.9	0.05	0.020	0.003	-0.020	0.002	0.019	0.005	-0.019	0.004
0.052	-0.049	1.9	0.10	0.042	0.006	-0.042	0.005	0.038	0.010	-0.038	0.009
0.084	-0.076	1.9	0.16	0.069	0.009	-0.067	0.008	0.065	0.005	-0.067	0.009
0.134	-0.116	2.4	0.25	0.108	0.034	-0.099	0.026	0.104	0.039	-0.100	0.030
0.025	-0.025	3.0	0.05	0.026	0.007	-0.026	0.006	0.027	0.007	-0.026	0.006
0.052	-0.048	3.0	0.10	0.055	0.014	-0.052	0.013	0.055	0.015	-0.053	0.013
0.135	-0.115	3.0	0.25	0.145	0.043	-0.121	0.025	0.148	0.043	-0.121	0.023
0.195	-0.156	3.0	0.35	0.228	0.086	-0.171	0.036	0.225	0.078	-0.171	0.039
0.026	-0.024	5.0	0.05	0.016	0.007	-0.016	0.007	0.017	0.007	-0.017	0.006
0.053	-0.047	5.0	0.10	0.036	0.012	-0.035	0.009	0.036	0.012	-0.035	0.009
0.145	-0.105	5.0	0.25	0.089	0.039	-0.076	0.017	0.088	0.040	-0.075	0.017
0.325	-0.175	5.0	0.50	0.177	0.112	-0.117	0.043	0.183	0.116	-0.120	0.051
0.028	-0.022	10.0	0.05	0.055	0.013	-0.041	0.009	0.057	0.014	-0.042	0.009
0.180	-0.070	10.0	0.25	0.283	0.208	-0.130	0.067	0.323	0.202	-0.143	0.056
0.401	-0.099	10.0	0.50	0.245	0.252	-0.172	0.112	0.222	0.235	-0.159	0.105

MTS and AwaSys both had similar crest and trough values for all regular cases with active absorption activated. AwaSys generated crests that were closer to the theoretical value for 10.0 s period and 0.25 m and 0.50 m wave height conditions. While the troughs were similar for both systems signifying that AwaSys does a better job generating longer waves. This is interesting given the results in figure 7.1 for the 10.0 s cases with AwaSys performing worse than MTS during absorption.

As expected, all regular trials without absorption had similar performances for both systems. This confirms that both systems are generating waves in a similar fashion while active absorption is deactivated. The absolute difference from the theoretical and calculated crest and trough values was computed and compared side by side for each system with and without absorption. The result was nearly identical for both of the systems.

The regular wave conditions that generated crests and troughs closest to the theoretical crest and trough with active absorption were all of the wave heights with a period of 5.0 s and 10.0 s for both MTS and AwaSys. According to Table 7.3, AwaSys generated a wave height of 0.05 m with a period of 1.4 s closer to the theoretical values with active absorption activated while MTS did not. This verifies the result at this frequency in Figure 7.1. Wave conditions with periods of 1.9 s, 2.4 s, and 3.0 s were closer to the theoretical crest and trough values when the active absorption system was deactivated for both systems. As a complement to Tables 7.3 and 7.4, appendix E contains the crests and trough as plots.

### 7.1.1 Experiments with a Passive Absorber

Preliminary results for the two wave conditions tested with a 1:12 slope beach will be briefly discussed. The regular beach wave cases could not be processed using separation of incident and reflected waves due to the removal of the ultrasonic wave gauges for the beach installation. The data was collected using four resistance wave gauges located closest to the wavemaker with the fifth resistance wave gauge also removed prior to testing.

The first wave condition discussed is the trial with a period of 10.0 s and a wave height of 0.5 m. Based on initial analysis it is evident that the crest exceeded that of the theoretical value for the cases tested with and without active absorption by the both systems. A difference between the uniformity of the crests and troughs cannot easily be spotted between the cases with and without active absorption with one exception. There are several higher crests at the beginning of the trial without active absorption after which the crests level out and become uniform as seen in figures 7.5a and 7.5b.

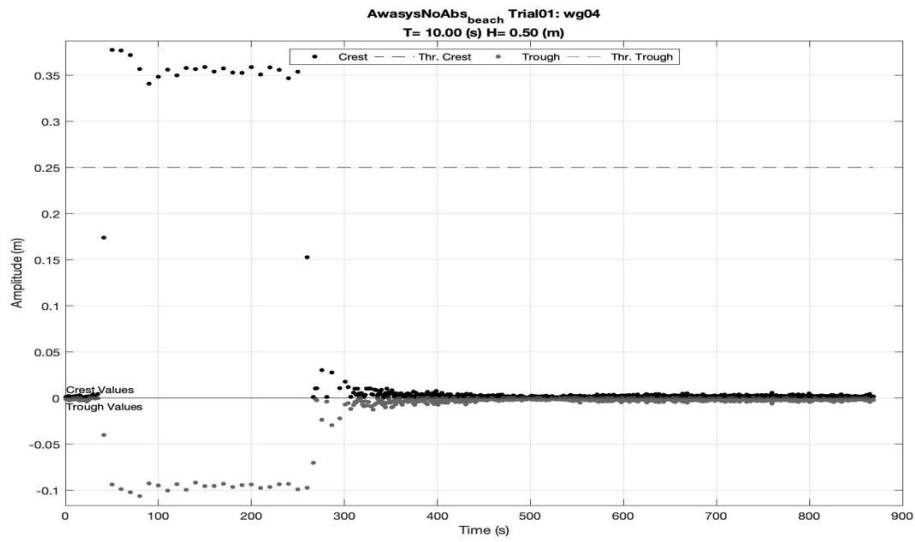


Figure 7.5a: Trend in crest and trough values without absorption tested with the AwaSys system.

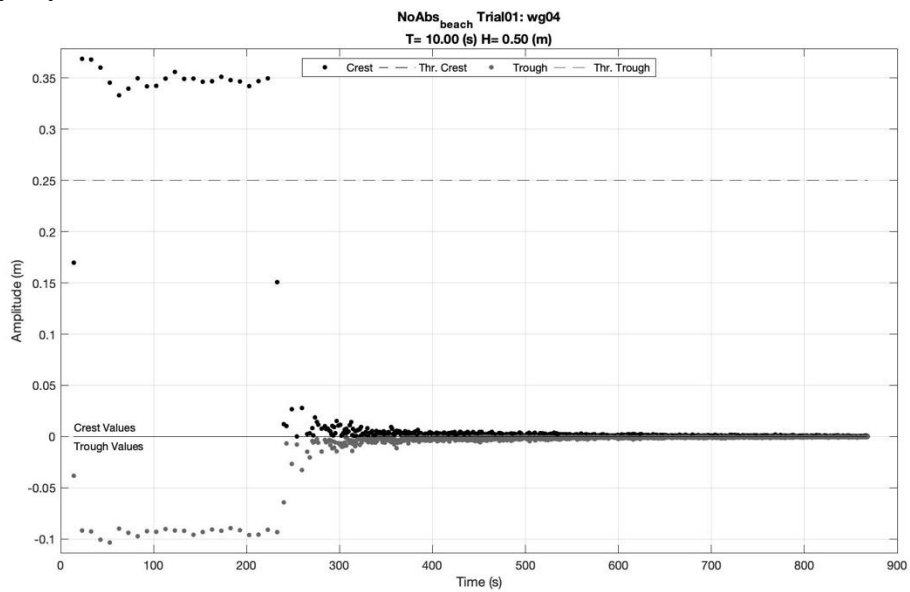


Figure 7.5b: Trend in crest and trough values without absorption tested with the MTS system.

Although it is difficult to make a concrete statement it appears that both systems exhibit greater uniformity in the troughs with active absorption as observed in figures 7.6a and 7.6b.

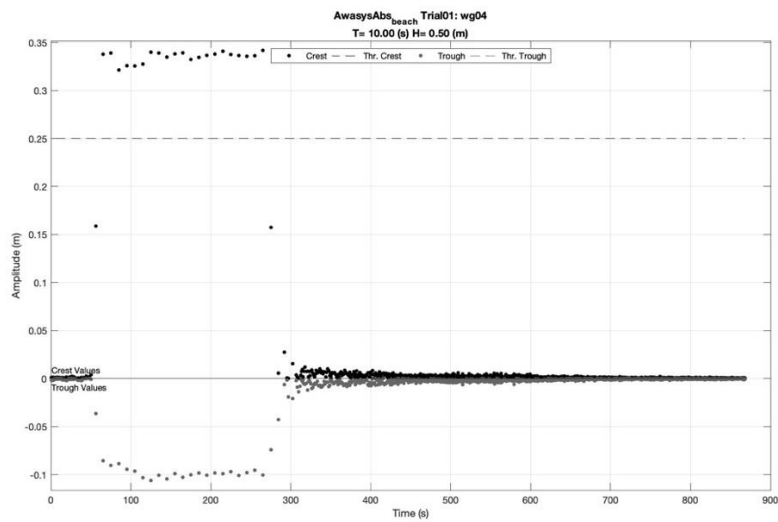


Figure 7.6a: AwaSys'  $T=10.0$  s,  $H = 0.5$  m trial with active absorption.

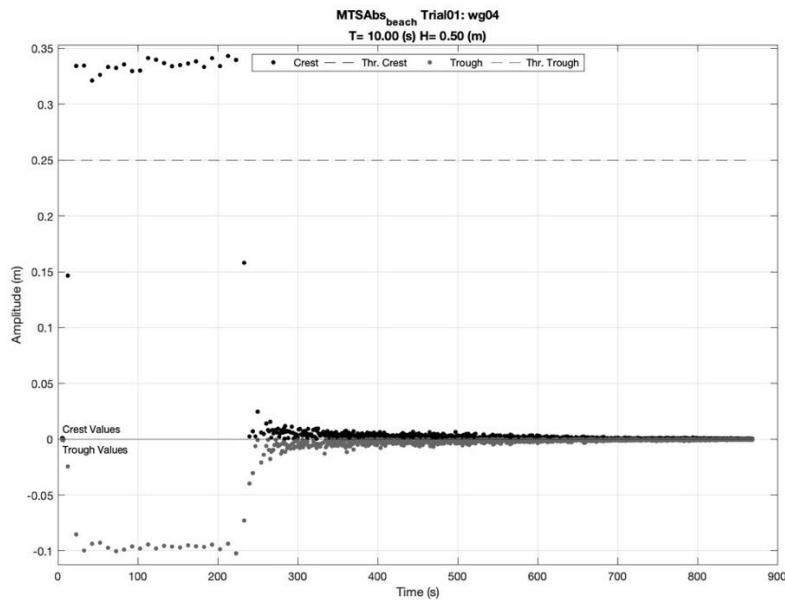


Figure 7.6b: MTS' regular beach trial with  $T=10.0$  s,  $H=0.5$  m with active absorption.

Both systems tested at this wave condition with and without active absorption were successful in eliminating the waves from the flume at the conclusion of the trial.

The second wave condition tested with the beach installed was the 3.0 s period with a 0.35 m wave height. This trial was the only regular wave trial of the entire experiment that was generated for a total of 10 minutes. During testing of the AwaSys system, the crests and troughs appear nearly identical with and without active absorption with the crests hitting the theoretical value with active absorption as shown in figures 7.7a and 7.7b.

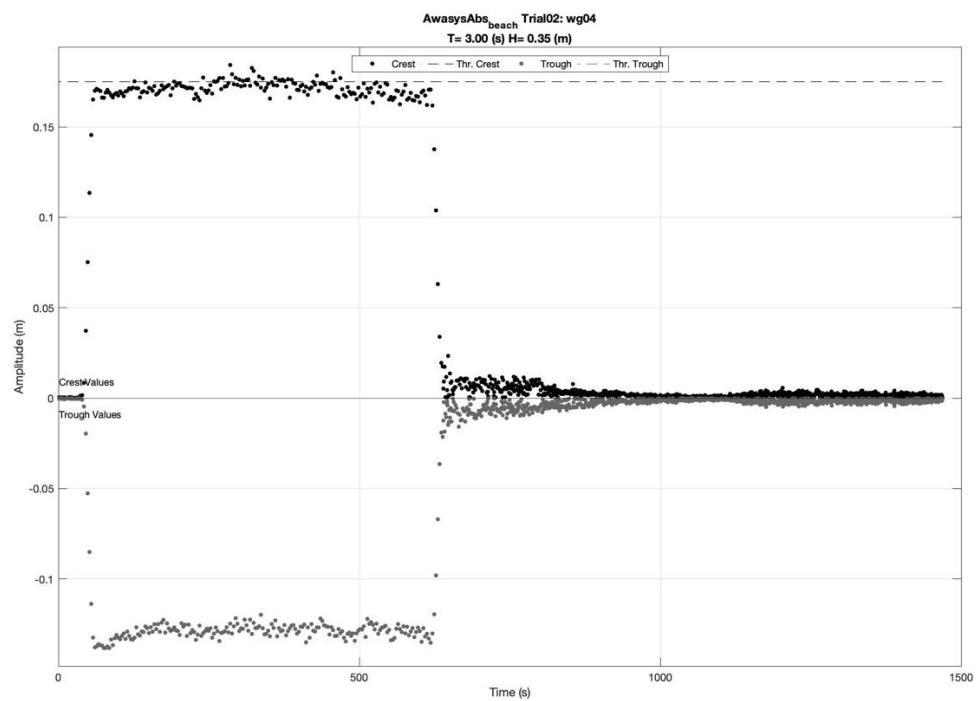


Figure 7.7a: AwaSys' T=3.0 s, H=0.35 m trial showing a relatively uniform run with absorption activated.

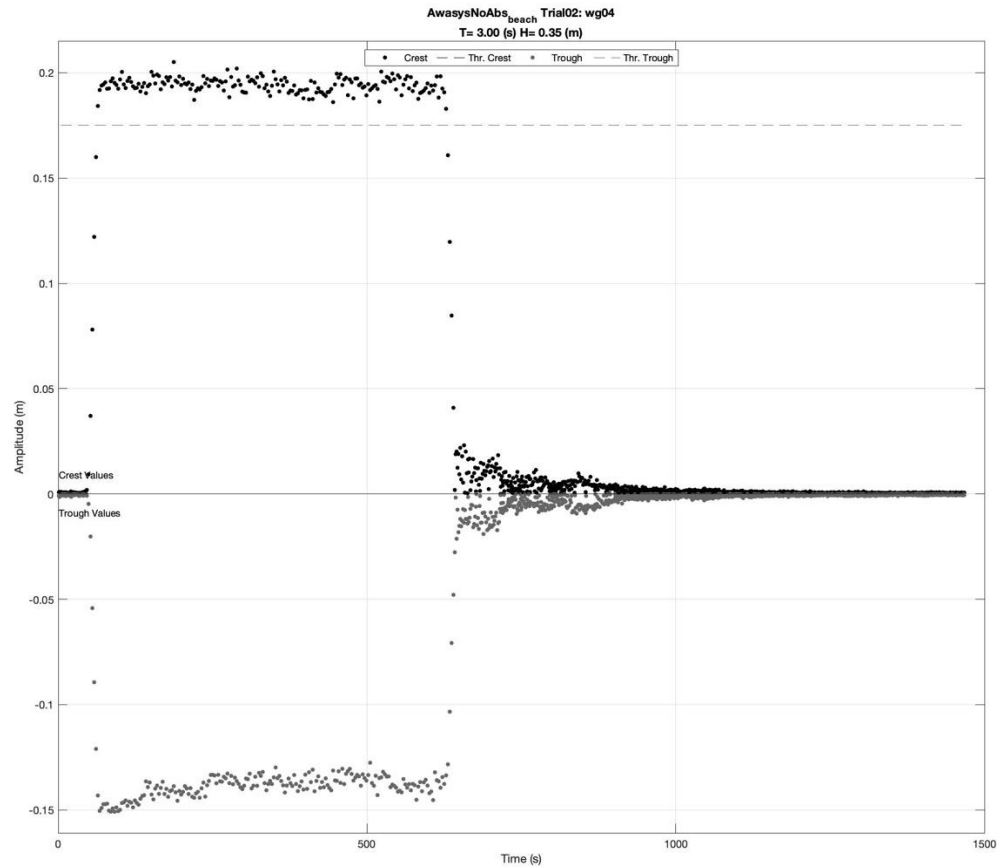


Figure 7.7b: AwaSys'  $T=3.0$  s,  $H=0.35$  m trial without absorption.

The flume quieted down immediately with and without absorption but had slightly better results with active absorption.

The 3.0 s wave case tested using the MTS system did have different results between the trials with and without active absorption. The active absorption trial generated non uniform crests and troughs with the flume quieting down relatively quickly as with the previous case (figure 7.8a).

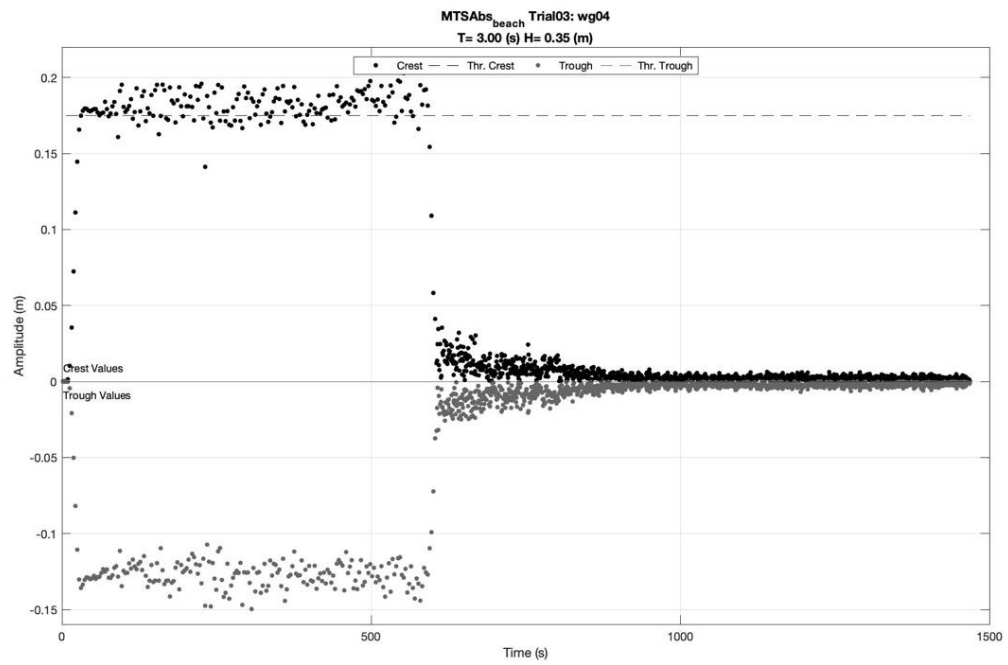


Figure 7.8a: MTS'  $T=3.0$  s,  $H=0.35$  m case with active absorption.

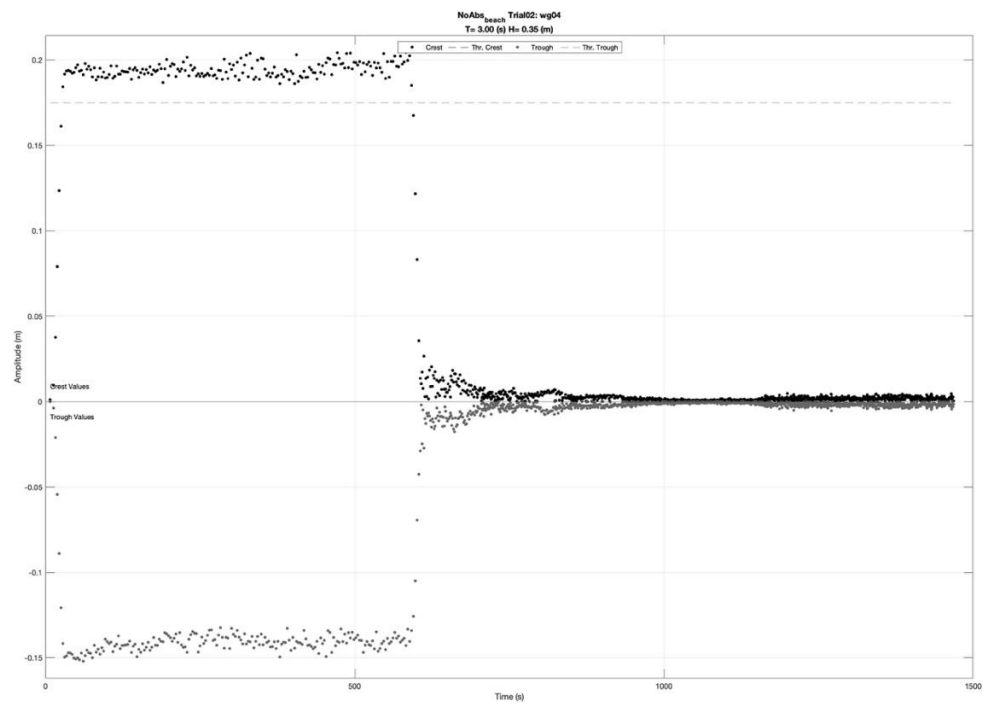


Figure 7.8b: MTS'  $T=3.0$  s,  $H=0.35$  m trial without absorption.

The wave condition was more successful when generated without the MTS active absorption system (Figure 7.8b). The crests and troughs were more uniform for the duration of the trial and the flume calmed down more efficiently as well. In addition, Figures 7.5a-7.5b are located in appendix D.

### *7.2 Irregular Wave Experiments*

Four irregular wave conditions at two different frequencies in the intermediate water regime were examined. No passive absorber (beach) was installed, so waves fully reflected from the vertical wall at the end of the flume. Percent variance was computed for the duration of the trial considering the full elapsed time series to examine the energy state while the percent variance calculated using smaller windows was used to calculate the performance of the active absorption system at the end of generation. The variance is, by definition, a form to compute the significant wave height of the time series. Hence, the computation of the variance will be an indication of the energy content in the flume.

By studying the change in variance, we see how energy changes over time for the test. As shown in Figure 7.9, the trials tested using both systems at  $T_p = 1.9$  s,  $H_s = 0.1$  m and  $H_s = 0.25$  m without active absorption showed variance increasing until a plateau was reached near the end of generation with cross waves and breaking waves occurring for the 0.25 m wave height. This trend shows that there is an increase of energy in the flume that is occurring during generation. In other words, for the full

reflective case, there is an energy build-up in the flume that reached 1.5 to 3 times the corresponding energy level in case of no reflection.

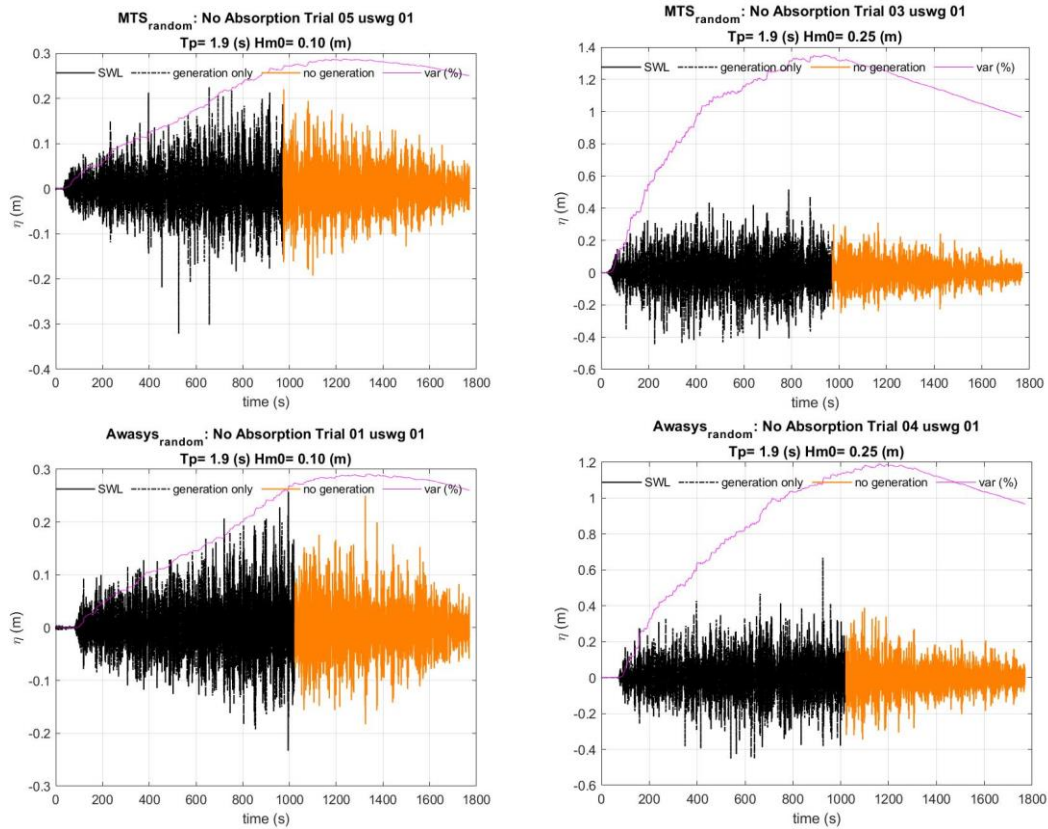


Figure 7.9: Variance for all  $T_p = 1.9$  s trials conducted without absorption for MTS and AwaSys.

While trials with a peak period of 5.0 s without active absorption showed increasing variance until a plateau was reached approximately two thirds of the way into generation, and a decrease at the culmination of generation as seen in figure 7.10. For both systems and periods, the larger wave height measured a greater variance.

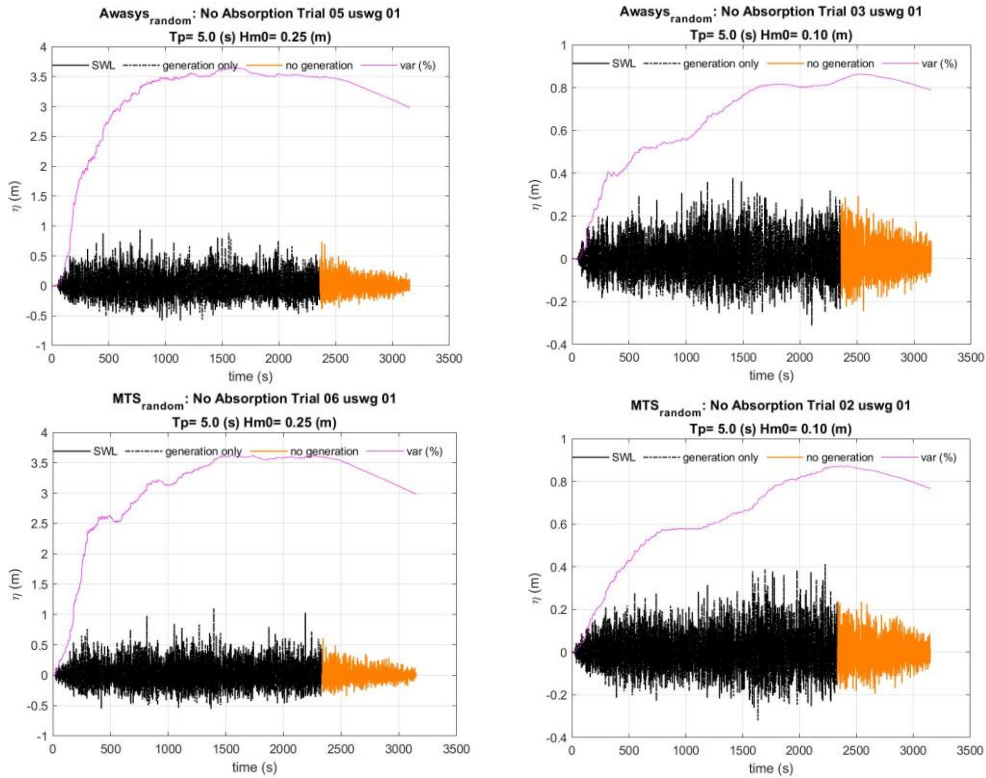


Figure 7.10: Variance for all  $T_p = 5.0$  s trials conducted without absorption for MTS and AwaSys.

The 1.9 s peak period and 0.1 m wave height case tested with absorption was successful using the AwaSys system while the MTS trial experienced an increase in variance followed by an instability at approximately 1500 s (Figure 7.11).

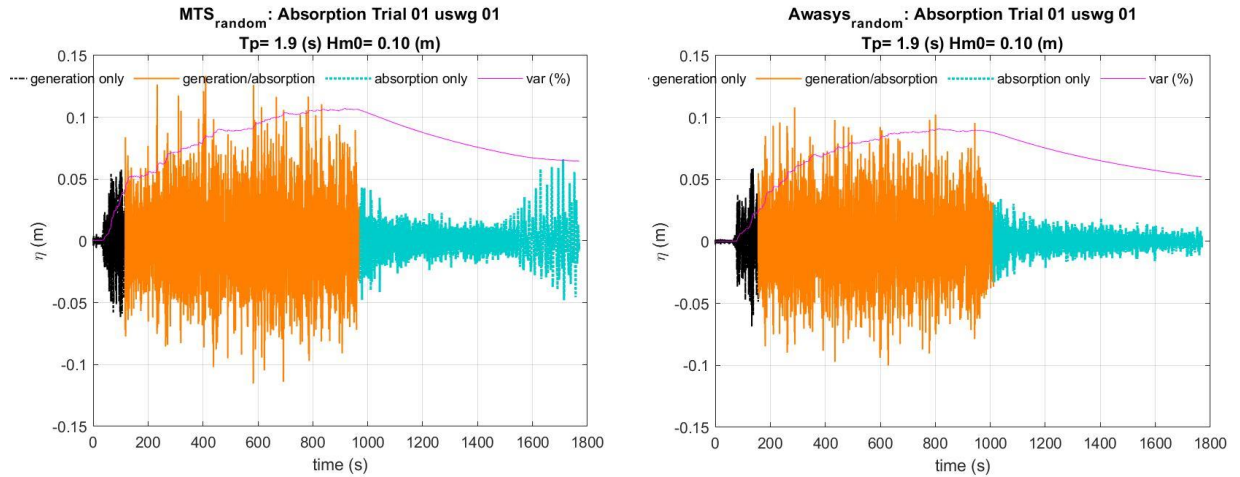


Figure 7.11: Comparison of AwaSys and MTS with absorption.  $T_p=1.9$  s trials with  $H_s=0.1$  m.

AwaSys' variance became stable prior to the end of generation without any instabilities present. Nevertheless, it would be advisable to turn the active absorption system off in order to avoid generating instabilities caused by highly reflective surfaces, such as a vertical structure. This could be due to the running filter calculating at exactly half of the period of the seiche generating an instability in the flume.

The 1.9 s and 0.25 m case tested with absorption was not completed using the MTS system with the wave height control manually deactivated 6.5 minutes ahead of schedule to prevent the wavemaker from hitting its limits. The plot shows that variance continued to increase during the trial with an instability forming quickly after the culmination of simultaneous generation and absorption. The AwaSys system' variance reaches a plateau with an instability forming during the absorption

only phase at around 1550 s (Figure 7.12). Cross waves were excited at the board and the system clipped 3% of the samples.

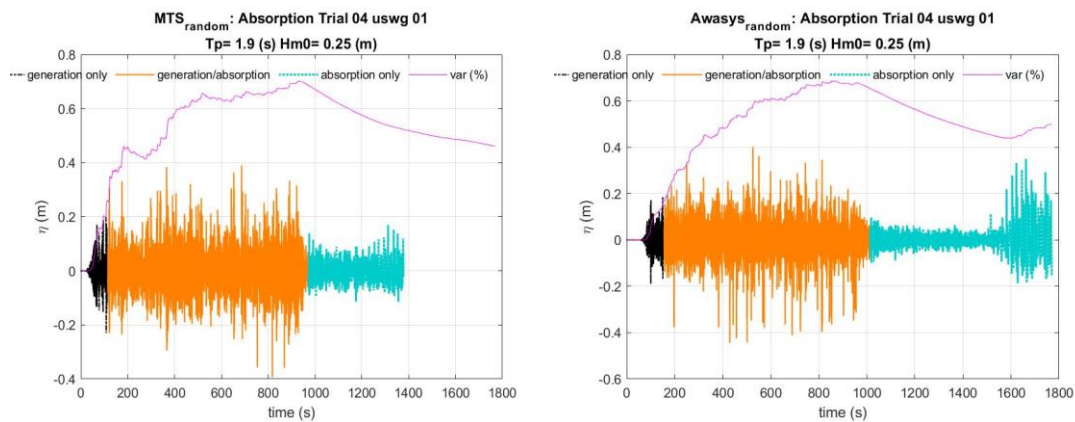


Figure 7.12: Comparison of both systems with active absorption for the  $T_p = 1.9$  s  $H_s = 0.25$  m case.

The 5.0 s and 0.1 m case failed under the MTS system. The MTS system immediately had issues with the cross waves excited at the wavemaker with the limit hit after 17 min (1020 s). The AwaSys system did exceptionally well for the first 1600 seconds of the trial. After this moment a generation of subharmonics (viewed in the AwaSys software during testing) occurred. This required a manual stop at the end of simultaneous generation and absorption which deactivated the active absorption ability in order to avoid reaching the limits of the wavemaker.

The 5.0 s and 0.25 m case failed under both systems. The MTS system hit a wave board limit 10 minutes into the test while AwaSys was aborted after 16 minutes of testing with sample clipping taking place prior to shut down.

The calm down time was used as a way to assess the performance of the active absorption and was calculated by fitting an exponential function to the variance and comparing the exponent's coefficient  $\alpha$  from equation  $e^{-\alpha t}$ , as shown in Figure 7.13. Note that the variance in this case do not consider the full elapsed time series, but a shorter window of  $\sim 100$  waves.

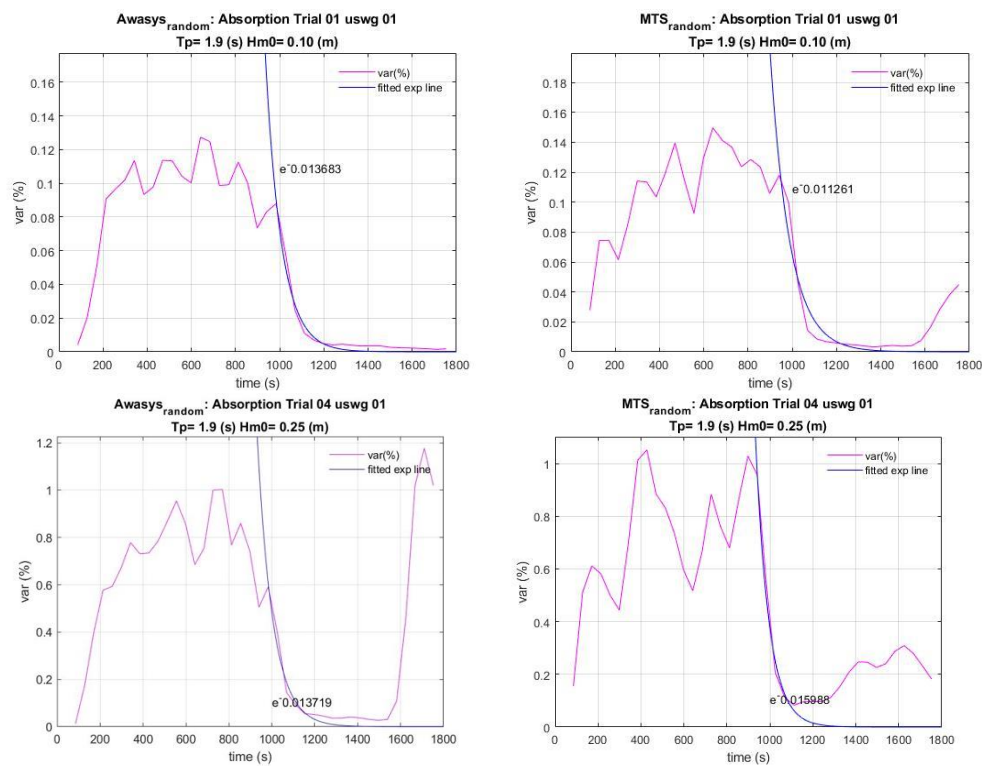


Figure 7.13: Fitted exponential function to the calculated percent variance.

Due to the unsuccessful runs of the 5.0 s peak period, only the 1.9 s cases were evaluated for performance of active absorption in reference to calming down and summarized in Table 7.5.

Table 7.5: Fitted exponent's coefficient for the calm-down times of irregular wave cases.

$T_p$ (s)	$H_{m0}$ (m)	MTS	AwaSys
1.9	0.1	-0.011	-0.014
1.9	0.25	-0.016	-0.014

The results in Table 7.5 show that AwaSys' active absorption system decreases the energy in the flume faster for the 0.1 m case while the MTS system performs better for the 0.25 m case with results being quite similar.

An additional analysis was done for the irregular wave trials by plotting the change in the incident  $H_{m0}$  for each analyzed window. The results verify the previously mentioned parameters.

As shown in Figure 7.14, both systems maintained a quasi-steady  $H_{m0}$  during simultaneous generation and absorption for the 1.9 s and 0.1 m case with a decrease seen at the end of generation. An instability developed at the end of the trial conducted with the MTS system. An increase in the  $H_{m0}$  is evident for both systems during generation only trials with a slower decline occurring at the end than with the active absorption cases. The  $T_p = 1.9$  s,  $H_s = 0.25$  m case behaves in a similar fashion with both systems developing an instability following a decline in  $H_{m0}$  in the trials conducted with active absorption (Figure 7.15).

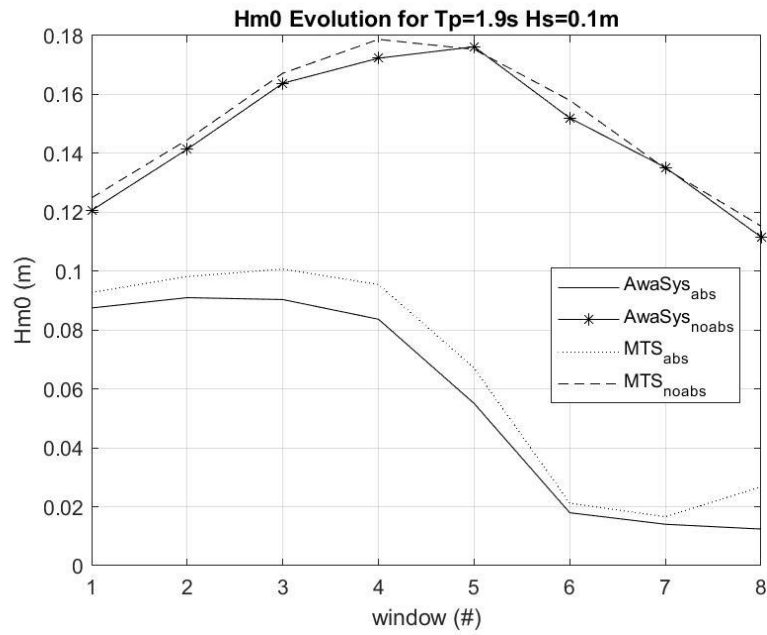


Figure 7.14: Evolution of  $H_{m0}$  for  $T_p=1.9s$  and  $H_s = 0.1m$ .

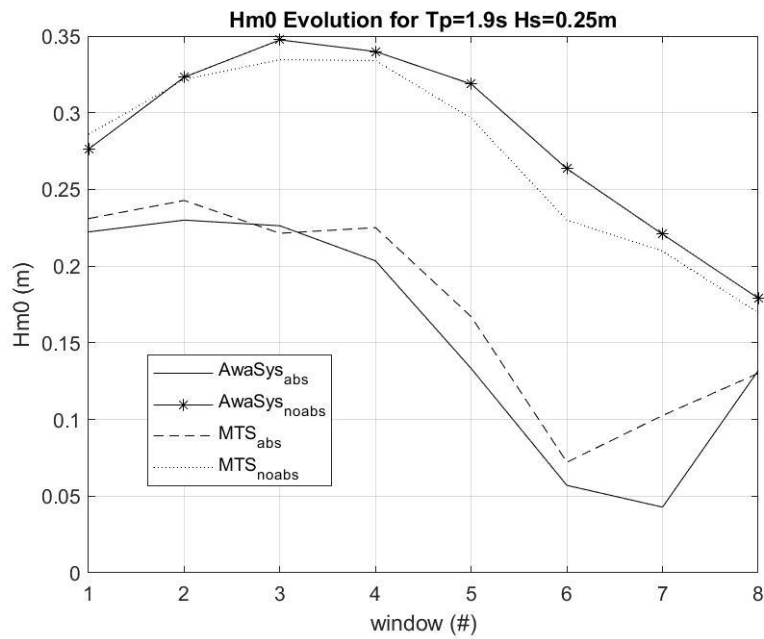


Figure 7.15: Evolution of  $H_{m0}$  for  $T_p=1.9s$  and  $H_s = 0.25m$ .

The cases with a peak period of 5.0 seconds were challenging for both of the systems. Therefore, the plots representing these trials have been omitted to prevent confusion. AwaSys was able to keep simultaneously absorbing and generating for a longer period of time until an instability was formed at around 1600 s. Both of the systems behaved similarly without active absorption present with an increasing trend in energy as seen in the  $T_p=1.9$  s trials.

In addition to the plots presented in the results chapter, the beach trial plots used for analysis, time series plots showing the incident and reflected waves traveling in the flume, wave height evolution, crest and trough plots, wave height plots, and variance plots are located in the appendices. Due to the large quantity of plots all appendices are in an electronic format except for appendix A, list of symbols, and appendix C, 1.4 s and 1.9 s incident wave height evolution.

In conclusion the data shows that for the regular wave cases, performance of both active absorption systems was analogous with AwaSys typically reaching a calm state in the same or shorter time frame. Due to the drastic change in performance of the AwaSys system for the 0.1 Hz tests, it is suggested that additional tests be conducted at this frequency. Additional testing will offer an opportunity to better fine-tune the filter settings used in AwaSys potentially leading to better performance of long wave absorption.

The wave conditions using the beach setup have been briefly analyzed at this time yielding preliminary results. Further testing using a beach profile should be conducted varying the frequency as well as the duration of the trials to provide more data for the difference in performance seen by the MTS system. However, it is important to say that AwaSys performed well for both wave conditions with and without active absorption.

Only two irregular wave conditions were tested with one having a peak period of 1.9 s that is close to the first mode of a cross wave that fits in the flume. The evidence of this was seen with cross waves propagating in the flume during testing. Further tests should be conducted with a slightly higher peak frequency. Although there was a presence of the cross waves, the AwaSys system did extremely well for the  $T_p=1.9$  s and  $H_s=0.1$  m case remaining stable for the entirety of the test. An instability was created at the end of the absorption only test for the  $T_p=1.9$  s and  $H_s=0.25$  m case with samples being clipped during the test. For the 5.0s peak period wave condition with a significant wave height of 0.1 m, AwaSys was able to work properly for a longer time frame than MTS. During the time it was working, the waves generated did not increase in energy. Awasys' active absorption system was aborted during generation for the  $T_p=5.0$  s and  $H_s=0.25$  m case and was manually stopped after generation ended due to a rapidly growing instability.

Although, AwaSys' results are not ideal, the program did outperform MTS for the irregular wave cases. This is most likely because MTS' wave height control was not

designed for irregular waves by only allowing one frequency to be absorbed by the system. Overall, MTS wave height control failed during the  $T_p=5.0$  s irregular wave trials with the system aborting for both of the trials. An instability was created for the remaining two  $T_p=1.9$  s trials after generation was complete.

As a side note, it is interesting to mention that due to a user error, the MTS system had as an input a wrong nominal period of 5.0 s for an irregular wave trial with  $T_p=1.9$  s,  $H_s=0.25$  m. While entering the proper nominal period for the  $T_p=1.9$  s cases had successful results, entering a wrong nominal period prevents the system from working properly. The wave height control receiving an incorrect period culminated with the wave board hitting its limits within 13 minutes.

Along with further testing of regular waves with a mild slope beach present, it would be interesting to see the trend in energy for the irregular wave cases with a beach. In addition to further testing, certain changes can be made to the system to improve performance of the active absorption system, for example:

- The wavemaker wave gauges on the face of the piston accumulate rust over time, potentially compiling errors in surface elevation readings. However, the cleaning of the instruments could lead to the exposure of the wiring, leading to faster corrosion. As stated previously by [5], the capability of self-calibration of the wavemaker wave gauges could improve the performance of the system.
- The make-up pump located in the vicinity of the wavemaker creates noise that was filtered out of the data. Though small, it does create unnecessary noise to the active absorption system. Therefore, the pump should be moved to the other end of the flume away from the wavemaker or lower its discharge point underneath the water surface.
- The bulk of the active absorption issues for the regular and irregular wave cases occurred at the end of wave generation. In order to improve

performance, the active absorption system should be deactivated at the culmination of wave generation. Unfortunately, this would need to be determined by the user of the system who will have to observe the conditions in the flume and decide on when the majority of the wave train has been absorbed.

It was not identified prior to testing that the 1.9 s regular and irregular cases would create a cross wave in the flume. However, the wavemaker wave gauges are offset on the wave board in order to cancel out this effect. To fully understand the repercussions of the development of the cross wave, further tests should be conducted with wave gauges on both sides of the flume to gain a better understanding of the quality of the wavemaker wave gauge offset.

Overall, in spite of the large amount of potential uncertainty, both of the systems perform equally well for the regular wave cases. With the performance leaning in AwaSys' favor with lower reflection coefficients for the regular cases and shorter calm down times. Both systems can be used for absorption of regular waves with AwaSys being a better choice for the 1.4 s and 1.9 s regular waves.

For tests with a beach installed in the flume, it would be advised to use either the MTS system without activating its wave height control or to use AwaSys with or without its active absorption turned on.

Though not ideal, the irregular wave cases were absorbed better by the AwaSys system. Therefore, future tests should utilize the AwaSys software for irregular wave absorption and disabling it after generation is complete.

## Bibliography

1. NOAA. *How much water is in the ocean?* 2018 06/25/2018 March 26, 2019]; Available from: <https://oceanservice.noaa.gov/facts/oceanwater.html>.
2. Kristen Crossett, B.A., Percy Pacheco, and Kate Haber. *National Coastal Population Report: Population Trends from 1970 to 2020*. NOAA's State of the Coast March 2013 March 26, 2019]; Available from: <https://aamboceanservice.blob.core.windows.net/oceanservice-prod/facts/coastal-population-report.pdf>.
3. Hughes, S.A., *Physical models and laboratory techniques in coastal engineering*. Advancer Series on Ocean Engineering. Vol. 7. 2005, Singapore: World Scientific.
4. Dalrymple, R.G.D.a.R.A., *Water Wave Mechanics for Engineers and Scientists*. Advanced Series on Ocean Engineering ed. P.L.-F. Liu. Vol. 2. 1991, Hackensack, New Jersey: World Scientific Publishing Co. Pte. Ltd.
5. Thomas Lykke Andersen, M.C., P. Frigaard, M. Losada, and J.I. Puyol, *A new active absorption system and its performance to linear and non-linear waves*. Coastal Engineering, 2016. **114**: p. 47-60.
6. Datta, Y.O.a.J., *A survey of wave absorbers*. Journal of Hydraulic Research 1986. **24**(4): p. 265-280.
7. Milgram, J.H., *Compliant Water Wave Absorbers*, M.I.o. Technology, Editor. 1965, MIT Library: MIT. p. 263.
8. Milgram, J.H., *Active water-wave absorbers*. Journal of Fluid Mechanics, 1970. **43**(4): p. 845-859.
9. Gilbert, G., *Absorbing wave generators*. Hydraulics Research Station Notes, 1978: p. 3-4.
10. Salter, S.H. *Absorbing Wave-Makers and Wide Tanks*. in *Conference on Directional Wave Spectra Applications*. 1981. University of California, Berkley, California: ASCE.
11. Schäffer, H.A.K., Gert, *Review of Multidirectional Active Wave Absorption Methods*. Journal of Waterway, Port, Coastal, and Ocean Engineering, 2000: p. 10.
12. Murton, G.N.B.a.G.J., *Performance of a Wedge-Type Absorbing Wave Maker*. Journal of Waterway, Port, Coastal, and Ocean Engineering, 1989. **115**(1): p. 1-17.
13. Hemming A. Schäffer, T.S.a.P.H. *Simultaneous Generation and Active Absorption of Waves in Flumes*. in *International Symposium: Waves-Physical and Numerical Modelling*. 1994. University of British Columbia, Vancouver, Canada: University of British Columbia.
14. Schäffer, H.A., *Active Wave Absorption in Flumes and 3D Basins*, in *Ocean Wave Measurement and Analysis*. 2001: San Francisco, California, United States. p. 1200-1208.
15. Jakobsen, H.A.S.a.K. *Non-linear wave generation and active absorption in wave flumes*. in *Long Waves Symposium*. 2003. Thessaloniki, Greece.
16. Williams, H., *University to make waves for research*, in *The Seattle Times*. 1972, Seattle Times: Seattle, Washington. p. 1.
17. Bundy, D., *University Researchers Intend To Make Waves*, in *Corvallis Gazette Times*. 1973, -: Corvallis, Oregon. p. 1.

18. Lab, O.H.H.W.R., *1982 LWF roof photo*. 1982.
19. University, O.S. *History*. 2019 [cited 2018 April 7, 2018]; History tab on the HWRL websites]. Available from: [https://www.nsf.gov/funding/pgm\\_summ.jsp?pims\\_id=503259](https://www.nsf.gov/funding/pgm_summ.jsp?pims_id=503259).
20. *Oregon wave lab best in world*, in *The Oregon Scientist*. 1991, -: Newburg, OR. p. 2.
21. Engineering, C.o. *Large Wave Flume*. - [cited 2019 March 15, 2019]; Description of the large wave flume]. Available from: <https://wave.oregonstate.edu/large-wave-flume>.
22. Frigaard, T.L.A.a.P., *Wave Generation in Physical Models: Technical documentation for AwaSys 6*. 2014, Aalborg, Denmark: Aalborg University Department of Civil Engineering.
23. Haiwen Zhang, H.A.S., *Approximate Stream Function wavemaker theory for highly nonlinear waves in wave flumes*. *Ocean Engineering*, 2007(34): p. 1290-1302.
24. Schäffer, H.A., *Second-Order Wavemaker Theory for Irregular Waves*. *Ocean Engineering*, 1996. **23**(1): p. 44-88.
25. Fenton, J.D., *Nonlinear Wave Theories*. *The Sea*, 1990. **9**.
26. Dalrymple, R.A. *Stream Function Wave Theory*. Java Applets for Coastal Engineering 1996 December 13, 1996 [cited 2019; Available from: [http://homepages.cae.wisc.edu/~chinwu/Coastal\\_Java/](http://homepages.cae.wisc.edu/~chinwu/Coastal_Java/).
27. Corporation, M.S., *2D Wave Generator User's Manual*. 2009, Oregon State University.
28. Palle Meinert, T.L.A., and Peter Frigaard, *AwaSys7 user manual*. 2017, Aalborg University: Aalborg, Denmark. p. 60.
29. Dibble, T.L.a.S., C.K., *New Designs for Acoustic and Resistive Wave Profilers*. 1989, Oregon State University: Corvallis, Oregon. p. 16.

## Appendices

## Appendix A: List of Symbols

$\eta$	Surface elevation
H	Wave height from crest to trough
k	Wave number equivalent to $\frac{2\pi}{L}$
L	Wave length from crossing to crossing
t	time in seconds
$\sigma$	Angular wave frequency equivalent to $\frac{2\pi}{T}$
S	Amplitude of wavemaker stroke
T	Wave period from crossing to crossing
$\omega$	Angular frequency equivalent to $\frac{2\pi}{T}$
$\phi$	Velocity potential
s	Nonlinearity parameter
a	Wave amplitude
h	Water depth
U	Ursell number
g	Gravity equal to $9.81 \frac{m}{s^2}$
z	Vertical axis, zero at water surface elevation and -h at bottom of theoretical flume
x	Horizontal axis representing position along flume
e	Wavemaker motion
$\gamma$	Peak enhancement factor
$d_{wg}$	Wave gauge distance from wavemaker face
$C_{0,2D}$	Biésel Transfer Function
$D_x$	Sum of transfer functions for the near field
$X_{gen}$	Wavemaker position during wave generation
$X_{abs}$	Wavemaker position during active absorption
$A_R$	Reflected wave amplitude
$A_{WG}$	Wave amplitude at wave gauge
$A_I$	Incident wave amplitude
$H(f)$	Active absorption transfer function
$C_g$	Group velocity
C	Wave celerity
$K_r$	Reflection coefficient
$K_a$	Absorption coefficient
$H_r$	Reflected wave height
$H_i$	Incident wave height
$H_s$	Significant wave height
$H_m$	Mean wave height
f	Wave frequency, equivalent to $\frac{1}{T}$

## Appendix B (electronic): Incident and reflected time series plots

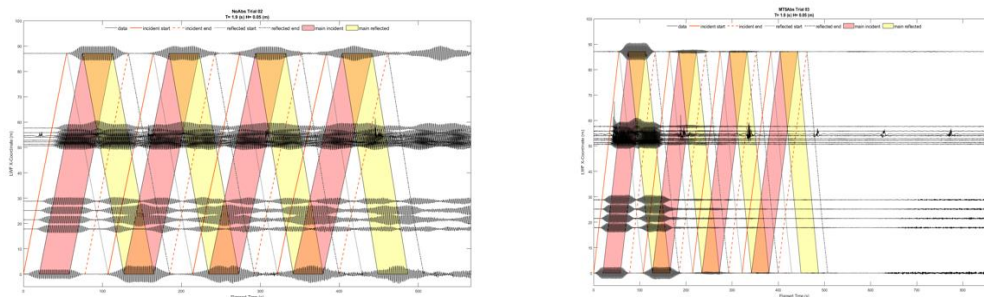
### Supplementary Data File:

#### Description:

The accompanying figures show each trial's time series on top of the incident and reflected time frames for the generated main waves and the ramp up and down waves.

These figures were only generated for the regular trials without a beach with and without absorption.

#### Sample plots:



#### Filenames:

##### Awasys\_Absorption:

Trial01.fig  
 Trial01.jpg  
 Trial03.fig  
 Trial03.jpg  
 Trial04.fig  
 Trial04.jpg  
 Trial05.fig  
 Trial05.jpg  
 Trial07.fig  
 Trial07.jpg  
 Trial08.fig

Trial08.jpg  
 Trial10.fig  
 Trial10.jpg  
 Trial11.fig  
 Trial11.jpg  
 Trial12.fig  
 Trial12.jpg  
 Trial14.fig  
 Trial14.jpg  
 Trial15.fig  
 Trial15.jpg

Trial17.fig  
 Trial17.jpg  
 Trial18.fig  
 Trial18.jpg  
 Trial20.fig  
 Trial20.jpg  
 Trial21.fig  
 Trial21.jpg  
 Trial23.fig  
 Trial23.jpg

## Awasys\_NoAbsorption:

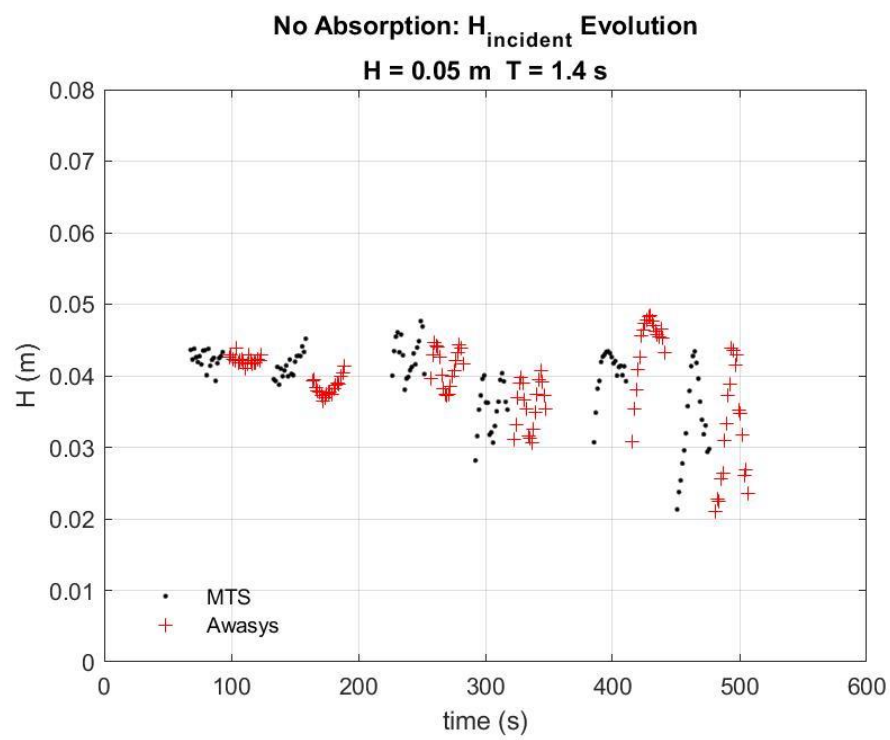
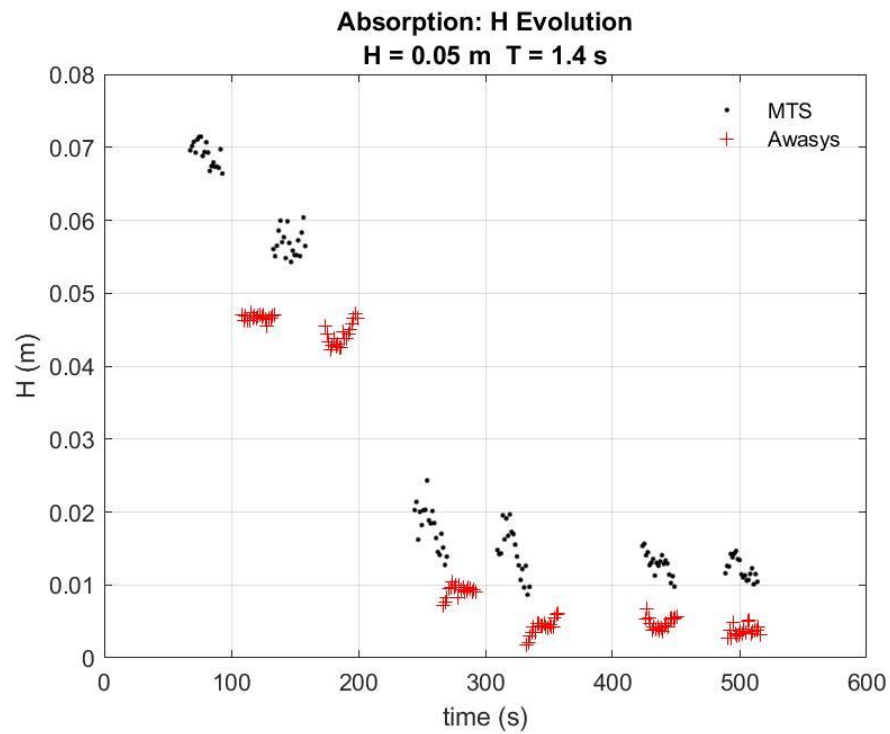
Trial01.fig	Trial07.jpg	Trial17.fig
Trial01.jpg	Trial08.fig	Trial17.jpg
Trial02.fig	Trial08.jpg	Trial18.fig
Trial02.jpg	Trial10.fig	Trial18.jpg
Trial03.fig	Trial10.jpg	Trial20.fig
Trial03.jpg	Trial11.fig	Trial20.jpg
Trial04.fig	Trial11.jpg	Trial21.fig
Trial04.jpg	Trial12.fig	Trial21.jpg
Trial06.fig	Trial12.jpg	Trial23.fig
Trial06.jpg	Trial14.fig	Trial23.jpg
Trial07.fig	Trial14.jpg	

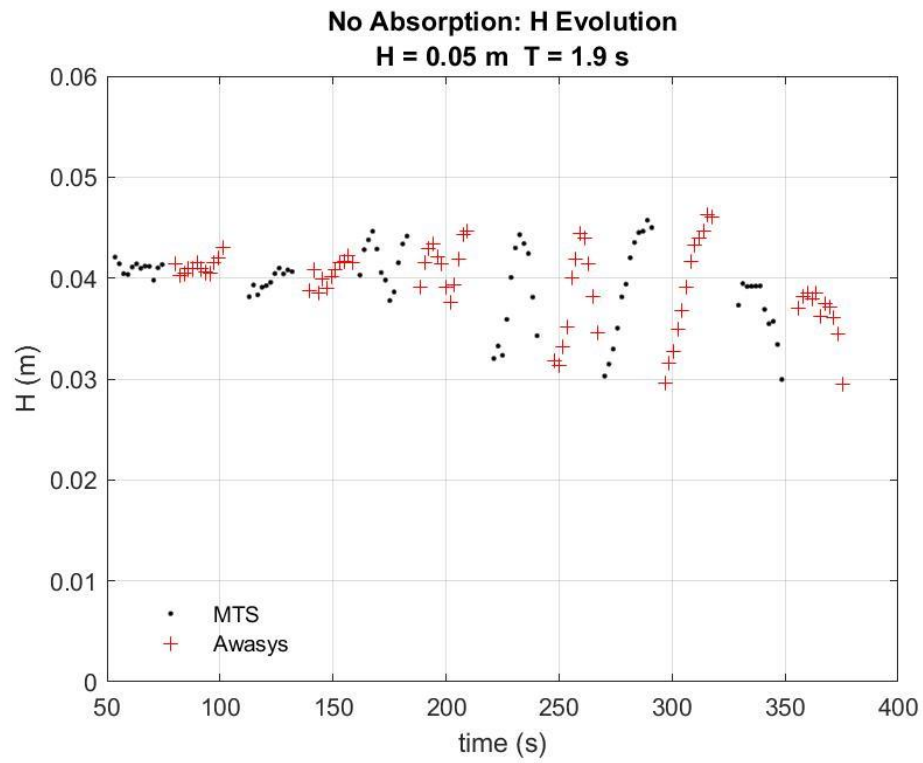
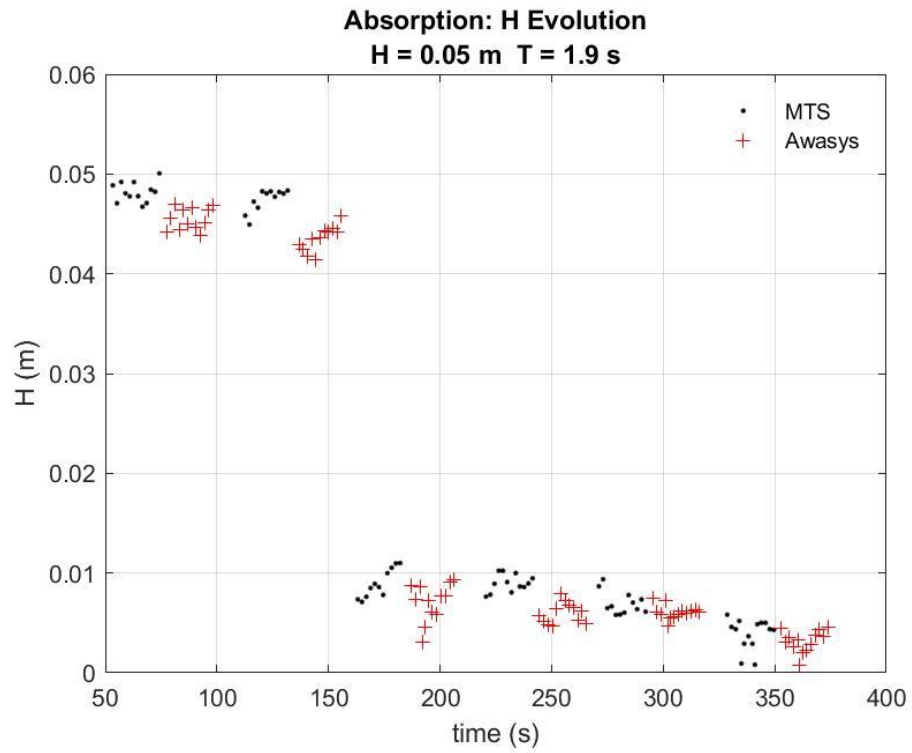
## MTS\_Absorption:

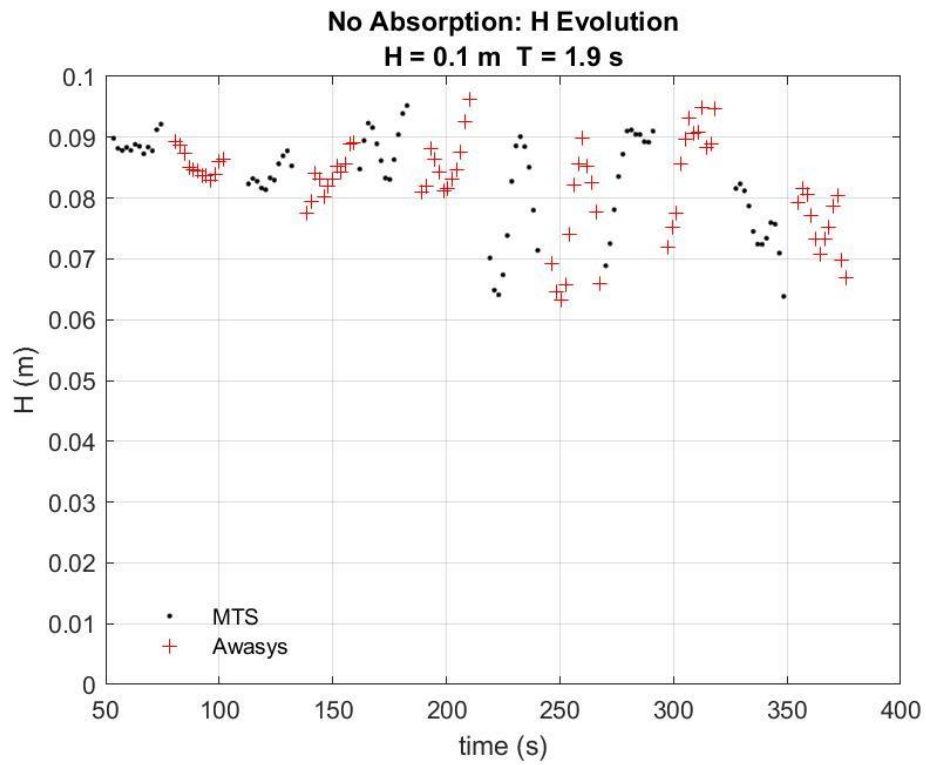
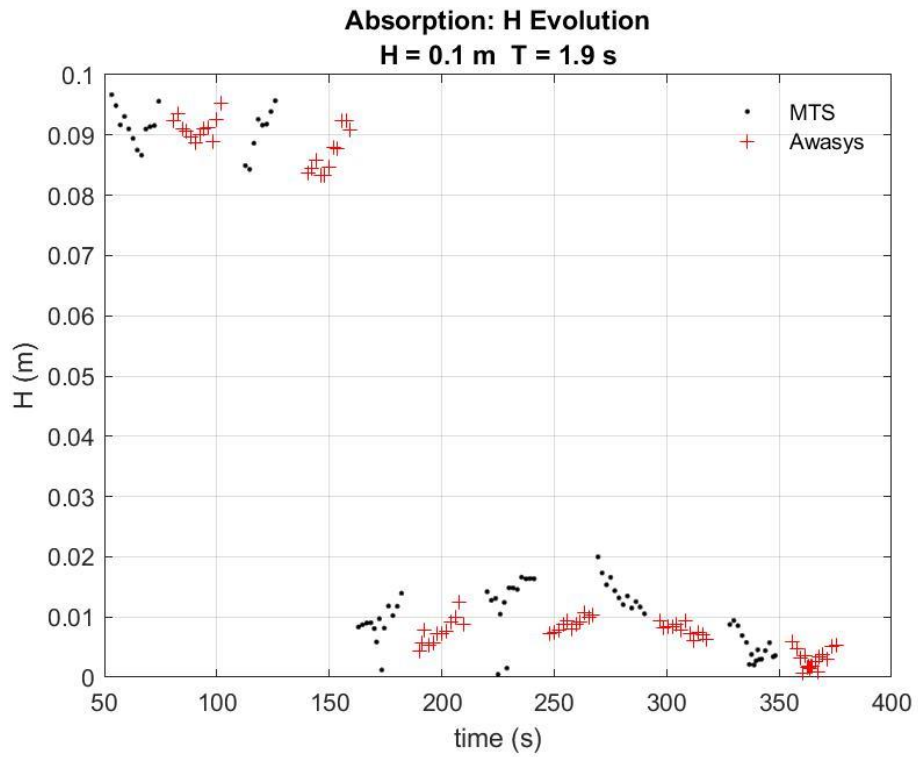
Trial02.fig	Trial08.jpg	Trial17.fig
Trial02.jpg	Trial09.fig	Trial17.jpg
Trial03.fig	Trial09.jpg	Trial18.fig
Trial03.jpg	Trial11.fig	Trial18.jpg
Trial04.fig	Trial11.jpg	Trial19.fig
Trial04.jpg	Trial12.fig	Trial19.jpg
Trial05.fig	Trial12.jpg	Trial20.fig
Trial05.jpg	Trial13.fig	Trial20.jpg
Trial07.fig	Trial13.jpg	Trial21.fig
Trial07.jpg	Trial16.fig	Trial21.jpg
Trial08.fig	Trial16.jpg	

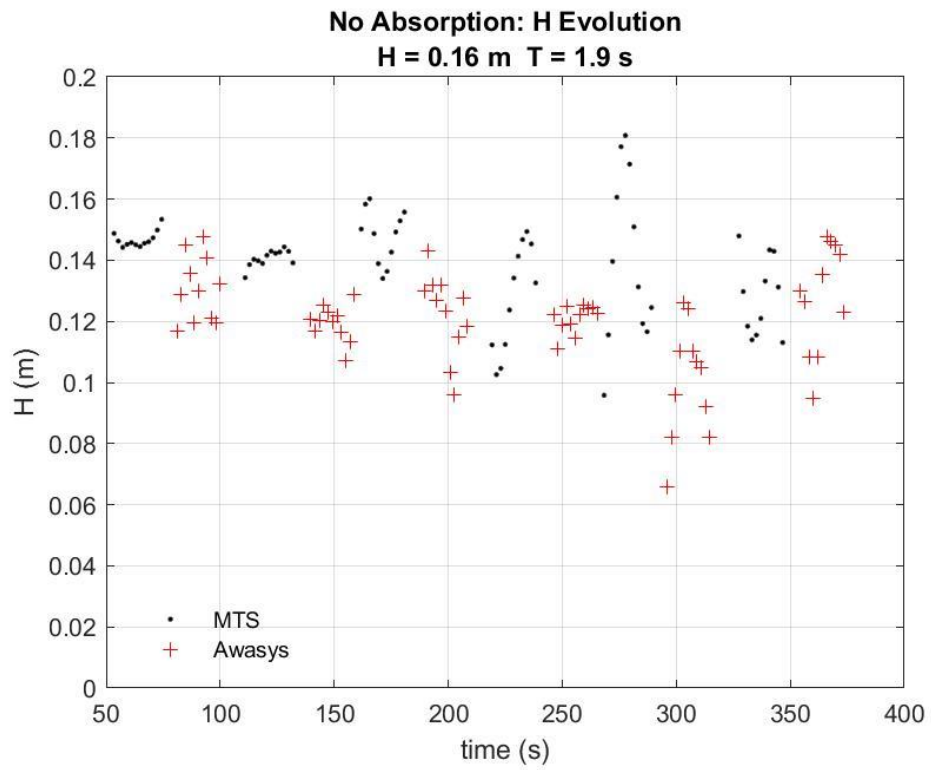
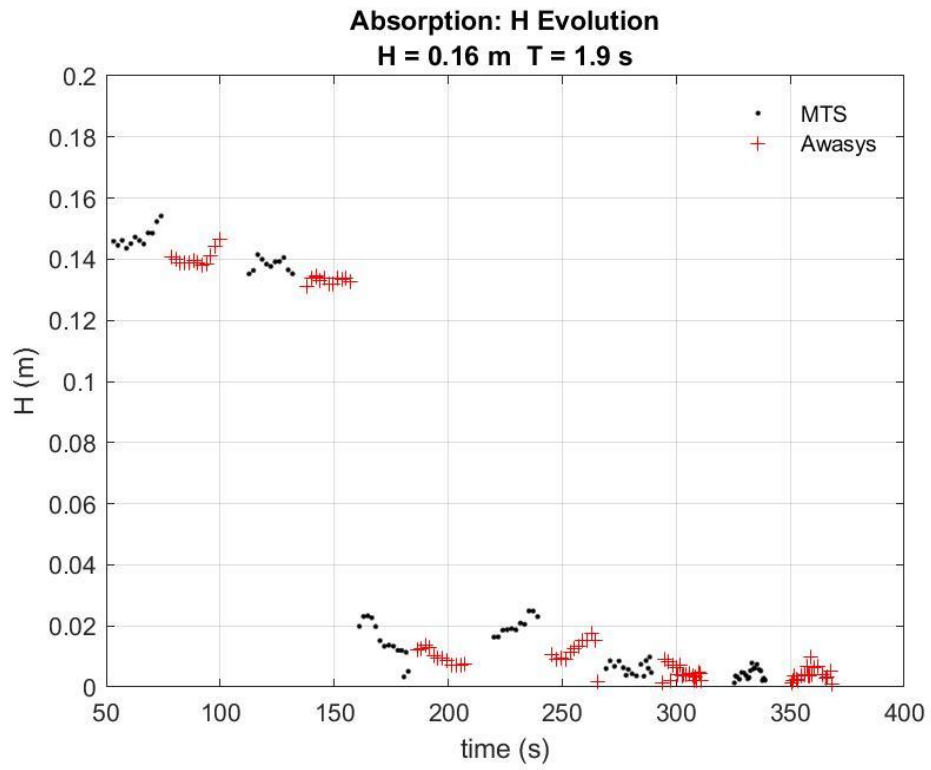
## MTS\_NoAbsorption:

Trial01.fig	Trial07.jpg	Trial15.fig
Trial01.jpg	Trial08.fig	Trial15.jpg
Trial02.fig	Trial08.jpg	Trial16.fig
Trial02.jpg	Trial10.fig	Trial16.jpg
Trial03.fig	Trial10.jpg	Trial17.fig
Trial03.jpg	Trial11.fig	Trial17.jpg
Trial04.fig	Trial11.jpg	Trial18.fig
Trial04.jpg	Trial13.fig	Trial18.jpg
Trial06.fig	Trial13.jpg	Trial19.fig
Trial06.jpg	Trial14.fig	Trial19.jpg
Trial07.fig	Trial14.jpg	

**Appendix C: 1.4 s and 1.9 s incident and reflected wave height evolution**







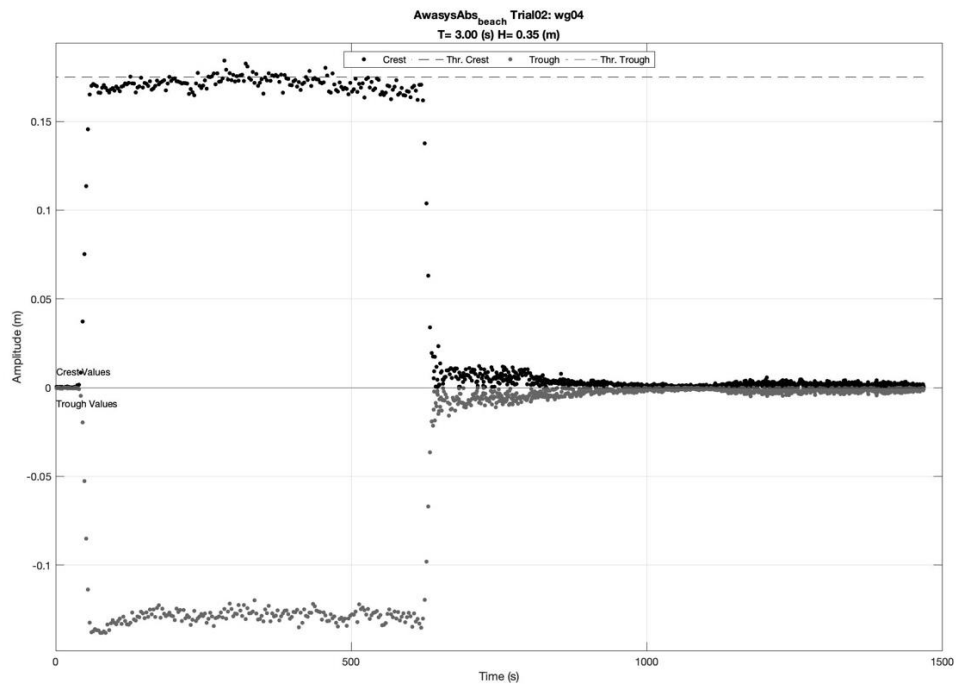
## Appendix D (electronic): Crest and trough evolution for beach trials

### Supplemental Data File:

### Description:

The figures included show how the crest and trough evolved over the duration of the entire test using resistive wave gauge 4 for the analysis.

### Sample Plot:



### File Names:

Awasy\_Absorption\3.0s\_case\timeserieswg04.fig

Awasy\_Absorption\3.0s\_case\timeserieswg04.jpg

Awasy\_Absorption\10.0s\_case\timeserieswg04.fig

Awasy\_Absorption\10.0s\_case\timeserieswg04.fig

Awasys\_NoAbsorption\3.0s\_case\timeserieswg04.fig

Awasys\_NoAbsorption\3.0s\_case\timeserieswg04.jpg

Awasys\_NoAbsorption\10.0s\_case\timeserieswg04.fig

Awasys\_NoAbsorption\10.0s\_case\timeserieswg04.fig

MTS\_Absorption\3.0s\_case\timeserieswg04.fig

MTS\_Absorption\3.0s\_case\timeserieswg04.jpg

MTS\_Absorption\10.0s\_case\timeserieswg04.fig

MTS\_Absorption\10.0s\_case\timeserieswg04.fig

MTS\_NoAbsorption\3.0s\_case\timeserieswg04.fig

MTS\_NoAbsorption\3.0s\_case\timeserieswg04.jpg

MTS\_NoAbsorption\10.0s\_case\timeserieswg04.fig

MTS\_NoAbsorption\10.0s\_case\timeserieswg04.fig

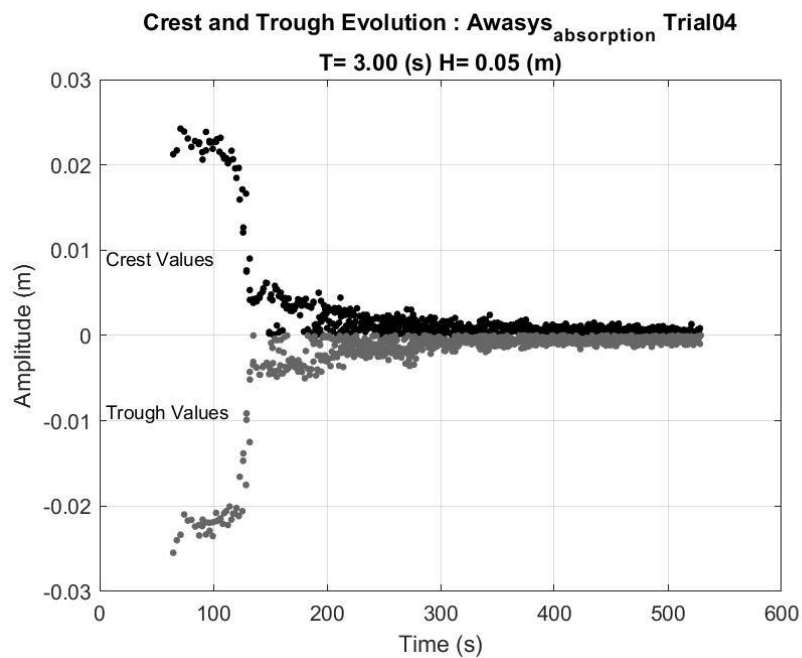
## Appendix E (electronic): Crest and trough evolution for regular cases without beach

### Supplemental Data File:

#### Description:

The figures in appendix E show how the crest and trough changed during the entire duration of a test. The plots included are for ultrasonic wave gauge 1 for the 1.4s and 1.9s cases with no gauge specification for the rest. The lower frequency plots were generated from the incident and reflected analysis that used several uswg to obtain one timeseries.

#### Sample plot:



#### File Names:

Awasys\_Absorption\Trial01\timeseriesuswg01.fig and .jpg

Awasys\_Absorption\Trial03\timeseriesuswg01.fig and .jpg

Awasys\_Absorption\Trial07\timeseriesuswg01.fig and .jpg

Awasys\_Absorption\Trial21\timeseriesuswg01.fig and .jpg

Awasys\_Absorption\CrestTroughEvolution\Trial04.fig and .jpg

Awasys\_Absorption\CrestTroughEvolution\Trial05.fig and .jpg

Awasys\_Absorption\CrestTroughEvolution\Trial08.fig and .jpg

Awasys\_Absorption\CrestTroughEvolution\Trial10.fig and .jpg

Awasys\_Absorption\CrestTroughEvolution\Trial11.fig and .jpg

Awasys\_Absorption\CrestTroughEvolution\Trial12.fig and .jpg

Awasys\_Absorption\CrestTroughEvolution\Trial14.fig and .jpg

Awasys\_Absorption\CrestTroughEvolution\Trial15.fig and .jpg

Awasys\_Absorption\CrestTroughEvolution\Trial17.fig and .jpg

Awasys\_Absorption\CrestTroughEvolution\Trial18.fig and .jpg

Awasys\_Absorption\CrestTroughEvolution\Trial20.fig and .jpg

Awasys\_Absorption\CrestTroughEvolution\Trial23.fig and .jpg

Awasys\_NoAbsorption\Trial01\timeseriesuswg01.fig and .jpg

Awasys\_NoAbsorption\Trial02\timeseriesuswg01.fig and .jpg

Awasys\_NoAbsorption\Trial06\timeseriesuswg01.fig and .jpg

Awasys\_NoAbsorption\Trial21\timeseriesuswg01.fig and .jpg

Awasys\_NoAbsorption\CrestTroughEvolution\Trial03.fig and .jpg

Awasys\_NoAbsorption\CrestTroughEvolution\Trial04.fig and .jpg

Awasys\_NoAbsorption\CrestTroughEvolution\Trial07.fig and .jpg

Awasys\_NoAbsorption\CrestTroughEvolution\Trial08.fig and .jpg

Awasys\_NoAbsorption\CrestTroughEvolution\Trial10.fig and .jpg

Awasys\_NoAbsorption\CrestTroughEvolution\Trial11.fig and .jpg

Awasys\_NoAbsorption\CrestTroughEvolution\Trial12.fig and .jpg

Awasys\_NoAbsorption\CrestTroughEvolution\Trial14.fig and .jpg

Awasys\_NoAbsorption\CrestTroughEvolution\Trial17.fig and .jpg

Awasys\_NoAbsorption\CrestTroughEvolution\Trial18.fig and .jpg

Awasys\_NoAbsorption\CrestTroughEvolution\Trial20.fig and .jpg

Awasys\_NoAbsorption\CrestTroughEvolution\Trial23.fig and .jpg

MTS\_Absorption\Trial02\timeseriesuswg01.fig and .jpg

MTS\_Absorption\Trial03\timeseriesuswg01.fig and .jpg

MTS\_Absorption\Trial07\timeseriesuswg01.fig and .jpg

MTS\_Absorption\Trial20\timeseriesuswg01.fig and .jpg

MTS\_Absorption\CrestTroughEvolution\Trial04.fig and .jpg

MTS\_Absorption\CrestTroughEvolution\Trial05.fig and .jpg

MTS\_Absorption\CrestTroughEvolution\Trial08.fig and .jpg

MTS\_Absorption\CrestTroughEvolution\Trial09.fig and .jpg

MTS\_Absorption\CrestTroughEvolution\Trial11.fig and .jpg

MTS\_Absorption\CrestTroughEvolution\Trial12.fig and .jpg

MTS\_Absorption\CrestTroughEvolution\Trial13.fig and .jpg

MTS\_Absorption\CrestTroughEvolution\Trial16.fig and .jpg

MTS\_Absorption\CrestTroughEvolution\Trial17.fig and .jpg

MTS\_Absorption\CrestTroughEvolution\Trial18.fig and .jpg

MTS\_Absorption\CrestTroughEvolution\Trial19.fig and .jpg

MTS\_Absorption\CrestTroughEvolution\Trial21.fig and .jpg

MTS\_NoAbsorption\Trial01\timeseriesuswg01.fig and .jpg

MTS\_NoAbsorption\Trial02\timeseriesuswg01.fig and .jpg

MTS\_NoAbsorption\Trial06\timeseriesuswg01.fig and .jpg

MTS\_NoAbsorption\Trial19\timeseriesuswg01.fig and .jpg

MTS\_NoAbsorption\CrestTroughEvolution\Trial03.fig and .jpg

MTS\_NoAbsorption\CrestTroughEvolution\Trial04.fig and .jpg

MTS\_NoAbsorption\CrestTroughEvolution\Trial07.fig and .jpg

MTS\_NoAbsorption\CrestTroughEvolution\Trial08.fig and .jpg

MTS\_NoAbsorption\CrestTroughEvolution\Trial10.fig and .jpg

MTS\_NoAbsorption\CrestTroughEvolution\Trial11.fig and .jpg

MTS\_NoAbsorption\CrestTroughEvolution\Trial13.fig and .jpg

MTS\_NoAbsorption\CrestTroughEvolution\Trial14.fig and .jpg

MTS\_NoAbsorption\CrestTroughEvolution\Trial15.fig and .jpg

MTS\_NoAbsorption\CrestTroughEvolution\Trial16.fig and .jpg

MTS\_NoAbsorption\CrestTroughEvolution\Trial17.fig and .jpg

MTS\_NoAbsorption\CrestTroughEvolution\Trial18.fig and .jpg

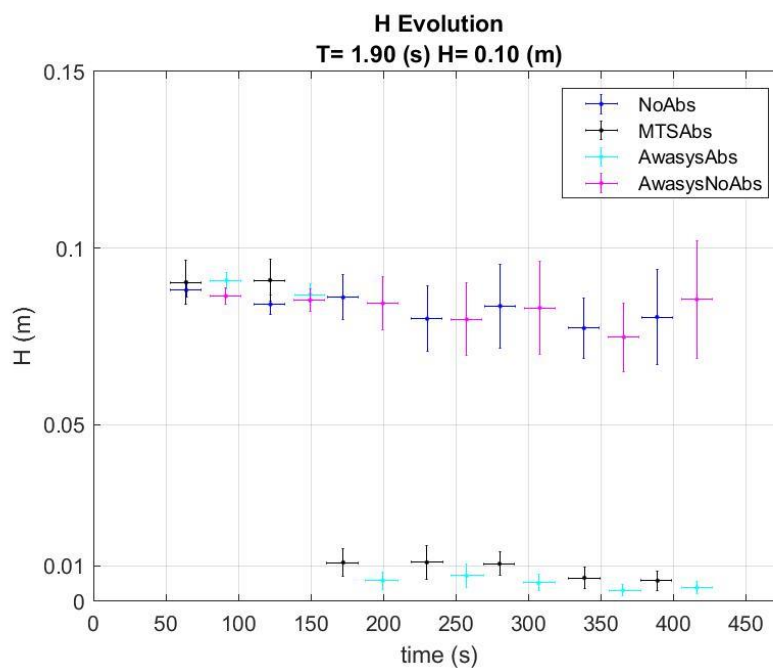
## Appendix F (electronic): H evolution for all 1.4 s and 1.9 s cases

### Supplemental Data File:

#### Description:

The figures in appendix F show the evolution of the wave height for both systems with and without absorption for each 1.4s and 1.9s wave condition. The wave heights are calculated by averaging the values for all of the ultrasonic wave gauges with calculated standard deviation.

#### Sample Plot:



#### File Names:

Combined\_H\_Evolution\_woexpfit0.1T1.9.fig and .jpg

Combined\_H\_Evolution\_woexpfit0.16T1.9.fig and .jpg

Combined\_H\_Evolution\_woexpfit0.05T1.9.fig and .jpg

Combined\_H\_Evolution\_woexpfit0.05T1.4.fig and .jpg

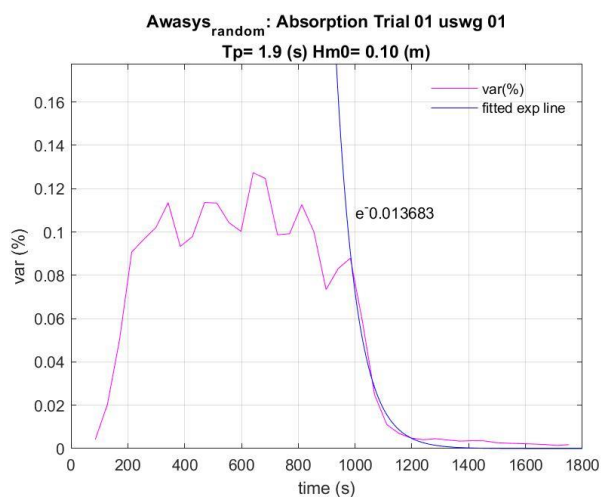
## Appendix G (electronic): Alpha values

### Supplemental Data File:

### Description:

The figures show the exponential line that was fit to the variance for the irregular  $T_p=1.9s$  cases with active absorption.

### Sample Plot:



### File Names:

AwasyRandom\_Absorption\Trial01\fitted\_uswg01.fig and .jpg

AwasyRandom\_Absorption\Trial04\fitted\_uswg01.fig and .jpg

AwasyRandom\_NoAbsorption\Trial01\fitted\_uswg01.fig and .jpg

AwasyRandom\_NoAbsorption\Trial04\fitted\_uswg01.fig and .jpg

MTSRandom\_Absorption\Trial01\fitted\_uswg01.fig and .jpg

MTSRandom\_Absorption\Trial04\fitted\_uswg01.fig and .jpg

MTSRandom\_NoAbsorption\Trial03\fitted\_uswg01.fig and .jpg

MTSRandom\_NoAbsorption\Trial05\fitted\_uswg01.fig and .jpg

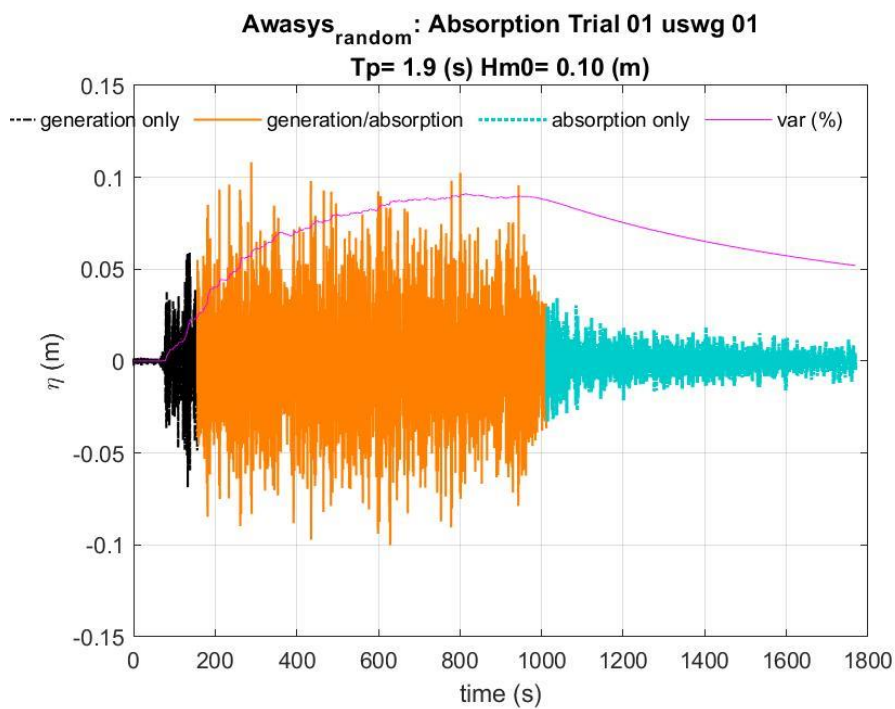
## Appendix H (electronic): Percent variance

### Supplemental Data File:

### Description:

The figures show the filtered ultrasonic wave gauge 1 data for the irregular trials with the percent variance plotted on top.

### Sample Plot:



### File Names:

MTSRandom\_NoAbsorption\Trial02\ uswg01.fig and .jpg

MTSRandom\_NoAbsorption\Trial03\ uswg01.fig and .jpg

MTSRandom\_NoAbsorption\Trial05\ uswg01.fig and .jpg

MTSRandom\_NoAbsorption\Trial06\ uswg01.fig and .jpg

MTSRandom\_Absorption\Trial01\ uswg01.fig and .jpg

MTSRandom\_Absorption\Trial02\ uswg01.fig and .jpg

MTSRandom\_Absorption\Trial04\ uswg01.fig and .jpg

MTSRandom\_Absorption\Trial05\ uswg01.fig and .jpg

AwasysRandom\_NoAbsorption\Trial01\ uswg01.fig and .jpg

AwasysRandom\_NoAbsorption\Trial03\ uswg01.fig and .jpg

AwasysRandom\_NoAbsorption\Trial04\ uswg01.fig and .jpg

AwasysRandom\_NoAbsorption\Trial05\ uswg01.fig and .jpg

AwasysRandom\_Absorption\Trial01\ uswg01.fig and .jpg

AwasysRandom\_Absorption\Trial02\ uswg01.fig and .jpg

AwasysRandom\_Absorption\Trial03\ uswg01.fig and .jpg

AwasysRandom\_Absorption\Trial04\ uswg01.fig and .jpg

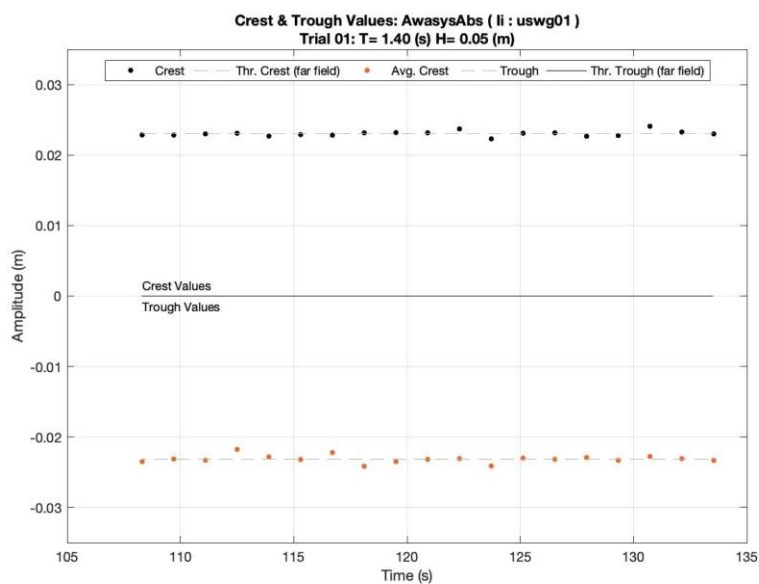
## Appendix I (electronic): Crest and trough values

### Supplemental Data File:

#### Description:

The figures show the filtered ultrasonic wave gauge 1 data for the regular wave trials with the crests and trough plotted with theoretical values for the first incident packet of waves.

#### Sample Plot:



#### File Names:

Awasy\_Absorption\Trial01\ CrestandTroughValuesIi\_strmfuswg01.fig and .jpg

Awasy\_Absorption\Trial03\ CrestandTroughValuesIi\_strmfuswg01.fig and .jpg

Awasy\_Absorption\Trial07\ CrestandTroughValuesIi\_strmfuswg01.fig and .jpg

Awasy\_Absorption\Trial21\ CrestandTroughValuesIi\_strmfuswg01.fig and .jpg

Awasy\_NoAbsorption\Trial01\ CrestandTroughValuesIi\_strmfuswg01.fig and .jpg

Awasy\_NoAbsorption\Trial02\ CrestandTroughValuesIi\_strmfuswg01.fig and .jpg

Awasys\_NoAbsorption\Trial06\ CrestandTroughValuesIi\_strmfuswg01.fig and .jpg

Awasys\_NoAbsorption\Trial21\ CrestandTroughValuesIi\_strmfuswg01.fig and .jpg

MTS\_Absorption\Trial02\ CrestandTroughValuesIi\_strmfuswg01.fig and .jpg

MTS\_Absorption\Trial03\ CrestandTroughValuesIi\_strmfuswg01.fig and .jpg

MTS\_Absorption\Trial07\ CrestandTroughValuesIi\_strmfuswg01.fig and .jpg

MTS\_Absorption\Trial20\ CrestandTroughValuesIi\_strmfuswg01.fig and .jpg

MTS\_NoAbsorption\Trial01\ CrestandTroughValuesIi\_strmfuswg01.fig and .jpg

MTS\_NoAbsorption\Trial02\ CrestandTroughValuesIi\_strmfuswg01.fig and .jpg

MTS\_NoAbsorption\Trial06\ CrestandTroughValuesIi\_strmfuswg01.fig and .jpg

MTS\_NoAbsorption\Trial19\ CrestandTroughValuesIi\_strmfuswg01.fig and .jpg

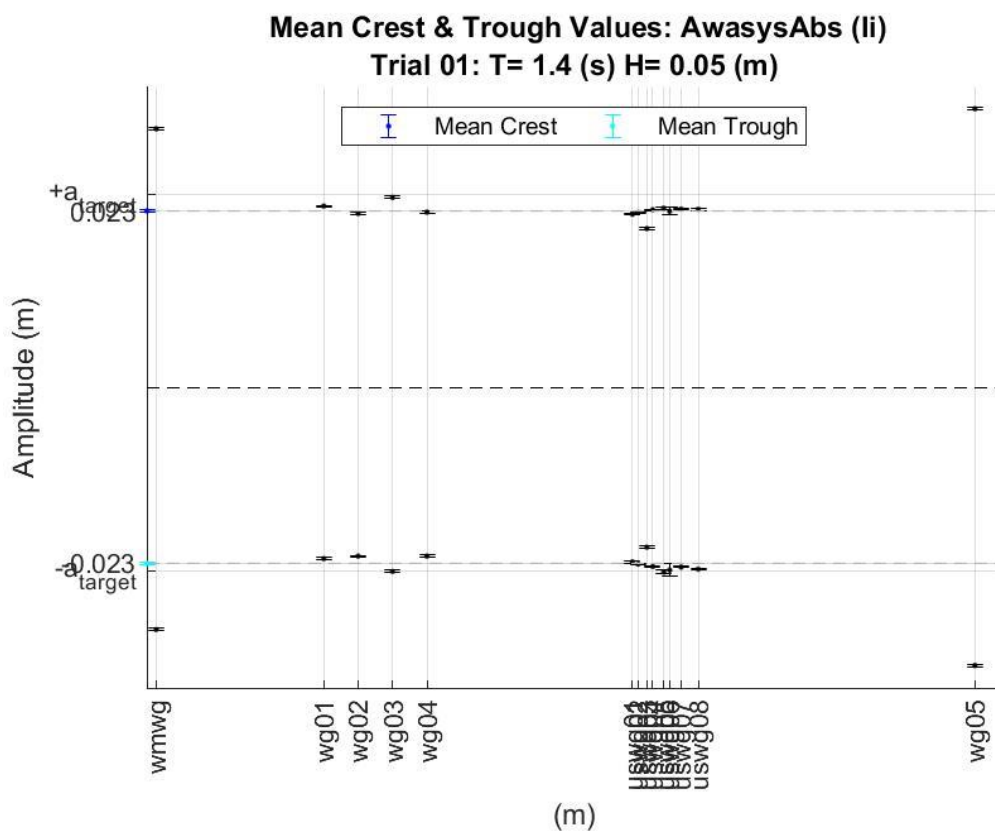
## Appendix J (electronic): Crest and trough values in space

### Supplemental Data File:

#### Description:

The figures show crest and trough data with std error for the wmwg, wg 1-5, and uswg 1-8 for the first incident wave packet for the regular 1.4s and 1.9s wave trials.

#### Sample Plot:



#### File Names:

MTS\_NoAbsorption\Trial01\ Ii\_mCandTrough\_stderr.fig and .jpg

MTS\_NoAbsorption\Trial02\ Ii\_mCandTrough\_stderr.fig and .jpg

MTS\_NoAbsorption\Trial06\ Ii\_mCandTrough\_stderr.fig and .jpg

MTS\_NoAbsorption\Trial19\ Ii\_mCandTrough\_stderr.fig and .jpg

MTS\_Absorption\Trial02\ Ii\_mCandTrough\_stderr.fig and .jpg

MTS\_Absorption\Trial03\ Ii\_mCandTrough\_stderr.fig and .jpg

MTS\_Absorption\Trial07\ Ii\_mCandTrough\_stderr.fig and .jpg

MTS\_Absorption\Trial20\ Ii\_mCandTrough\_stderr.fig and .jpg

Awasys\_NoAbsorption\Trial01\ Ii\_mCandTrough\_stderr.fig and .jpg

Awasys\_NoAbsorption\Trial02\ Ii\_mCandTrough\_stderr.fig and .jpg

Awasys\_NoAbsorption\Trial06\ Ii\_mCandTrough\_stderr.fig and .jpg

Awasys\_NoAbsorption\Trial21\ Ii\_mCandTrough\_stderr.fig and .jpg

Awasys\_Absorption\Trial01\ Ii\_mCandTrough\_stderr.fig and .jpg

Awasys\_Absorption\Trial03\ Ii\_mCandTrough\_stderr.fig and .jpg

Awasys\_Absorption\Trial07\ Ii\_mCandTrough\_stderr.fig and .jpg

Awasys\_Absorption\Trial21\ Ii\_mCandTrough\_stderr.fig and .jpg